Published in "Fundamentals of Cosmic Physics", Vol. 19, pp. 319-422, 1998.

Observations of the Magnetic Fields Inside and Outside the Solar System: From Meteorites (~ 10 attoparsecs), Asteroids, Planets, Stars, Pulsars, Masers, To Protostellar Cloudlets (< 1 parsec)

Jacques P. Vallée

Herzberg Institute of Astrophysics, National Research Council of Canada,
5071 West Saanich Road, Victoria, B.C., Canada V8X 4M6

Abstract. Moving outward from the Earth, one first observes magnetism in older well-formed stars and planets, then one observes magnetism in advanced protostellar disk systems, and one ends inside very young starforming cloudlets (it is akin to moving from old to young star systems). This review covers a range in magnetic field strength from 10^{-6} Gauss up to 10^{15} Gauss. I review here our *observational* knowledge of magnetic fields in interplanetary, stellar and starforming spaces, surveying meteorites (~ 0.3m or 10 attoparsecsin size; 1 parsec = 3.1×10^{16} m = 3.2 light-years), asteroids (~ 30 km or 1 picoparsec), planetary realms (~ 1 nanoparsec), interplanetary space (~ 1 microparsec), circumstellar space (~ 1 milliparsec), protostellar systems (~ 1 centiparsec), out to interstellar starforming cloudlets (up to ~ 1 parsec in size). Spacecrafts from Earth have measured in situ the magnetic field shapes and strengths just outside several planets, moons, and asteroids, as well as the general ubiquitous interplanetary magnetic field. Telescopes on Earth have performed measurements of the magnetic field strengths and shapes in circumstellar environments, protostellar disks, and interstellar cloudlets. Magnetic processes are essential to a detailed understanding of their internal physics and evolution. On small scales, active dipolar dynamo-type magnetic fields can play a dominant role in the dynamics of gas and dust around compact objects. Published theories in protostellar disks and starforming cloudlets are classified along physical parameters. There is little here on the magnetism of objects with sizes > 1 parsec (magnetism on scales > 1 parsec was reviewed in Vallée, 1997).

Key-Words: Magnetic fields; solar system magnetism; stellar system magnetism; magnetized stars; remanent magnetism; masers; protostellar magnetism; magnetic field and star formation; dynamo magnetism; quantum magnetism; magnetized protostellar cloudlets.

Table of Contents

- INTRODUCTION
  - Man-made Magnetism
  - Natural Magnetism
  - Aims of this Review
- MAGNETIC FIELDS IN SMALL BODIES: METEORITES, COMETARY NUCLEI, ASTEROIDS, MOONS, PLANETS
  - Remanent Magnetism
  - Dipolar-shaped Magnetic Field
  - Magnetic Moment and Angular Momentum
- MAGNETIC FIELDS IN STARS AND IN THE INTERPLANETARY MEDIUM
  - Sun (~ 10^6 km; ~ 10^{-7} pc) (~ 10 Gauss)
  - Spiral-shaped Interplanetary Magnetic Field (~ 10^8 km; ~ 10^{-6} pc) (~ 10^{-5} Gauss)
  - Normal Stars (~ 10^6 to 10^7 km; ~ 10^{-7} pc)
  - Degenerate Stars, White Dwarfs (~ 2000 km) (~ 10^6 Gauss)
  - Neutron Stars (~ 10 km)

- CIRCUMSTELLAR MAGNETIC FIELDS (OUT TO 200 AU; ~ 10^{-3} PC)
  - Cataclysmic Binary Objects (~ 10^{5} km) (~ 10^{6} Gauss) and Polars (~ 6×10^{7} Gauss)
  - Late-type Variable Giant Stars (~ 10^{8} km), Young Stars
  - Double Stars and Symbiotic Stars (~ 10^{10} km; ~ 10^{-3} pc)
  - Masers at Centimeter and Millimeter Wavelengths (~ 10^{9} km; ~ 10^{-4} parsec)
  - Circumstellar Gas (out to ~ 3×10^{10} km; ~ 0.001 pc)

- METHODOLOGY AND INSTRUMENTATION FOR PROTOSTELLAR AND INTERSTELLAR DETECTION
  - Basic detection concepts at Radio, Extreme IR, Far IR, and Mid IR Wavelengths
  - Instrumentation at Long Infrared Wavelengths

- PREDICTED MAGNETIC FIELDS IN PROTOSTELLAR DISKS (OUT TO ~ 2000 AU OR SO; ~ 10^{-2} PARSEC) AND DENSE INTERSTELLAR STARFORMING CLOUDLETS (0.1 TO 1 PC)
  - Distinctions of sizes
  - Magnetic Fields and Star Formation Onsets
  - Collapse models
  - Magnetic Disk Classes
  - Expected B with Time
  - Other Theoretical Ideas

- OBSERVED MAGNETIC FIELDS IN PROTOSTELLAR DISKS (OUT TO ~ 200 AU OR SO; ~ 10^{-2} PC) AND DENSE INTERSTELLAR STARFORMING CLOUDLETS (0.1 TO 1 PC)
  - Excess line width for small objects (sizes < 1 parsec)
  - Magnetic Field Strengths
  - Polarization Percentages and Physical Parameters
  - Polarization Position angles and Physical Parameters
  - Some Mapping Results So Far (10^{-3} Gauss)
  - Many Unanswered Questions

- STRIPES AND CLOUDLETS AT NEAR-INFRARED, OPTICAL, AND ULTRAVIOLET WAVELENGTHS (~ 10^{-6}) GAUSS)
  - Gas Stripes near Planetary Nebulae
  - Cloudlets in Filaments
  - Diffuse Interstellar Dust Near and in between Stars

- CONCLUSION

- REFERENCES

1. INTRODUCTION

Is Magnetism a Life form ? The varied manifestations of magnetism have puzzled many people. Some terms used for these magnetic manifestations are: cosmic unrest, organism-like, biological form, and some actions of magnetism are described as: feeding, reproducing, active, altering, etc. "It appear that the radical element responsible for the continuing thread of cosmic unrest is the magnetic field. [...] The magnetic field exists in the Universe as an 'organism', feeding on the general energy flow from stars and galaxies. [...] Magnetic fields (and their inevitable offspring the fast particles) are found everywhere in the universe where we have the means to look for them. [...] What is this fascinating entity that, like a biological form, is able to reproduce itself and carry on an active life in the general outflow of starlight, and from there alter the behaviour of stars and galaxies?" - Parker (1979, his chapter 1).

1.1. Man-made Magnetism

The most powerful magnets on Earth have a magntic field strength near 160 000 Gauss $\approx$ 16 Tesla [1 Tesla = 10^4 Gauss] (e.g., Scanlan 1997), certainly strong enough to make frogs levitate two meters of the ground (e.g., Main 1997; Woloschuk 1997). Diamagnetic (e.g., going against the ambient magnetic field) materials such as water, hazelnuts, plastic, wood, tulips, and many living creatures on Earth, have been levitated already in artificial magnetic fields in labs in the Netherlands, in Grenoble, and the USA (e.g., Buchanan 1997).

Can strong magnetic fields affect humans? A study with a 10 Gauss magnetic field suggested that such a field could elicit

epileptic activity in sick people preparing for brain surgery (e.g., Fuller et al. 1995; Kirschvink 1997).

Are small magnetic fields affecting humans ? An electronic current betrays its presence by generating its own magnetic field. Numerous electrical appliances in a kitchen will generate at a short distance a magnetic field. Moving a magnet across electrical wires in a bike's dynamo will produce enough electricity to light up a lamp. In a 5-year, US $5 million study, various magnetic field levels and configurations in residential homes, ranging in intensity from 0.1 μ Tesla = 1 mGauss, up to 1 μ Tesla = 10 mGauss, and with various shapes (thickness of electrical wires, distance of wires), have been carefully tested with over 1200 children, and the results showed no biological effects (e.g., Taubes 1997). All putative biological side effects due to small magnetic fields < 10 mGauss have remained unproven so far (being too weak or negligible), and putative magnetic effects on our dreams are still unproven (e.g., Saint-Germain 1996).

1.2. Natural Magnetism

1.2.1. *Compass*

Near the Earth's surface, geomagnetic effects are readily detectable with a simple compass. A natural bar magnet, mounted on a pivot, will do. The Earth's magnetic field strength near the surface is half a Gauss ($\approx$ 50 microTesla), and surface magnetic field lines are pointing towards and entering the Earth's crust near the North geographic pole - the entry point in the crust is currently near 70 - 75° longitude West, and near 79 - 80° latitude North.

Are some animals endowed with a sixth (magnetic) sense ? Migratory sea turtles can detect changes in the Earth's magnetic field strength at different places in their trips, as well as changes in the Earth's magnetic field inclination/direction (Lohmann & Lohmann, 1996). The Earth's magnetic field direction can also be detected or sensed by many types of bees and birds, notably pigeons and garden warblers (Weindler et al. 1996; Gould 1996b), as well as by many types of whales and fish, notably eels, salmons, yellowfin tunas, sea turtles, and trouts (e.g., Gould 1996a; Kirschvink 1997).

The threshold of magnetic intensity variation necessary to induce behavioral responses is around 1000 milliGauss for some birds, honeybees, pigeons, and whales, while it is 500 milliGauss in rainbow trouts (Walker et al. 1997).

In rainbow trouts, a study identified an area in the olfactory nose of the trout where a form of biogenic magnetite could be found, attached to the ramus (ros V) of the trigeminal sensory nerve going to the brain. The apparent proximity of the magnetic sensor and the olfactory reception raises the possibility that olfactory impairment would also produce magnetic impairment, which is the case in homing pigeons (e.g., Walker et al. 1997).

1.2.2. *Auroras*

From time to time, energetic jets of particles are emitted by the Sun and are channeled by the Earth's magnetic field toward the two poles of the Earth, where they encounter at high speed the gas particles in the atmosphere. The ensuing collisions energize the local gas particles; these auroral particles then de-excite by emitting flashes of optical light at an altitude of about 100 km. Against solar particles, the Earth's magnetic field acts as a shield protecting Life, and as a channel for space particles. The existence of the Earth's magnetic field is thus revealed when illuminated by the auroral particles in the atmosphere, producing a show often described as 'dancing curtains'. The dancing is due to the intermittent and varied arrivals of different amounts of solar particles at different times and directions.

1.2.3. *Space Storms*

Figure 1 shows typical transmission lines on Earth, above the ground. Solar magnetic storms can have effects on these above-ground transmission lines, through their magnetic induction. In 1989, the Canadian province of Québec suffered a massive electricity blackout, brought on by a space surge, costing Hydro-Québec $10 M Cdn; the large surge in electrical activity from space had short-circuited these electric transmission lines and the overall system on Earth.

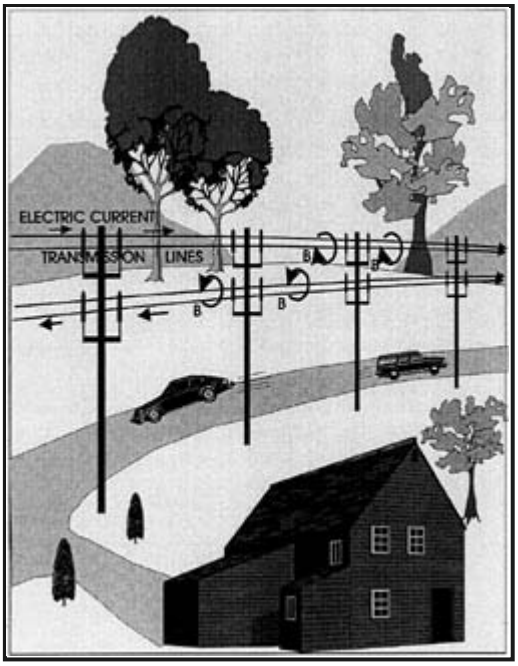

Figure 1. Typical example of electrical transmission lines to transport electricity on Earth. Magnetic fields are shown following the usual right-handed screw system (right thumb towards direction of electric current I). Since the electric currents are mostly alternating, the senses of the assoicated magnetic fields will also reverse with time. The above-ground lines can be seriously affected by the passage of solar magnetic storms speeding away from the Sun and encountering the Earth.

In 1994, Canada's Anik-E1 and Anik-E2 communication satellites were hit by a magnetic blast from the Sun, disrupting Canadian TV operations for days. In January 1997, another solar energy burst permanently disabled the US AT&T satellite, costing nearly $150 millions US (e.g., Curren 1997) - it did this pushing the Earth's magnetosphere boundary much closer to Earth, inside the satellite's orbit around Earth, exposing the satellite to the Sun's blasts (e.g., Kiernan 1997).

1.3. Aims of this Review

"Cherchez le Champ Magnétique" is slowly becoming a well known saying in astronomy. Magnetic fields exist almost everywhere in Space, filling Space to a very large extent. The review below includes the small scale magnetic fields, on the scale from ~ 10^{-17} pc up to 1 pc. The search for a magnetic field ouside the Earth starts with *magnetometers* inside spacecrafts (planetary and interplanetary magnetic fields) and continues further with *polarimeters* inside telescopes on Earth (stellar and interstellar magnetic fields). The large majority of recent observations in interplanetary space have been made with detectors on board spacecrafts, notably Galileo, Ulysses, Voyager I, and Vega I and II.

The study of magnetic fields in circumstellar, protostellar and interstellar objects do impose some extra complexities for theorists in their equations (more terms are added, often non-linear), and do require extra time for observers in their measurements (to see the weak polarized signals above a detection threshold).

The large majority of recent observations of magnetic fields in protostellar disks and interstellar cloudlets have been made in the field of radio astronomy called the Extreme Infrared (submillimeter wavelengths), Current theories for the formation of protostellar disks and interstellar cloudlets prefer a strong magnetic field. Yet strong magnetic fields could (i) prevent gravitational free-fall collapse of the gas, decreasing the star formation rate there; (ii) limit the random motions of individual disks and cloudlets, dragging along low density gas; (iii) transfer momentum between cloudlets, removing angular momentum during condensation; (iv) be a source of extra pressure, creating non-linear magneto-hydro-dynamical (MHD) waves (e.g., Elmegreen 1993). Can we match theories with observations ?

Section 2 deals with magnetism in small bodies and planets, as sampled by artificial satellites launched from Earth. Section 3 deals with stars and the large interplanetary medium. Section 4 deals with circumstellar magnetic fields. Section 5 deals with the methodology and instrumentation involved in sampling interstellar space with radio telescopes. Section 6 deals with the predictions while Section 7 deals with the observations of magnetic field *B* for protostellar disks and small interstellar cloudlets, up to 1 parsec in size. Section 8 deals with large stripes and cloudlets seen at near IR, optical, and UV wavelengths. In what follows, one Astronomical Unit equals 150 million km (1 AU = Earth-Sun distance).

2. MAGNETIC FIELDS IN SMALL BODIES: METEORITES, COMETARY NUCLEI, ASTEROIDS, MOONS, PLANETS

2.1. Remanent Magnetism

Remanent magnetization is familiar through everyday occurrence of permanent magnetism. Ferromagnetic substances may acquire or lose magnetization under some circumstances. Thus ferromagnetic material which cools from a high temperature to a lower one while held in a magnetic field is very efficiently magnetized (called thermo-remanent magnetization). Also, the growth of mineral grains in the presence of a magnetic field produces chemical-remanent magnetization. And the accretion of magnetic particles in the presence of a magnetic field produces depositional-remanent magnetization. The total magnetization of a natural object is often a superposition of magnetization components acquired through several processes over its lifetime. And these different components can be later disentangled, giving some details about the conditions prevailing under each acquired magnetization. Virtually all meteorites carry natural remanent magnetization (e.g., Levy & Sonett 1978).

2.1.1. *Meteorites (~ 0.1 to 1 m; 10^{-17} pc)*

How did our solar system form ? The answer lies in part within the asteroidal belt, located about 3 Astronomical Units (~ 4.5×10^8 km) from the Sun, and containing ~ 10^5 small rocky planetesimals/asteroids. The asteroidal belt is the origin of many meteorites found on Earth. Among the meteorites, the chondrites contain abundant millimeter-sized silicate spherules (chondrules) which were formed ~ 4.5×10^9 years ago within the solar nebula, and have remained relatively unchanged since. Unravelling this record may provide constraints on the type and duration of processes that occurred within the solar nebula.

Chondrites are not entirely pristine, as a few processes may have occurred in the solar nebula, changing the original primary characteristics of chondrites (e.g., Brearly 1997). Examples are the many alterations, either within the original solar nebula before coalescence or accretion into an asteroid, or after accretion within the interior of an asteroid.

The magnetic properties of meteorites are studied to know more about the physical conditions in the early solar system. The meteorites could have been magnetized during the accretion and cooling stages of the formation of the Solar nebula.

2.1.1.1 *Origin* Estimates of the primordial magnetizing fields (the fields responsible for the remanence) have been made through various techniques. Careful measurements of the magnetic field properties of meteorites, based on the thermo-remanent magnetization model, have revealed the primeval magnetic field strength required to give the observed remanent magnetization. The evidence seems to show that chondrules (~ 1 mm in size) inside meteorites (~ 10 cm to 1 m in size) were probably magnetized by the interplanetary magnetic field. A predicted theoretical magnetic field in the early solar nebula (~ 30 μT = 0.3 Gauss), which was inherited from an earlier interstellar cloudlet, is about the correct value needed to magnetize the carbonaceous chondrites. In addition to chondrules, small interstellar grains (~ 1 μm in size) have been discovered in meteorites (notably silicon carbide SiC grains, graphite grains, and corundum Al_2O_3 grains), The distribution of their sizes follows a log-normal equation (e.g., Sandford 1996).

A possible magnetic field for the early solar nebula may have had a dipolar shape with a strength around 1 Gauss. The magnetic field lines could have been perpendicular to the elongated nebular disk, in a dynamo model with a differentially rotating protosolar nebula (gas density 3×10^{-10} cm^{-3}, temperature ~ 200 K, magnetic field ~ 1 Gauss, diameter ~ 7 Astronomical Units, e.g. Levy & Sonett 1978). Such large early interplanetary magnetic fields may have decayed with the dispersal of the early nebular gas, on a time scale of 10 million years (e.g., Umebayashi & Nakano 1984).

2.1.1.2 *Evolution* In the case of a well-preserved meteorite, such as the Allende meteorite which fell to Earth on 8 February 1969 in Mexico, paleomagnetism has shown that its chondrules may have acquired their random remanent magnetization before accretion into the meteorite. During or soon after accretion into the meteorite, a sulfidation event occurred which remagnetized most of the meteorite, but a fraction of the pre-accretion remanent magnetism survived. A subsequent shock slightly rotated the chondrules in the meteorite.

2.1.1.3 *Chemistry* Magnetic minerals in meteorites are quite often different from those in terrestrial rocks. Kamacite is by far the most abundant and the most common magnetic mineral in meteorites. Others include tretataenite, magnetite, and

titanomagnetite. Shu et al. (1997) proposed a model where a magnetosphere in a high magnetic state (inner disk radius located far from star) with low gas temperature (500 K) would allow partial retention of Na and K in rocky chondrules located in the protostellar disk, while a magnetosphere in a low magnetic state (inner disk radius located close to star) with high gas temperature (1500 K) would evaporate Na and K and leave only Ca-Al oxides and silicates in ordinary chondrites in the protostellar disk.

Caveat: a difficulty in meteorite magnetism is that nobody knows what may have happened to the meteorites after their fall to Earth. Generally, atmospheric entry in the Earth affects a meteorite's magnetization only in the outer few centimeters, and it does not interfere with identification of the inner primordial magnetization (e.g., Levy & Sonett 1978). Artificial magnets on Earth may have been used later to identify meteorites - such contacts with artificial magnets could produce a large remanent magnetization in some types of meteorites (e.g., ordinary chondrites), but not in others (e.g., achondrites). Shocks and heat in the absence of a magnetic field may demagnetize the meteorites. A good review on these topics can be found in Sugiura and Strangway (1988).

2.1.2. *Comets' Nuclei (~ 1 to 10 km; ~ 10^{-13} parsec)*

Spacecrafts visit comets rarely, for only brief time intervals in their flythroughs, and at different places along the cometary tails. Near the nucleus of a comet, the general ubiquitous interplanetary magnetic field (~ 50 μGauss at 1 AU) gets compressed by the pressure of cometary static ions, to values ~ 50 nT (= 0.5 milliGauss) at 1 AU from the Sun (e.g. Spinrad et al. 1994). There is usually no need for an intrinsic cometary magnetic field attached to the cometary nucleus; all effects are *extrinsic*. Magnetic disturbances in the interplanetary magnetic field, due to the presence of comet Halley, have been measured by the spacecrafts Giotto (Mazelle et al. 1995), Vega I and Vega II (Mikhajlov and Maslenitsyn 1995).

2.1.3. *Asteroids (~ 10 to 100 km; ~ 10^{-12} pc)*

Big asteroids could be viewed as micro-planets. A few of them have been surveyed at a distance by spacecrafts, and deviations of the interplanetary magnetic fields have been measured in their vicinity. The small radius of the asteroid does not permit the setting up of a dynamo magnetic field. The magnetic moment of the asteroid is weak, weak enough that the magnetic field cannot set up a bow shock and cannot carve a recognizable cavity against the solar wind ram pressure, but it may be strong enough to generate a bow wave and dispersive anisotropic MHD waves (e.g. Baumgärtel et al. 1997). An asteroid generates disturbances in the interplanetary plasma flow, launching whistler waves that are swept downstream by the flowing plasma (e.g., Kivelson et al. 1995). The interaction of the solar wind flow with the asteroid may depend on the properties of the asteroid, such as its magnetization and its electrical conductivity. The interplanetary field may become draped around the asteroid (Wang & Kivelson, 1996).

2.1.3.1 *Gaspra* The Galileo spacecraft acquired data in 1990 during its passage at 1600 km from Gaspra, consistent with a diversion of the interplanetary flow by the asteroid 951 Gaspra (e.g., Baumgärtel et al. 1994; Kivelson et al. 1995). It is thought that some remanent magnetization, left over from the time of formation of the asteroid, could create a somewhat chaotic magnetic field (perhaps like an imperfect non-ideal line dipole).

Gaspra orbits at a mean distance of 2 AU from the Sun, where the interplanetary magnetic field strength is ~ 2 nT = 20 μGauss. Gaspra's magnetic moment (= $B_{surf}\, r^3_{surf}$) has been estimated around 1.5×10^{11} Gauss m^3, predicting a chaotic surface magnetic field around B_{surf} ~ 0.5 Gauss at a radius r_{surf} ~ 7 km (e.g. the dipole model of Baumgärtel et al. 1994). However, the dipole model also predicted a change of magnetic field magnitude which was not observed in the data of the Galileo probe (Wang & Kivelson, 1996). Thus the real magnetic field on Gaspra may be random (not dipolar).

2.1.3.2 *Ida* The Galileo spacecraft acquired data in 1993 during its passage at 2400 km from Ida, consistent with a diversion of the interplanetary flow by effects from the asteroid 243 Ida (e.g., Burnham 1994; Kivelson et al. 1995). The asteroid Ida (radius ~ 15 km) may have revealed to the Galileo spacecraft a weak magnetic field, probably remanent. Ida affects the magnetic field of the solar wind sweeping past it. It is not yet known if a model with a conducting Ida or a model with a magnetic moment for Ida could produce the observed signature in the interplanetary flow (Kivelson et al. 1995).

2.1.4. *Big Moons Without Dynamos*

2.1.4.1. *Earth's Moon* The data for Earth's Moon do not show a large scale golbal magnetic field, so the magnetic moment < 1×10^{12} Gauss. m^3 (e.g., Lin et al. 1998). The radius of Earth's Moon is ~ 1740 km. The Moon is located at 60 Earth radii from the Earth's center. The magnetic field strength at the equatorial surface is < 2 μGauss (e.g. Kivelson et al. 1996b). The solar wind normally flows virtually unimpeded to the lunar surface, where it is absorbed.

2.1.4.2. *Europa* Europa, a large rock at 9 Jupiter radii from Jupiter's center, seems to have an *extrinsic* magnetic field induced

by a current-carrying ionosphere, maintained by Jupiter's background magnetic field of strength ~ 420 nT (= 4.2 milliGauss), as seen by the Galileo probe (Kivelson et al. 1997). The data for Europa are consistent with some kind of passive magnetic dipole, of strength ~ 9×10^{15} Gauss m^3. The radius of Europa is ~ 1570 km. The magnetic field strength at the equatorial surface amounts to 240*nT* = 2.4 mGauss (e.g. Kivelson et al. 1997).

2.1.4.3. *Callisto* The Galileo spacecraft detected a small enhancement of the field strength related to small changes in the jovian plasma environment caused by Callisto's presence. Internal magnetic anomalies in the crust of Callisto could also affect the result, being more probable than an internal dynamo.

Callisto, with a radius of 2400-km, is a moon rock at 26 Jupiter radii from Jupiter's center. It shows little or *no intrinsic* magnetic field (< 30 nT; < 300 microGauss); the magnetic moment is < 4×10^{15} Gauss m^3, as measured by the Galileo probe (e.g., Khurana et al. 1997; Gurnett et al. 1997).

2.2. Dipolar-shaped Magnetic Field

Figure 2 shows a dipolar shape for the magnetic field around a natural bar magnet usually made from a ferrous oxyde. In theory, this would be the ideal unperturbed shape of the magnetic field of the Sun or most stars on a global scale, for some inner planets such as Earth and Mercury, as well as for some giant planets such as Jupiter, Saturn, Uranus, Neptune.

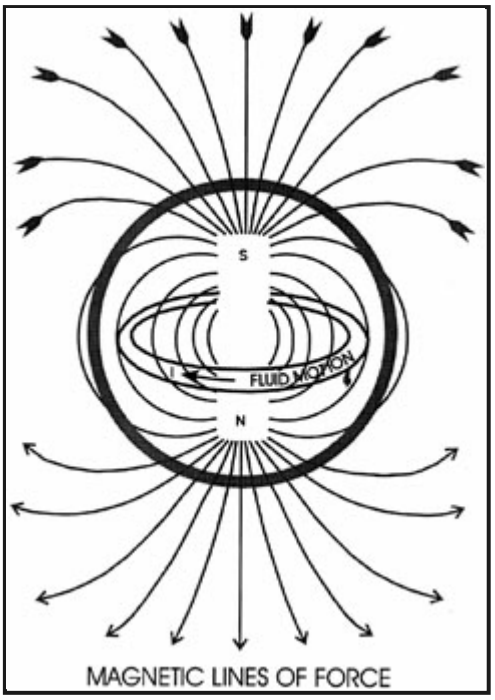

Figure 2. Dipolar-shaped magnetic field lines of a bar magnet. An ideal shape for the magnetic field close to the surface (thick circle) of a star or a planet, as produced inside these bodies by fluid motions (dynamos).

Outside the body's surface, the magnetic field of a dipole decreases roughly as the inverse cube of the distance,

$$B(r) = B_{\rm surf} \cdot r_{\rm surf}^3 / r^3 = M_{\rm surf} \cdot r^{-3}$$

where $B_{\rm surf}$ is the magnetic field strength at the surface of the object of radius $r_{\rm surf}$. It is customary to define the 'dipole magnetic moment' as

$$M_{\rm surf} = B_{\rm surf} \cdot r_{\rm surf}^3$$

and to express its units as Gauss m^3 .

Inside the body's surface, the three basic ingredients needed for a dynamo are a large volume of electrically conducting fluid in the body's interior, an energy source (such as convection) to circulate the fluid, and the body's overall rotation to organize the resulting fluid motions.

2.2.1. *Big Moons With Dynamos (~ 10^3 to 10^4 km; ~ 10^{-10} pc) (~ 10^{-2} Gauss)*

Big moons could be viewed as mini-planets.

2.2.1.1 *Ganymede* The discovery of the magnetic field of Ganymede (one of the moons of the planet Jupiter) by the spacecraft Galileo (e.g., Kivelson et al. 1996a) has shown that remanent magnetization is very unlikely. The internal magnetic field is strong enough to carve out a magnetosphere with clearly defined boundaries within Jupiter's own magnetosphere - Ganymede's magnetic field is several times larger than Jupiter's ambient magnetic field (120 nT = 1.2 milliGauss) at Ganymede's distance. Ganymede is at 15 Jupiter radii from Jupiter's center.

The data are consistent with an *active* Ganymede-centered magnetic dipole of ~ 1.4×10^{17} Gauss m^3, tilted by about 10 degrees relative to the spin axis of the moon. The radius of Ganymede is ~ 2650 km. The magnetic field strength at the equatorial surface amounts to 750 nT = 7.5 mGauss (e.g. Kivelson et al. 1996a).

The source of Ganymede's magnetic field could be a dynamo action, located in a molten iron core (or a salty-water internal ocean). Ganymede is "almost certainly" operating its own dynamo, albeit altered by Jupiter's own magnetic field (Sarson et al. 1997).

2.2.1.2. *Io* Voyager I spacecraft detected magnetic fields from Jupiter's moon Io (e.g., Ness et al. 1979). The Galileo spacecraft confirmed this finding. A part of Io's magnetic field could be *extrinsic*, induced externally by a *current-carrying ionosphere* (Kivelson et al. 1996c), and a part could come from an internal dipole. The extrinsic part is maintained by Jupiter's own magnetic field (Sarson et al. 1997), *via* magnetoconvection processes induced by Jupiter's ambient field of strength ~ 1800 nT (= 18 mGauss). Io is at 6 Jupiter radii from Jupiter's center.

The data for Io are consistent with some kind of passive magnetic dipole, anti-aligned with Jupiter's magnetic dipole, of strength ~ 8×10^{16} Gauss m^3. The radius of Io is ~ 1820 km. The magnetic field strength at the equatorial surface amounts to 1300 nT = 13 milliGauss (e.g., Kivelson et al. 1996b). The recent evidence suggests that Io has a large molten iron-sulfide core and that adequate tidal heating is present to drive a small dynamo field (e.g., Kivelson et al. 1996b).

2.2.2. *Planet Earth (~ 10^4 km)*

The Earth's interior can be subdivided into 4 main volumes. At the center one has the core, composed of (i) a 1200-km radius solid crystalline metallic 'inner core', (ii) which is surrounded by a 2300-km thick "liquid" molten (iron-alloy) metallic 'outer core'. On top of that one has the 2900-km solid oxide shell, composed of (iii) a 'lower mantle', and (iv) an 'upper mantle'.

Inside the Earth, the magnetic field may be generated and maintained somewhere in the outer core by dynamo action. The rough extent of the dynamo region is above 0.2 and below 0.5 Earth radii. It is motions in the "liquid" molten metallic 'outer core' that produce the Earth's magnetic field, through MHD processes in the electrically conducting fluid of the outer core, where the magnetic field there can reach 300 Gauss (e.g., Fig. 3 in Jeanloz & Romanowicz 1997). The temperature at the top of the outer core is near 4000 K, while it is about 5000 K at the top of the inner core. An important energy source for the dynamo is the crystallization of iron at the inner-outer core boundary, releasing latent heat and light constituents, driving convection in the liquid outer core (e.g., Olson 1997). Geo-dynamo theories have predicted the shape of the magnetic field inside the Earth, aligned along the rotation axis in the inner core, but more complex in the outer core due to convective fluid (Glatzmaier and Roberts, 1996).

The data for Earth are consistent with some kind of *active* magnetic dipole, of strength ~ 1.3×10^{20} Gauss m^3. The radius of Earth is ~ 6400 km. The magnetic field strength at the equatorial surface amounts to about 0.5 Gauss (e.g., Lanzerotti & Krimigis 1985). The Earth's magnetic field has reversed polarity many times in the past, the last ones being 780 000 years ago and 990 000 years ago. The duration of the reversal is short, about 4000 years during which the average intensity of the Earth's field is not zero but small, decreasing to about a quarter of its usual value (e.g., Merrill 1997).

Outside the Earth, the magnetic field strength in the Earth's ionosphere (ionized atmosphere at 100 km above the surface of the Earth) is about 0.3 Gauss. The effects of the solar wind on the Earth's original dipolar-shaped magnetic field is to push or deform the Sun-facing side into a smaller lobe, and to pull/expand the opposite side into a long trailing lobe. The full length of the magnetotail on the extended/night side can reach as fas as 220 Earth radii. The Moon is at 60 Earth radii.

Figure 3 shows a sketch of the Earth's magnetic field (or shield), which has a roughly dipolar form and a surface strength of about 0.5 Gauss. The lines of force of the Earth's magnetic field come into the Earth's geographic North pole, and exit through the Earth's geographic South pole. When the needle from a compass points to the Earth's North, the needle's own North pole aligns itself with the Earth's geographic North pole direction. An "equivalent bar magnet" inside the Earth would be upside down (have opposite polarity) to the earth's geographic North and South poles.

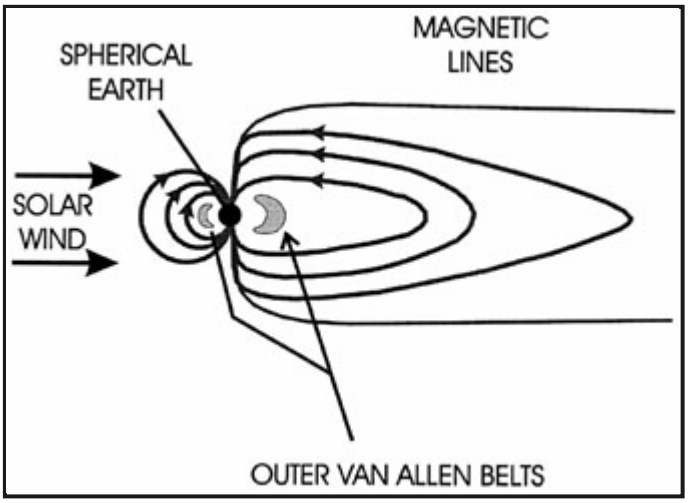

Figure 3. Earth's magnetic field, as deformed from its ideal bar-magnet shape by the ram-pressure effects of the solar wind.

2.2.3. *Planets (~ 10^4 to 10^5 km; ~ 10^{-9} parsec) (~ 0.1 Gauss)*

Aside from Earth, planetary magnetic fields have been detected so far through in-situ spacecraft measurements, for Mercury and the giant planets Jupiter, Saturn, Uranus, Neptune (e.g., Fig. 5 in Kivelson et al. 1996b).

For a planetary dipolar-shaped magnetic dynamo, the time-variation of the magnetic field *B* follows the interaction between a diffusion term and an induction term

$$\frac{\partial B}{\partial t} = \beta \nabla^2 B + \nabla \times (V \times B)$$

where ∂ signifies a partial differential operator, *t* is the time, *B* is the global magnetic field, β is the magnetic diffusivity ($\beta < 10^7$ cm^2 sec^{-1}) and *V* is the velocity field relative to the rigidly rotating frame defined by the external magnetic field (e.g., chapter 6 in Hubbard 1984).

2.2.3.1 *Mercury* The data for Mercury are consistent with some kind of active magnetic dipole, of strength × 5 × 10^{16} Gauss m^3. The radius of Mercury is ~ 2440 km. The magnetic field strength at the equatorial surface amounts to about 3.5 milliGauss (e.g. Lanzerotti & Krimigis 1985).

In Mercury, the magnetic field may be generated and maintained somewhere in the liquid outer core by dynamo action. The rough extent of the dynamo region is above 0.4 and below 0.6 Mercury radii (Schubert et al. 1988), and the dynamo is driven by release of gravitational energy and latent heat upon inner core growth.

2.2.3.2 *Venus* The data for Venus do not show a magnetic field, so the magnetic moment < 6.6 × 10^{16} Gauss m^3. The radius of Venus is ~ 6050 km. The magnetic field strength at the equatorial surface is < 0.3 milliGauss (e.g. Lanzerotti & Krimigis 1985).

Dynamo theory does not predict much magnetism for Venus, due to the *very slow rotation* of ~ 243 days of Venus as a whole, < 0.6 milliGauss (e.g., chapter 20 in Parker 1979).

2.2.3.3 *Mars* The data for Mars show a very weak magnetic field, about 800 times weaker than Earth's or about 0.6 milliGauss (e.g., Cohen 1997a; Kerr 1997; Lanzerotti & Krimigis 1985), so the mean magnetic moment is ≈ 2.3 × 10^{16} Gauss m^3. Mars' radius is ~ 3370 km.

The Global Surveyor probe found some patchy magnetic areas on Mars' surface, showing a random distribution of rocky bar magnets scattered all over the surface, sometimes reaching a few milliGauss - this is not a global magnetic field. The random magnetic patches are thought to be the remnants of an ancient field (e.g., Cole 1997).

The planetary core of Mars may extend up to 0.5 Mars radius. Dynamo theory does not predict much magnetism for Mars, due to the current *absence of thermal convection* inside the core (e.g., Schubert et al. 1992). Such a very weak magnetism implies that the planetary core must have cooled quickly and the current magnetism may be the relic of a *dead turn-off dynamo*, a fossilized remnant left in crustal rocks of earlier interior activity.

2.2.3.4 *Jupiter* The data for Jupiter are consistent with some kind of active magnetic dipole, of strength ~ 1.5×10^{24} Gauss m^3. The radius of Jupiter is 71,370 km. The magnetic field strength at the equatorial surface amounts to ~ 4.1 Gauss (e.g. Lanzerotti & Krimigis 1985).

Substantial polarized synchrotron radio emission comes from Jupiter, implying the presence of a strong dipolar magnetic field, rotating with the same period as for the planet as a whole. The position of the moon Io seems to affect the intensity of the radio emission coming from the magnetosphere of Jupiter, possibly due to the matter being spurned out from the volcanoes of Io.

A substantial dynamo can be sustained by a highly turbulent MHD flow inside Jupiter (e.g., Hubbard 1984), involving a convecting electrically conducting dynamo in the planet's interior.

2.2.3.5 *Saturn* The data for Saturn are consistent with some kind of active magnetic dipole, of strength ~ 9×10^{22} Gauss m^3. The radius of Saturn is ~ 60330 km. The magnetic field strength at the equatorial surface amounts to ~ 0.4 Gauss (e.g., Lanzerotti & Krimigis 1985).

In Saturn, the magnetic field may be generated and maintained somewhere in the outer core by dynamo action. The rough extent of the dynamo region is above 0.4 and below 0.6 Saturn radii, in the outer core of liquid-metallic-hydrogen and semiconducting-molecular-hydrogen (Hubbard & Stevenson 1984).

2.2.3.6 *Uranus* The data for Uranus are consistent with some kind of active magnetic dipole, of strength ~ 5×10^{20} Gauss m^3. The radius of Uranus is ~ 12800 km. The magnetic field strength at the equatorial surface amounts to about 0.23 Gauss (e.g., Table 3.2 in Lang 1992).

In Uranus, the magnetic field may be generated and maintained by dynamo action. The rough extent of the dynamo region is above 0.3 and below 0.7 Uranus radii, through nonuniform motions in a highly ionic conducting fluid (Podolak et al. 1991).

2.2.3.7 *Neptune and Pluto* The data for Neptune are consistent with some kind of *active* magnetic dipole, of strength ~ 2.5×10^{20} Gauss m^3. The radius of Neptune is ~ 12380 km. The magnetic field strength at the equatorial surface amounts to about 0.13 Gauss (e.g., Table 3.2 in Lang 1992).

In the large planets Uranus and Neptune, it has been argued that the magnetic field could also be generated in a shell at intermediate depth in the planetary interior, not in the core (Kivelson et al. 1997).

2.3. Magnetic Moment and Angular Momentum

2.3.1. *Empirical Law*

The angular momentum A of a spherical object of radius r_{surf} is

$$A = 0.4\,\omega\,(\mathrm{mass}) r_{surf}^2$$

where $\omega = 2\pi$ (rotation period)$^{-1}$, and mass is the mass of the object. Thus for the Sun ($\omega = 2.9 \times 10^{-6}$ sec^{-1}) one gets $A \approx 10^{42}$ kg m^2 sec^{-1}; the Sun's magnetic moment $M_{surf} \approx 3 \times 10^{27}$ Gauss m^3 . For Mercury ($\omega = 1.2 \times 10^{-6}$ sec^{-1}), $A \approx 10^{30}$ kg m^2 sec^{-1}, and $M_{surf} \approx 5 \times 10^{16}$ Gauss m^3.

A direct relationship is often but not always observed between the magnetic dipole moment M_{surf} of an object and its angular momentum A. This often observed relation is given approximately by

$$M_{\rm surf}({\rm Gauss\ m^3}) \approx 4 \times 10^{-9} [A({\rm kg\ m^2\ sec^{-1}})]^{0.83}$$

Figure 4 shows this equation (dashed), along with the observational data. Originally proposed only for the planets, this empirical law has been extended to include the Sun (e.g., Blackett 1947; Russell 1978), and big moons such as Ganymede and Io (Kivelson et al. 1996a, 1996b).

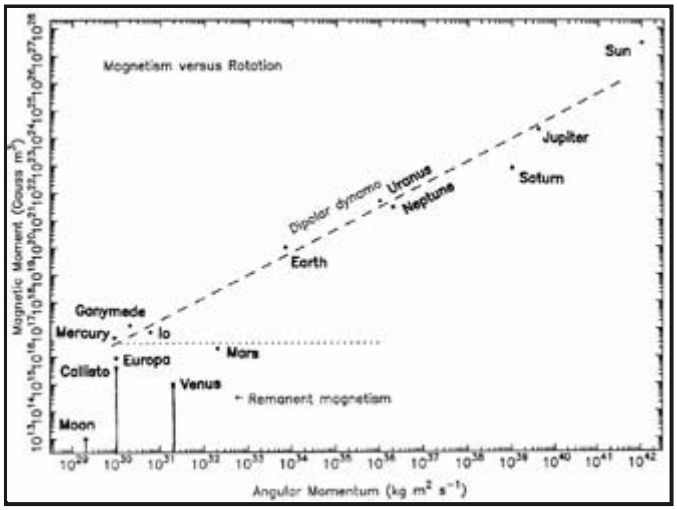

Figure 4. Observed relation between the magnetic moment and the angular momentum of moons, planets, and the Sun. The dashed line follows the equation for a dipolar dynamo, with a slope of $\approx$ 0.8. Many data are from Kivelson et al. (1996b), the rest from this text. Below a certain strength and a certain angular momentum (at bottom left), remanent magnetism is often found.

2.3.2. *Interpretation*

Such a law has been called a "magnetic Bode's law" (Russell 1978), and was though to be a "long-sought connection between electromagnetic and gravitational phenomena" (Blackett 1947), and has also been called "an effect more along 'meteorological' lines" (e.g., chapter 18 in Parker 1979).

This relationship may now be better called a "dipolar dynamo law", for three reasons. (1) All the moons, planets and star(s) that obey so far this relation do have a dipolar dynamo. (2) All the moons and planets without a significant magnetic dynamo (Earth's Moon, Venus, Mars) do not follow this law - the observed data for Earth's Moon, Venus, and Mars fall significantly *below* the $M_{\rm surf}$ values predicted by this law (e.g., Kivelson et al. 1996b). (3) The relationship may not work for other (not dypolar) dynamo types - thus our Milky Way galaxy has a planar disk with an axisymmetric spiral (not dipolar) dynamo magnetic field, with $A \approx 3 \times 10^{67}$ kg m^2 sec^{-1} and $M_{\rm surf} \approx 9 \times 10^{55}$ Gauss m^3, and thus the equation above would predict only $M_{\rm surf} \approx 4 \times 10^{47}$ Gauss m^3 - about 10^8 times lower than observed.

Physically, no direct physical justification for this law has been found. Mathematically, since $M_{\rm surf} = B_{\rm surf} \cdot r^3_{\rm surf}$ for a sphere, and since $A \sim$ (mass) $\cdot\ r^2_{\rm surf} \sim$ (density) $\cdot\ r^5_{\rm surf}$ then it can be seen that $M_{\rm surf}$ and A are strong powers of $r_{\rm surf}$, so the apparent correlation of these two quantities should predict $M_{\rm surf} \sim r^3_{\rm surf} \sim A^{0.60}$. This mathematical argument would predict that the data for all planets would follow this law - this argument does not explain why the observed data for some planets or some moons fall below the predictions of this law.

3. MAGNETIC FIELDS IN STARS AND IN THE INTERPLANETARY MEDIUM

3.1. Sun (~ 10^6 km; ~ 10^{-7} pc) (~ 10 Gauss)

Current magnetic fields in stars could have originated in pre-stellar matter (fossil theory), and be influenced later by (i) magnetic diffusion and (ii) breaking in the protostellar cloud as well as by (iii) plasma motions and (iv) dynamo effects inside stars (e.g., Shi-Hui 1994). The contraction of an initial protosolar cloud permeated by a magnetic field may have followed the equation

involving diffusion, magnetic induction, as well as buoyancy and turbulence.

The internal structure of the Sun is reasonably well understood. The current internal structure of the Sun is understood to have a nuclear-burning core (out to ~ 0.2 solar radius), followed by a radiative zone or shell (out to ~ 0.6 solar radius), and by a convection zone or envelope (out to ~ 0.98 solar radius). The visible surface of the Sun is called the photosphere.

It is believed that the main energy source of the solar dynamo is the differential rotation inside the stable stratified '*overshoot layer*' of thickness ~ 20000 km, sandwiched near 0.6 solar radius between the solar radiative zone and the solar convection zone (e.g., Zwaan 1978; Parker 1993). In this 'overshoot layer', the magnetic field needs to be ~ 100000 Gauss and the gas density ~ 10^{23} cm^{-3}, and some of this magnetic field may then wind up later on at the solar surface with a 22-year complete solar cycle (e.g., Ossendrijver & Hoyng 1997). Such a thin-shell dynamo model for the Sun cannot generate a poloidal field fast enough to maintain a large scale field stretching across the entire sun; the field is therefore an oscillating dipole (e.g., Parker 1983).

The large scale solar magnetic field near the poles of the Sun is basically dipolar (with a strength of about 10 Gauss). The 11-year sunspot pattern occurs for each half of a 22-year complete solar cycle, and after each half the poles of the sun change again their large-scale magnetic sense. The polarity of the north geometric pole of the Sun changed in mid-1958, and in mid-1971, and again in mid-1980, etc. (e.g., chapter 7 in Shi-Hui 1994).

The data for the Sun's large scale magnetic field are consistent with some kind of *active* magnetic dipole, of strength ~ 3×10^{27} Gauss m^3. The radius of Sun is ~ 700000 km. The magnetic field strength at the polar surface amounts to about 10 Gauss.

In practice, such a large-scale dipolar magnetic field shape will be distorted by environmental effects (solar rotation, solar wind) or by local surface effects (sunspots) or by tidal effects (combined effects or planets, nearby passing star).

There are small scale magnetic fields on the Sun. Magnetic activity on the scale of months or years appears away from the solar poles, usually as bipolar active regions (sunspots) covering small surface areas, where the magnetic field strength can reach about 2000 Gauss and sunspots tend to be paired by a localized dipolar magnetic field (small scale magnetic fields). Recent work by Westendorp Plaza et al. (1997) gave evidence for gas and magnetic field lines to rise near the center of a sunspot, and to turn horizontal in a penumbral canopy, and then to bend downward in the outer penumbral region at the outer edge of the sunspot. The gas density in the penumbral canopy is an order of magnitude smaller than in the inner penumbra and the canopy has 14 times smaller magnetic flux, implying a non-conservation of mass and field in the canopy, and explained by the field bending and downward mass motion at the outer edge of the sunspot. Over the course of the first half of a 22-year complete solar cycle, the mean sunspot latitude starts around 40° and then slowly tends to decrease toward the solar equator, after which (~ 11 years) the poles of the Sun change their magnetic sense (large-scale dipole).

3.2. Spiral-shaped Interplanetary Magnetic Field (~ 10^8 km; ~ 10^{-6} pc) (~ 10^{-5} Gauss)

Figure 5 shows a sketch of the interplanetary magnetic field, as measured between the planets by the spacecrafts launched from Earth. The interplanetary magnetic field takes its source from the Sun. As the Sun rotates, the escaping magnetic field takes a spiral shape - also called Archimedean, akin to a water jet escaping from a rotating carrousel.

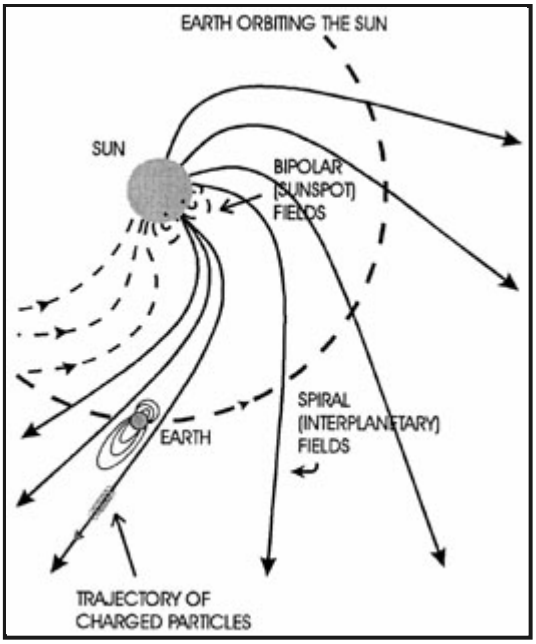

Figure 5. Interplanetary magnetic field, as originating in the Sun and as deformed by the effects of the solar rotation and solar wind.

The interplanetary magnetic field strength is about 50 microGauss near the Earth (1 AU from the Sun), and near 20 microGauss at a distance of 2 AU from the Sun. The solar wind near 2 AU is about 1 proton / cm^3, and flows at ~ 300 km/s (e.g., Baumgärtel et al. 1994). The solar wind has a permanent slow component and an irregular gusty fast component (up to ~ 800 km/s). The slow component seems to come from long narrow structures towering over the arched magnetic fields of the streamer belt near the solar equator. The fast component emerges from isolated patches of open field lines over most of the solar surface and including coronal holes near the two solar poles, allowing the hot gas to rush out unimpeded (e.g., Glanz 1997).

The Ulysses spacecraft, going out of the ecliptic plane after an encounter with Jupiter, was deflected into a polar orbit around the Sun. It confirmed that the overall interplanetary magnetic field was *dipolar*, with the same polarity as that at the Sun's surface outward for both the Northern hemisphere of the Sun and for the interplanetary space; inward for both the Southern hemisphere of the Sun and for the interplanetary space, in 1995 (e.g., Forsyth et al. 1996). The solar equator is inclined by 7° from the ecliptic plane (Earth's orbital plane), so the Earth rises above and below the solar equator.

The interplanetary magnetic field lines with their origin in the Sun are swept out by the solar wind. This sweeping creates two broad regions of opposite magnetic polarity (outward for 180°, inward for 180°) in solar longitudes, separated by a current 'sheet' (often warped) near the plane of the solar equator (latitude 0°).

There is a single warp of the equatorial sheet. The Ulysses spacecraft, while in the ecliptic plane, observed the current 'sheet' lying close to the equator, but being *warped* up to +20° and down to -20° in solar latitudes, much like a double-peaked cosine function as one goes around the solar equatorial longitudes (e.g., Forsyth et al. 1996). Near the equator, outward magnetic field lines were found in 1995 near solar longitudes 285° and 105° (due to a current 'sheet' warped down to ~ - 20° latitude); inward magnetic field lines were found near longitudes 195° and 15° (due to a current 'sheet' warped up to ~ + 20° latitude). Thus *four* 'magnetic sectors' were encountered in the equatorial plane going around the solar longitudes. Hence as the Earth orbits in a year around the Sun, it encounters an outward-going interplanetary magnetic field (for ~ 3 months), then an inward-going field (for ~ 3 months), then an outward-going field (for ~ 3 months), and finally an inward-going field (for ~ 3 months).

Figure 6 shows a simplified sketch of the heliospheric magnetism in 1995, as seen by Ulysses. As the Earth orbits a full circle around the Sun, these four interplanetary magnetic sectors are crossed, leading to observational effects on Earth such as *geomagnetic storms* (e.g., Parker 1958; Vallée 1969; Lapointe and Vallée 1970; Vallée 1982). Geomagnetic activity can thus change significantly, depending on which magnetic sector the Earth is in (i.e., depending on the number of sunspots and the particle-emitting activity of the sunspots, in that magnetic sector).

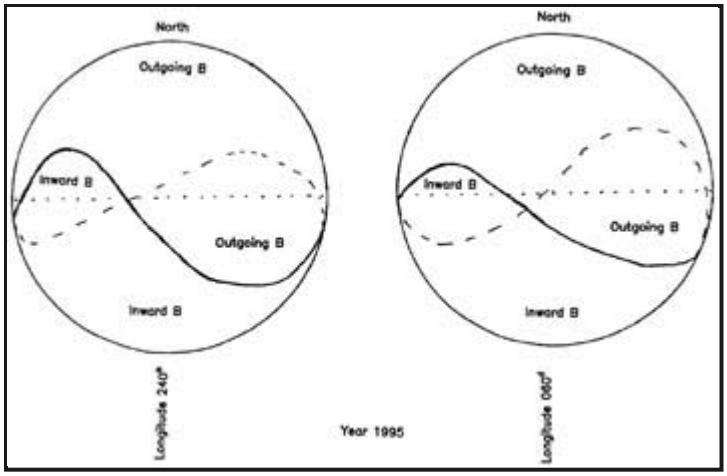

Figure 6. A sketch of the heliospheric magnetic field in 1995, with the location of the neutral sheet (double-cosine curve, also shown dashed on the back side of the Sun), adapted from Forsyth et al. (1996) . When moving along the equatorial plane (dots), one encounters 4 magnetic polarities, hence 4 magnetic sectors in interplanetary space due to the solar wind.

3.3. Normal Stars (~ 10^6 to 10^7 km; ~ 10^{-7} pc)

In normal stars, dynamos can explain the basics of a stellar magnetic field, as long as a convective envelope exists in the stellar interior. But theoreticians have yet to arrive at an adequate, complete, self-consistent MHD dynamo model of a convective envelope that can reproduce quantitatively *all* relevant observations at the same time (e.g., Donati et al. 1997).

3.3.1. *Dipolar Magnetic Field Shape*

The internal structure of a star is reasonably well understood. The energy released in the interior of stars and in the assemblages of stars by the action of nuclear and gravitational forces keeps electrically conducting fluids in turbulent motion. Magnetic field in cool stars originate from the *base* of the outer convection zone and migrate towards the stellar surface through magnetic buoyancy. The magnetic field entrained in the fluid (ionized gas) is stretched and folded by the fluid motion (nonuniform rotation and cyclonic convection), gaining energy in the process (e.g., Parker 1983). Main sequence stars rotate and have vigorous convective zones (like the Sun), so it follows that there is a dynamo effect in these stars. The younger stars would seethe with activity, but their magnetic virility would decline over a period of 10^8 years (e.g., chapter 21 in Parker 1979).

An important mechanism to detect stellar magnetic fields at optical wavelenths is the Zeeman effect, where emitted lines from chemical elements (e.g., sodium) placed in a magnetic field are splitted into components and the state of splitting depends on the direction and strength of the magnetic field. The application of the Zeeman effect to the optical spectra of certain other classes of star has shown that some stars do possess magnetic fields. Different absorption lines can be used for the Zeeman effect, depending on the star's surfae temperature and hence on the star's spectral type (from hot *O*-type and *B*-type stars, normal *A*-type, *F*-type, and *G*-type stars, to cool *K*-type and *M*-type stars).

There is typically one large scale dipole and many small localized surface scale dipoles. Stellar-type magnetic fields often have a basic large scale dipolar shape near the stellar surface.

Rapidly rotating active stars generally display stellar spots near their two poles, which is a way to prevent dynamo saturation at high rotation rate (e.g., Solanski et al. 1997). A dynamo could start saturating when rotation is too high, due to the back reaction of the magnetic field on the stellar convection and differential rotation. Slower rotators like the G-type Sun tend to have their spots near the equatorial plane. The magnetic flux tubes are rising from deep inside the star, due mainly to magnetic buoyancy and Coriolis force, and secondarily to magnetic tension and drag.

A detection of a magnetic field in a supposedly 100% convective star or in a 100% radiative star could be challenging for dynamo theories. Some low-mass pre-main-sequence objets (such as V410 Tau) are claimed to have no inner radiative zone, being 100% convective stars, yet they may have a detectable magnetic field. Some high-mass pre-main-sequence objects (such as HD 104237) are claimed to have no convective envelope, being 100% radiative stars, yet they may have a magnetic field - in such cases, the theoretical work is being concentrate on the possible presence of a small sub-photospheric layer with turbulent motions (e.g., Donati et al. 1997).

3.3.2. *A_p stars (~ 10^4 Gauss)*

Many stars in a sub-class of spectral type *A* stars, called peculiar *A* stars or A_p stars, have strong surface magnetic fields. The magnetic dipole axis are often perpendicular or oblique with respect to the star's rotation axis, causing a periodic change in the Zeeman line data.

Thus in an ideal case the "effective" magnetic field *B*, or "longitudinal" magnetic field, or the "line-intensity weighted average over the visible stellar hemisphere of the line-of-sight component of the magnetic vector", is obtained from Stokes *V* observations and should vary with time *t* during the rotation period *p* as

$$B \sim B_{\rm pole}[(\cos i)(\cos \beta) + (\sin i)(\sin \beta)\cos(2\pi t/p)]$$

where $B_{\rm pole}$ is the polar magnetic field, *i* is the angle between the axis of the magnetic field dipole and the axis of rotation of the star, and β is the angle between our line of sight and the axis of rotation of the star. The observed separation between the two Zeeman line components is proportional to the strength of the magnetic field, ie $\Delta \lambda \sim \lambda_0 g_e <B>$ where λ_0 is tl normalization wavelength and g_e is the average effective Landé factor (~ 1, within a factor 2). Current observed effective magnetic field strengths are ~ 10000 Gauss.

Also in the ideal case the "surface" magnetic field, or the "mean field modulus", or the "line-intensity weighted average over the visible stellar hemisphere of the modulus of the magnetic vector", is obtained from Stokes I observations at sufficiently high spectral dispersion showing the spectral lines splitted into several magnetic components. The observed line separation between red and blue components for the Zeeman doublet of the Fe II line at λ6149.258 Åis given as $\Delta \lambda \sim \lambda_0^2 g <B>$ where λ_0 is the normalization wavelength and *g* is the Landé factor of the split level $\approx$ 2.7 here (e.g., Mathys et al. 1997). Current observed surface magnetic field strengths are ~ 3 kG to 10 kG.

The simultaneous consideration of both the "effective" field and of the "surface" field is required to derive meaningful constraints on the geometrical structure of the magnetic field. Such considerations suggest the following: the magnetic field covers most of the stellar surface, and the two poles within a star often have different strengths, so one magnetic pole could be nearer the stellar surface than the other magnetic pole (e.g., Mathys et al. 1997).

The stellar envelope of A_p stars is hot and radiative, and the magnetic field is thought to be "fossil" - a remainder of the magnetic flux previously in the interstellar medium from which the star formed (e.g., Babel and North 1997).

Some stars have a bow shock. Some X-ray emitting gas around peculiar Ap stars may be due to a shock near such a star, The dipolar magnetic field of 1000 Gauss is able to bend the 500 km/s stellar wind towards the magnetic equatorial disk extending out to 4 stellar radii, resulting in shocked gas near 106 K (Babel & Montmerle 1997).

Calcium emission lines from stellar spots, where the magnetic field is strong, will follow a time variation due to the stellar spot cycle. Since many sun-like, *G*-type stars show such calcium line variation over time, it has been inferred that about half of the stars similar to the Sun may have magnetic fields.

3.3.3. *M-type stars*

M-type stars, with a smaller mass than the *G*-type Sun, are rotating faster than the Sun. All *M* stars in the Pleiades are rapid rotators (e.g., Jones et al. 1996). They are thus expected to have (i) a predominently polar magnetic field and (ii) temporal magnetic activity possibly concentrated near the stellar poles. Essentially all *M* stars should display polar, rather than equatorial, temporal magnetic activity. A physical result is that stellar spin-down should be negligible for *M* stars (e.g., Buzasi 1997)

3.3.4. *Stars with a Residual Disk*

A small number of stars may have a circumstellar disk (not planets) around, even a long time after star formation. The gas in the circumstellar disk of diameter 0.7 AU around the Be star SS2883 has been modeled with a gas density of 10^{10} cm^{-3} and a radial/toroidal magnetic field of 30 Gauss (thin disk) and with a gas density of 10^8 cm^{-3} and a poloidal magnetic field of 14 kiloGauss (thick disk), as inferred from the modulation of the RM and DM of the distant orbiting pulsar PSR B1259-63 (e.g., Melatos et al. 1995).

3.3.5. *Quadrupolar Magnetic Field Shape*

A very small number of stars (< 10) are known to have a global quadrupolar type magnetic field, much like that resulting from two antiparallel dipoles slightly displaced from each other.

This is the case for the *B*-type star HD37776 with a diameter ~ 8×10^6 km and a magnetic field reaching 2000 Gauss (e.g., Thompson & Landstreet 1985; Borra & Landstreet 1978). This is also the case for the B_p star HD133880, whose very non-sinusoidal magnetic field curve indicates a non-dipolar field geometry, but rather a predominently quadrupolar magnetic field shape with a strength ~ 10000 Gauss (Landstreet, 1990). The A_p star HD137509 has recently been found to exhibit such a quadrupolar magnetic shape with a strength ~ 25000 Gauss (Mathys & Hubrig 1997).

Clearly any mass loss, atmospheric parameter, diffusion velocity, and other quantity that depends on magnetic field strength and shape will be affected by this system of quadruple poles. This is even more so if the magnetic field strength is weak (say 3000 Gauss) at 2 opposite poles and strong (say 10000 Gauss) at the other 2 opposite poles.

Donati & Cameron (1997) proposed a novel method to analyse Stokes *V* data, requiring a single spectral line fit to over 1500 spectral lines from λ0.470 μm to λ0.710 μm, assuming all 1500 line shapes/profiles to be additive, self-similar, and scalable in width and depth. These and other assumptions (weak magnetic field so that Zeeman splitting is small compared to the intrinsic line width; limb darkening is constant with wavelength) sound rough and should be investigated later. Studying the rapidly rotating (0.5 day) KO dwarf star AB Dor with this novel method, Donati & Cameron (1997) found (i) 6 active magnetic loops with *B* ~ 500 Gauss located at high latitudes on the stellar surface and corona, and (ii) several other low-latitude spots. Further analysing their data, they deduced (iii) some clues for a possible surface toroidal magnetic field at high latitudes going in opposite direction to the surface toroidal field at intermediate latitudes, predicting (iv) another two zones of opposite magnetic polarity in the other stellar hemisphere; hence they theorized (v) a large scale poloidal magnetic structure ("octupole") inside the star, giving rise to the four surface toroidal magnetic structure through the interaction with differential rotation.

3.4. Degenerate Stars, White Dwarfs (~ 2000 km) (~ 10^6 Gauss)

A breakdown of classical theory is expected. A moving electron must spiral around a magnetic field line in a circle with radius r_L; the stronger *B* is, the smaller r_L is. The classical electromagnetic theory breaks down at small scales $r_L \sim 10^{-9}$ m, where quantum electromagnetic theory takes over. This occurs at a magnetic field strength $B_t > 10^7$ Gauss, where r_L can take only certain definite quantized values. In ordinary classical conditions, a small external *B* does not affect the internal structure of an atom. But when immersed in a high external *B*, the electronic orbits around atomic nuclei become very oblate ellipses. The study of magnetic field > 10^7 Gauss is a relatively new area of physics, and it is difficult to create such magnetic fields in terrestrial laboratories, so the astronomical research on dwarfs and pulsars having huge magnetic fields may continue to inspire physicists for a while.

A dipolar magnetic field shape can be seen also in some degenerate stars.

Several white dwarf stars have a dipolar magnetic field strength ~ 10^7 Gauss and a mean gas density ~ 10^{31} cm^{-3} (e.g., Fig. 9.8 in Shi-Hui 1994), but most white dwarfs may have a smaller field strength $\leq 10^6$ Gauss and a radius ~ 2000 km. Dwarfs have exhausted their nuclear-burning fuels, and they contract until gravity is balanced by the pressure of degenerate electrons.

Degenerate objects such as white dwarfs and neutron stars have highly conducting degenerate matter and do not require dynamo action to sustain their magnetic fields, and their magnetic fields have very long decay times. Thus a "fossil" magnetic field is predicted.

3.5. Neutron Stars (~ 10 km)

When immersed in a strong magnetic field $B \geq 10^{12}$ Gauss, the atom takes a cigar-shaped structure, since the Coulomb force becomes more effective for binding electrons in the direction parallel to the magnetic field axis while the electrons are extremely confined in the direction transverse to the magnetic field axis. Using the atomic unit $a_0 = 0.5 \times 10^{-10}$ m, one finds that the mean transverse separation of the electron and proton in the hydrogen atom is $L \sim [2m + 1]^{0.5} / [426\, B_{12}]^{0.5}$ atomic units, where $m = 0, 1, 2, 3, ...$, and where B_{12} is the magnetic field in units of 10^{12} Gauss. The ionization energy of the atom becomes $E_H = 161$ eV for $B_{12} = 1$ and rises as $E_H \approx 161\, [\ln(426 B_{12}) / \ln(426)]^2$ eV (e.g., Lai & Salpeter 1997).

3.5.1. *Normal Pulsars (~ 10^{12} Gauss)*

When a normal star with radius $R \sim 10^6$ km collapses to form a rotating neutron star or pulsar with radius ~ 10 km, the magnetic flux B will be conserved ($B \sim R^{-2}$) and the surface magnetic field will increase from ~ 100 Gauss to ~ 10^{12} Gauss. A previously dipolar shaped magnetic field will remain dipolar shaped. The magnetic field shape of pulsars is generally dipolar, and a magnetosphere is created around the pulsar (e.g., Radhakrishnan & Cooke 1969; Navarro et al. 1997). Neutron stars typically have a gas density decreasing from 10^{42} cm^{-3} at the center to 10^{12} cm^{-3} at the surface.

The data for normal pulsars are consistent with some kind of *passive frozen-in* magnetic dipole, of strength ~ 10^{24} Gauss m^3. The radius of a normal pulsar is ~ 10 km, with a mass ~ 1 solar mass, and a rotation period ~ 0.1 sec, giving an angular momentum ~ 5×10^{39} kg. m^2 s^{-1} (not far from the dipolar dynamo law for other bodies).

The basic radio emission process is essentially the same in millisecond-period pulsars and in slower pulsars. The nearby ~ 100 pc PSR J0437-4715 pulsar has a 5.8 millisecond period, a characteristic age of 2.5×10^{10} years, and a dipole magnetic field of 2×10^8 Gauss. This pulsar shows evidence of inertial dragging of its magnetic field lines in the outer magnetosphere, with the low frequency radio emission coming from higher altitudes in the pulsar magnetosphere (e.g., Navarro et al. 1997).

In recent models, the pulsar magnetosphere is divided into closed magnetic field lines (where particles are trapped for long periods of time) and open magnetic field lines (where particles are not confined and are eventually lost to the interstellar medium). In addition, recent models have added a secondary magnetospheric shell, having 1% of the number of particles in the primary shell (e.g., Fig. 4 in Eastlund et al. 1997).

The time evolution of the magnetic field with time in a pulsar is still controversial, a major issue in compact object astrophysics. While some theories favor no magnetic field decay over a long time (e.g., Romani 1990), most theories favor a magnetic field decay of some sort (e.g., Wang 1997). In the decay theories, the pulsar's evolution is divided into three phases: (i) the dipole phase, in which the pulsar spins down through magnetic dipole radiation, ending when the ambient material's ram pressure overcomes the pulsar's wind pressure; (ii) the propeller phase, in which ambient material fills the corotating magnetosphere in a shell above the Alfvénic radius, ending when the shrinking Alfvénic radius becomes smaller than the corotation radius; (iii) the accretion phase, in which the matter accretes directly on the polar cap of the neutron star. In the first (dipolar) and second (propeller) phases, the magnetic field decays either as a law

$$B = B_0 \cdot [1 + (t/t_d)]^{-1} \qquad \text{or else} \qquad B = B_0 \exp(-t/t_d),$$

with $t_d \approx 10^8$ years, and $B_0 \approx 10^{12}$ Gauss. In the third (accretion) phase, there is no magnetic field decay and the field strength remains steady. The 8.4-second pulsar RX J0720.4-3125 may be in the third or accretion phase (e.g., fig. 1 in Wang 1997).

Mukherjee & Kembhavi (1997) used statistics to obtain a lower limit on the decay timescale of pulsar magnetic fields (> 160 millions years).

The distance to a pulsar is best determined when one uses a detailed model of the distribution of free electrons in the disk of the Galaxy. Taylor & Cordes (1993) have provided such a distribution model, with electron density enhancements in four spiral arms and near the Gum nebula (their equ. 11 and Fig. 1, using a value of 8.5 kpc for the Sun-Galactic Center distance). From the electron density distribution, one can compute the plasma frequency and the group velocity at which a radio signal at a frequency ν can propagate in the interstellar medium. Comparing time arrivals at two or more frequencies, yields the dispersion measure DM, an integral of the free electron density over the distance to the pulsar. Thus the observed DM and the use of the distribution model for the free electrons will yield the pulsar distance, to an accuracy of 25%.

3.5.2. *Magnetars (~ 10^{15} Gauss)*

Extreme pulsars are called magnetars. They typically have a dipolar magnetic field strength ~ 10^{15} Gauss and a mean gas density ~ 10^{40} cm^{-3} (e.g., Thompson & Duncan 1996; Frail et al. 1997). The data for extreme pulsars (magnetars) are consistent with some kind of *passive frozen-in* crustal magnetic dipole, of strength ~ 10^{27} Gauss m^3. The radius of an extreme pulsar is ~ 10 km. Rotating with a period of a few seconds, with a mass ~ 1.4 solar masses, magnetars have an angular momentum ~ 10^{38} kg m^2 s^{-1}. When a magnetic field stronger than 1 - ^{14} Gauss is dragged through the pulsar crust by the diffusive motions in the pulsar core, Hall turbulence is excited and leads to multiple fractures tha will release enough energy to power soft gamma ray bursts.

The physical upper limit to the neutron star's magnetic field strength is the virial equilibrium value ~ 10^{18} Gauss (Lai & Salpeter, 1997).

4. CIRCUMSTELLAR MAGNETIC FIELDS (OUT TO ~ 200 AU; ~ 10^{-3} PC)

Complex polarimeters have been designed for optical and near-infrared polarimetry. Many involve a combination of half-wave and quarter-wave plates, polarizers, analysers, retarders, prisms, and collimating lenses. Various types of optical polarimeters have been described by Serkowski (1974).

Evocative names have started to appear, such as "Beauty (computer section) and the Beast (polarimeter section)" (Manset & Bastien 1995), "TNTCAM" = Ten aNd Twenty micron CAMera (Klebe et al. 1996), "PIREX" =Polarimetric InfraRed EXplorer (Clemens 1996).

4.1. Cataclysmic Binary Objects (~ 10^5 km) (~ 10^6 Gauss) and Polars (~ 6×10^7 Gauss)

Cataclysmic variable objects consist of two stars orbiting each other in a few hours up to a few days. The primary star is a white dwarf star. The secondary could be a red dwarf star. Mass transfer occurs, from the extended secondary star to the environment of the smaller primary white dwarf.

In some cataclysmic variables, magnetic fields from the white dwarf star then guide the mass transfer through funnels of gas, toward shocked accretion sites on the stellar surface of the white dwarf star (e.g., Wickramasinghe 1988). The size of the overall system is about 60 white dwarf radii, or 1×10^5 km, and the circumstellar magnetic field is about 10^6 Gauss.

In other cataclysmic variables, the mass transfer falls first onto an accretion disk around the white dwarf, and later joins the white dwarf itself (e.g., Lamb & Melia 1988). These binary star accretion disks are considered to be thin, and are fed by a stream of gas originating from the secondary star. To remove excess angular momentum, disk magnetic fields have been proposed. Small-scale "magnetic cells" in the disk have been envisioned, as well as a large-scale poloidal field; both may require a disk dynamo (e.g., ch. 11 in Campbell 1997).

"Polars" are defined as two stars in a closed binary system, one being a red *M* dwarf secondary and the other being a white dwarf primary, with the white dwarf having an accretion disk and a strong magnetic field which can range from ~ 10 million Gauss up to 230 million Gauss, with an average near 60 million Gauss. They are also called AM Herculis-type binaries (e.g., Burwitz et al. 1997). Polars are thus high-magnetic field cataclysmic variables.

4.2. Late-type Variable Giant Stars (~ 10^8 km), Young Stars

Variations in optical and radio emission of old red giant stars (size ~ 10^8 km) have been found. Mechanisms for such variations could involve radial pulsations and asymmetric dust distributions. Other less likely mechanisms of variability for red giant variable stars could involve magnetic fields, analogous to the solar activity cycle - however, the convection zones are extremely deep and the rotation rate slow, so a convective dynamo is unlikely to produce a significant surface magnetic field (Willson, 1988).

The polarization properties of young stars, including T-Tauri stars and young near IR stellar objects, has been reviewed by Bastien (1988). He found that models with dust aligned by magnetic fields have severe problems, while dust scattering models have little or no problems. These optical and near IR observations would say nothing on the magnetic fields there.

Observations of huge late-type supergiant stars, such as Rigel with a radius ~ 9×10^7 km, have shown absorption components in the Hα spectral line. The absorption components vary in time and wavelength, suggestive of stellar rotation and of a large "magnetic loop" (~ 1×10^8 km) in the corona near the equator, with coronal gas density ~ 5×10^{11} cm^{-3} and magnetic field B ~ 10 Gauss, and with photospheric surface gas density ~ 5×10^{12} cm^{-3} and magnetic field B ~ 25 Gauss (Israelian et al. 1997). Thus Rigel has an inhomogeneous circumstellar envelope with localized magnetic fields similar (but with larger sizes) to the dipolar magnetic regions near the equator of our Sun.

4.3. Double Stars and Symbiotic Stars (~ 10^{10} km; ~ 10^{-3} pc)

Binary (double-star) systems hold important clues to stellar magnetism. RS Canum Venaticorum shows optical light variations which differ from the orbital period, thus implying the presence of starspots and associated magnetic fields on one star of this system. Others show the presence of polarized radio emission from synchrotron electrons trapped in a magnetic field. The presence of a strong magnetic field in a close binary system can modify the standard structure of the system.

Symbiotic stars are interacting binary stars, with an orbital period of years to decades. One of the two stars in interaction is a late-type red giant star or a Mira variable star, emitting a stellar wind that goes around the system (circumbinary gas). The other star in the interaction is a source of ionization for a circumbinary wind. Typical values for the circumstellar gas are: electron density n ~ 10^7 cm^{-3}, electron temperature ~ 15000 K, dust temperature ~ 460 K, size ~ 100 AU ($\approx 1.5 \times 10^{10}$ km), so the

nebular mass ~ 10^{-6} $M_\odot$ (Schulte-Ladbeck 1988). Significant mass loss is occurring from the red giant star, with a portion of that neutral gas being ionized by a hot star somewhere in the wind - there is radio emission from the ionized gas (Seaquist et al. 1984). Here most of the variation in intensity and polarization may be due to asymmetric mass loss and asymmetric dust distribution and dust/molecule scattering (Moffat 1988), not to aligned dust in magnetic fields.

4.4. Masers at Centimeter and Millimeter Wavelengths (~ 10^9 km; ~ 10^{-4} parsec)

Masers are small regions located in the compressed shell between the shock front and the ionization front around an expanding object in a star formation site. A pump mechanism is required to start and maintain the maser activity (Elitzur 1982; Elitzur 1992). Circumstellar masers are important signs indicating the late stages of stellar evolution, associated with stellar mass loss. Maser stars are often (i) Mira variables or semi-regular variables in the process of becoming planetary nebulae, or (ii) supergiant stars on their way to becoming Wolf-Rayet stars or supernovae.

Magnetic fields in masers or hot spots can be measured by the Zeeman method. Zeeman splitting at centimeter and millimeter wavelengths, acting on *circularly* polarized radiation emitted by neutral molecules (SiO, H_2O), allows the study of magnetic fields on substellar hot spots at high thermal gas densities and small sizes (< 1 pc). Here the line splitting in frequency is proportional to the strength of the *B*-vector component parallel to the line-of-sight.

4.4.1. *SiO masers (~ 10 Gauss)*

SiO masers typically have a gas density ~ 10^{12} cm^{-3}, a size ~ 3×10^8 km ~ 10^{-5} pc, and a magnetic field ~ 40 Gauss (e.g., Barvainis et al. 1987).

One of the best known SiO maser lines is at 43 GHz (λ7.0 mm). Maser images show in each case that maser spots lie in a ring of ~ 3 stellar radii in the extended atmosphere of the associated star, inside the dust-formation region. The ring structure suggests an ordered outflow (e.g., Cohen 1997b).

In one important model of SiO masers, the maser polarization depends on the geometric relation between the magnetic field direction and the propagation direction. Pumping is mainly by collisions. The circular polarization is generated by a large 10-100 Gauss magnetic field (e.g., McIntosh & Predmore 1996). Observed narrow maser lines are not saturated, in support of this model and in contrast to saturation models with radiative pumping (e.g., Nedohula & Watson 1994).

Advances in very long baseline interferometry (VLBI) now allow polarimetric imaging of the SiO masers in the extended atmosphere of late-type stars. Radio images made at 43 GHz (λ7 mm) of the Mira variable TX Cam located at 317 pc show an orderly magnetic field over the shell with diameter ~ 10 AU. A tangential polarization structure around the shell, with a mean magnetic field strength of 5 to 10 Gauss, is indicative of a global poloidal magnetic field in the shell (Kemball & Diamond 1997).

4.4.2. *H_2O masers (~ 0.1 Gauss)*

H_2O masers typically have a gas density ~ 10^{10} cm^{-3}, a size ~ 3×10^9 km ~ 10^{-4} pc, and a magnetic field ~ 100 milliGauss (e.g., Fiebig & Gusten 1989).

One of the best known H_2O maser lines is at 22 GHz (λ1.3 cm), and others reach all the way to 658 GHz (λ456 μm).

In Sagittarius B2, the twenty H_2O maser features in the middle area exhibit an increase in velocity with an increasing angular distance from the center, suggesting that the features are located in/near an expanding envelope which has a radial velocity gradient (e.g., Elmegreen et al. 1980).

4.4.3. *OH masers (~ 10^{-3} Gauss)*

OH masers typically have a gas density ~ 10^7 cm^{-3}, a size ~ 3×10^{10} km ~ 10^{-3} pc, and a magnetic field ~ 4 milliGauss (e.g., Bloemhof et al. 1992).

OH masers in starforming regions are pumped radiatively by the strong far IR radiation from the dust near the HII region. Two peaks are observed in a typical maser line near the shell center at 1612 MHz (λ18.6 cm), characteristic of an expanding shell (the peak separation indicates twice the shell expansion velocity).

A radio image of an expanding HII shell and of its increasing angular diameter across the line of sight can be combined with the maser's expansion velocity along the line of sight to give an estimate of the distance to the shell (with an accuracy of 5%). The picture that is emerging from proper motion studies of masers is that of clumpy mass loss, with discrete maser cloudlets moving through relatively stationary regions where maser action is excited (Cohen, 1997b).

OH masers at 1720 MHz (λ17.4 cm) in supernova remnants are pumped collisionnally by the H_2 molecules in the postshocked gas just inside the remnant edges. Typical gas density ~ 3×10^5 cm^{-3}, kinetic temperature ~ 80°, and magnetic field ~ 0.2 milliGauss are found in three nearby SNR shells (e.g., Claussen et al. 1997). For these SNR masers, the path of maximum amplification occurs when the acceleration from the shock is transverse to the line of sight - it is along this direction that the velocity gradient is small and the largest coherent path length large.

4.5. Circumstellar Gas (out to ~ 3×10^{10} km; ~ 0.001 pc)

Here we take a circumstellar gas to mean gas located close to a star, closer than in a young protostellar nebula. Hence we shall take as circumstellar objects those stellar-powered nebula with an envelope extending up to 200 AU or so (~ 3×10^{10} km; ~ 0.001 pc).

Young Stellar Objects (YSO) are usually low-mass stars, such as T Tauri stars or Herbig Ae/Be stars, usually visible at optical wavelengths and the near infrared, showing variable linear polarization (e.g., Bastien 1996). The time variations may be due to binarity (two stars), spots on a rotating stellar surface, orbiting dust condensations, comet-like activity (e.g., Bastien 1996). The earlier interpretation with a model involving the alignment of grains by a magnetic field is no longer valid, and *nothing can be said about the magnetic fields* there from these data at optical and near infared wavelengths.

More detailed optical polarization maps show (i) a small pattern of linearly aligned vectors close to the central source, due to multiple scattering by dust in a central disk, (ii) an extended centrosymmetric pattern, suggesting single scattering of light by dust in an envelope, and (iii) two null points in polarization, located at the transition between the linearly aligned vectors (i) and the centrosymmetric vectors (ii).

Fischer et al. (1994) studied theoretical models of dust scattering around young starforming objects without magnetic fields, and found that (i) grains in the inner regions of the dust disk (optically thick) give *E*-vectors of polarization aligned parallel to the disk plane; (ii) grains in the outer regions of dust disk (optically thin) and in the surrounding envelope/lobe around the disk (optically thin) give *E*-vectors of polarization with a centro-symmetric polarization pattern around the center of the object.

The apparent polarization disk is much larger than the true, centrifugally supported "planetary range" or "accretion disk" $\leq$ 200 AU (~ 3×10^{10} km; 0.001 pc). Dust and gas beyond 200 AU may not be centrifugally supported but may be infalling toward the center.

5. METHODOLOGY AND INSTRUMENTATION FOR PROTOSTELLAR AND INTERSTELLAR DETECTION

5.1. Basic detection concepts at Radio, Extreme IR, Far IR, and Mid IR Wavelengths

How can we detect from Earth the distant interstellar magnetic fields ? Special particles affected by the magnetic field near them will emit a tell-tale polarized signal which we can capture on Earth. Thus by rotating a polarimeter attached to a radio telescope on Earth, we can detect this tell-tale polarized signal.

Figure 7 shows that high-energy relativistic electrons are trapped inside magnetic flux tubes or magnetic pipelines, in which the electrically-charged particles can glide along the lines by spiralling around them. While spiralling, they emit a synchrotron radio wave with its *E*-vector polarized in a direction perpendicular to the magnetic flux tube, and it is often emitted strongly at centimeter and meter wavelengths.

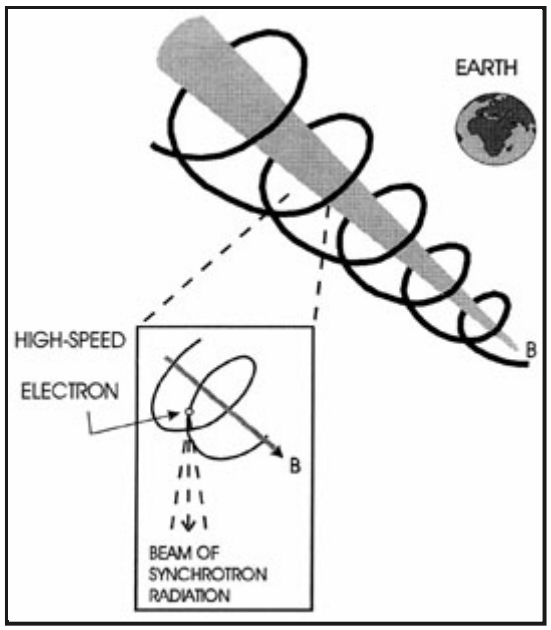

Figure 7. High-energy relativistic electrons are trapped by a magnetic field and forced to orbit around the field line. A plaintive synchrotron (non-thermal) signal from a trapped relativistic electron is emitted strongly at meter and centimeter wavelengths.

Figure 8 shows dust grains trapped and aligned by a magnetic field. Dust grains do emit a thermal continuum emission. The needle-like grain turns end-over-end around its center, akin to a pirouette; here the grain's short axis of rotation is aligned along the magnetic field line as proposed by some grain alignment theories - other grain alignment theories predict the grain's long axis to be aligned along the magnetic field line (e.g., Lazarian et al. 1997). The grain emits primarily in the plane of the rotation/pirouette, and its *E*-vector emission is polarized in a direction parallel to the grain's long axis, hence here perpendicular to the magnetic field lines. The signal is emitted strongly at Extreme IR wavelengths and at Far Infrared wavelengths.

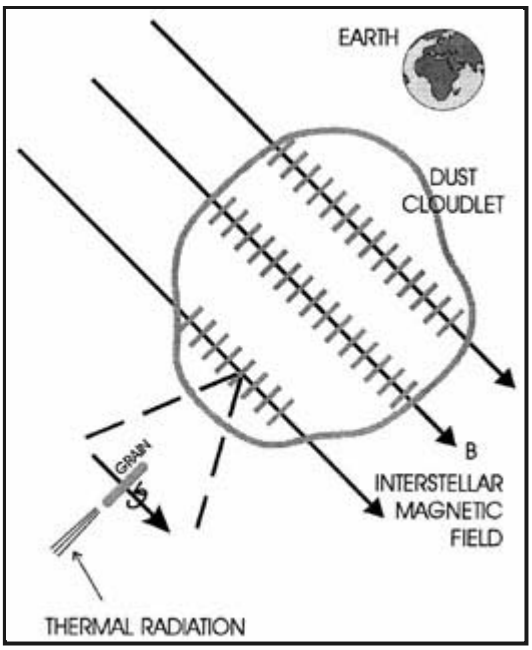

Figure 8. Elongated dust grains are aligned by an ambient magnetic field and forced to spin around the field line. A plaintive (thermal) signal from a trapped dust grain is emitted strongly at millimeter and submillimeter wavelengths.

Original unpolarized background *optical* stellar light is mostly *absorbed* by dust if the photon's *E*-vector is in the plane of the grain's long axis, and mostly transmitted if the photon's *E*-vector is in the plane of the grain's short axis, so at optical and near Infrared wavelengths we observe more optical photons with their *E*-vectors *parallel* to the ambient magnetic field lines.

Expressing the Planck function in the optically thin régime, one gets

$$S_\nu = 2h\nu^3 c^{-2}[e^{[h\nu/kT]} - 1]^{-1}\Omega\tau,$$

where Ω in steradians is the solid angle of the source as seen from the Earth, *h* is the Planck constant, and *c* is the speed of light and τ is the "optical" depth at frequency ν, where

$$\tau = 2.55 \times 10^{-24}[Q_\lambda a^{-1}\rho^{-1}](M_d/M_g)N_{H_2},$$

with Q_λ is the grain emissivity, *a* in cm is the grain radius, ρ in g cm^{-3} is the grain density, M_d / $M_g \approx 0.01$ is the dust mass to grain mass in a cubic centimeter, and N_{H_2} in cm^{-2} is the column density of molecular hydrogen, and $Q_\lambda = 3.8 \times 10^{-4}[250 / \lambda]^2$, with λ in microns.

Hildebrand (1983) has reviewed the derivation of dust characteristics and cloudlet masses from submillimeter/Extreme IR thermal emission, independent of grain models. He found that the dust mass $M_d = (4/3)[a\ \rho / Q_\nu][S_\nu\ D^2 / B_{\nu,T}]$, where S_ν is the flux density at frequency ν, *D* is the distance from the Earth to the source, $B_{\nu,T}$ is the Plank function with frequency ν and temperature *T*, Q_ν is the grain emissivity at frequency ν, $a \approx 0.1\ \mu$m is the grain radius, ρ is the grain density. Typically the value $a\rho \sim 2.8 \times 10^{-5}$ g cm^{-2}, and the value $(4/3)[a\rho / Q_\nu] \sim 0.1$ g cm^{-2}, at $\lambda = 250\ \mu$m. Hence one derives:

$$[M_g/M_\odot] = [S_\nu/\mathrm{Jy}][D/\mathrm{kpc}]^2[e^{47.1\nu/T} - 1]\nu^{-5}/21.1$$

where ν is in TeraHertz and *T* is the dust temperature (e.g., Little et al. 1990). For an early review, see Heiles et al. (1991).

In addition, the first detection of a *linearly* polarized (non-masing) molecular line has been obtained with the 15m James Clerk Maxwell Telescope (JCMT) in CO 2-1 (230 GHz, λ1300 microns) (e.g., Greaves et al. 1996). This is a potentially useful probe

of magnetic field as predicted earlier (e.g., Kylafis 1983). Here the percentage of linear polarization reaches a maximum for an 'optical' depth near 1 but it does not depend on the strength of the magnetic field. Also, the polarization position angle can be independent of the magnetic field direction (for a weak magnetic field) or else either parallel or pendicular to the magnetic field direction (for a strong magnetic field >> 1 microGauss). Glenn et al. (1997b) also detected ~ 0.8% linear polarization at PA ~ -70° in CS 2-1 (near λ3000 μm), but attributed this amount of polarization entirely to the elongation of the envelope of the giant branch star IRC+102216; they also claimed that the magnetic field there is either negligible or else is weak (<< 2 mGauss) and radially directed by the stellar wind.

5.2. Instrumentation at Long Infrared Wavelengths

5.2.1. *Mid-InfraRed/Far InfraRed Wavelengths*

Long Infrared wavelengths start in the Mid-IR (~ λ10 μm), cover the Far-IR (~ λ100 μm) and eventually extend to the Extreme-IR (~ λ1000 μm; submillimeter) wavelengths.

The first Mid-IR imaging polarimeter in the world, called NIMPOL, has recently been commissioned on the 3.9m Anglo Australian Telescope, and very limited observational results include the Galactic Center and η Carinae (Smith et al. 1997). The preliminary dust emission data show that the magnetic fields are going parallel to the three main filamentary arms within 1 parsec of the Galactic Center (their Fig. 5), and that the magnetic fields are doing a figure-8 loop centered on the accretion disk of the η Carinae nebula (their Figure 6).

The first observations in Far-IR polarimetry was made by Harwitt and his students in the late 1970's, toward the BN/KL object in Orion (e.g., Hildebrand 1996).

Hildebrand et al. (1995) found measurable polarization > 1% in many clouds, but usually less than 10%. In many clouds, the polarization position angle stays relatively constant over the clouds. The maximum polarization decreases with increasing 'optical' depth more rapidly than expected due to opacity alone, suggestive of additional factors (grain properties, grain alignment, inclination of magnetic field, unpolarized clumps). Davidson et al. (1995) found that the observed magnetic field in OMC1 could be due to a simple compression of an external large scale magnetic field, where the contraction of the cloud was predominently along the direction of the large scale magnetic field lines, and that the estimated strength of the magnetic field was strong enough ~ 3 m Gauss to have severely decreased the star formation rate in OMC1, by preventing gravitational collapse and by preventing the [nearby] HII region from more severely compressing the molecular cloud.

In the long IR régime, absorption by dust scattering becomes weaker at all the longer wavelengths, since scattering varies with the wavelength λ as λ^{-4} (e.g., Tamura et al. 1988; Bhatt & Jain 1992). Thus there is no significant absorption by dust scattering at Far IR and Extreme IR, as well as at millimeter wavelengths. Goodman (1995) argues in favor of Far IR and Extreme IR polarimetry (aligned dust emission) and against background starlight optical polarimetry, in order to map the magnetic field inside dense regions of the interstellar medium, because the physical size and type of grains inside dense clouds or clumps (larger, rounder on average, fluffier) are different than those outside clumps (smaller, more elongated on average).

5.2.2. *Submillimeter/Extreme InfraRed wavelengths*

In the long IR, emission by thermal radiation from dust particles becomes stronger from Extreme-IR to Far-IR wavelengths (flux density proportional to λ^{-4}). This emission allows the study of magnetic fields in objects of moderate thermal gas densities. Lazarian et al. (1997) claim that far-IR emission polarimetry selects warm grains near young massive stars, and these grains are in an environment far from equilibrium, possibly rotating suprathermally because of radiative torques from stellar photons.

The first successful observations of polarization in the submillimeter/Extreme IR régime was made by Murray (1991), Flett & Murray (1991), with the JCMT in Hawaii at 450 μ, 800 μm, and 1100 μm.

At submillimeter wavelengths, the instruments are as follows. (1) A few polarimetric observations have been done near 100 μm, with the Kuiper Airborne Observatory's Stokes polarimeter until 1996, with a nominal resolution of 35" (e.g., Davidson et al. 1995; Hildebrand et al. 1995; Goodman 1995). (2) The 15-m JCMT on Mauna Kea in Hawaii offers polarimetry at 450, 800, and 1300 microns (the old Aberdeen/QMW polarimeter was used from 1990 to 1996; it has been replaced with the SCUBAPOL in 1998). (3) The 10-m CalTech Submillimeter Observatory in Hawaii has recently used the Hertz submillimeter polarimeter, (e.g., Schleuning et al. 1997). (4) A polarimeter for the SOFIA (replacing the KAO plane) is being planned, and the telescope should start around 2002. It is optimized for 70 μmeters, although flight times will be limited so only moderately bright sources will be observable. (5) A BOL polarimeter is being planned for the Far InfraRed and Submillimeter Telescope (FIRST), to be launched in space around 2005. It is optimized for 250, 350 and 500 μmeters (Greaves et al. 1997).

The few Far IR and Extreme IR polarimetric data so far available hint at a complex interplay between magnetic field directions and strengths and other large disk and cloudlet variables, such as self-gravity, turbulence, radiation field, and thermal instabilities. Efforts have been made to understand the patterns of the projected magnetic field directions associated with these objects, with limited success so far owing to the lack of a large polarization survey at Extreme Infrared (e.g., Myers 1991).

At present, there are few studies at far IR or extreme IR of the magnetic structures over a range of physical parameters, and they are biased towards regions with strong flux density values. Many of the present and future polarimetric programs aim to answer questions related to the magnetic field shape and directions in protostellar disks and interstellar cloudlets, by analysing the submm and mm emission from dust. Up to now, few polarimetric programs have run on submm telescopes, and new results are expected to add significantly to our knowledge.

Schleuning et al. (1997) made a 350 μm map of Orion OMC-1, finding that the percentage of polarization ranges from ~ 1% up to 7%, while the polarization angle is fairly the same across the map at ~ 30° (East of North). A 'polarization hole' (lower percentage of polarization) is seen at the peak of the total intensity emission (Stokes I).

5.2.3. ***Millimeter/Radio wavelengths***

The first successful millimeter polarimetry was by Barvainis and his colleague in 1988 (e.g., Hildebrand 1996). At millimetric wavelengths, the instruments are as follows. (1) The portable Millipol instrument was used with the 12-m NRAO Kitt Peak telescope (Barvainis et al. 1988; Clemens et al. 1990), operating at 1.3 mm. (2) A Sapphire halfwave plate was attached to the FCRAO telescope (Novak et al. 1990) to operate at 1.3 mm wavelength. Both are owned by private groups (Millipol was built by a Boston-based group; the Sapphire half-wave plate was built by the Amherst-based group operating the 14m FCRAO telescope). (3) A polarimeter operating at 3000 microns at Kitt Peak has been provided for general use (e.g., Payne et al. 1993). (4) Polarimetry with an interferometer is also possible with the Owens Valley Array, which works at 1300 and 3000 microns.

Novak et al. (1990) found that the magnetic field near the bipolar outflow from the KL nebula in Orion is nearly parallel to the axis of the outflow. Cloud collapse is expected to occur along field lines, leading to a flattened gas disk; an outflow forming later in such a disk will expand more easily along the largest density gradient hence along the field lines. Barvainis et al. (1988) found at 1.3 mm wavelength a polarization percentasge near 3% in Orion, somewhat higher than the 2% found at 270 μm and 77 μm (but within the 2 rms error).

5.2.4. ***Typical Polarimetric Run***

Figure 9. The primary 15-meter diameter surface of the JCMT on Mauna Kea, one of the few large facility designed to opeate at Extreme InfraRed wavelengths. Also shown are the small secondary surface as supported by legs, and at right the windscreen.

Figure 9 shows, as an example, one of the radio telescopes in Hawaii. The JCMT is chosen here because it is the largest (15m) facility in the world specifically designed to operate at Extreme IR wavelengths, The primary 15-meter surface (bottom left) collects incoming photons from space coming through the huge windscreen (top right). The photons thus collected on the 15-m surface are first re-directed to the secondary surface (supported by the spider-like legs, at top right), where now the photons are bounced downward through the gaping hole in the 15-m surface (bottom center). Inside the hole below the primary surface, several instruments are located to detect these photons, to analyse their polarization properties, and to make recordings for future uses. The polarimeter there has a rotating half-wave plate inside, followed by a wire-grid analyser. Thus the intensity *I*, as seen at any position angle of the half-wave plate, is given by (e.g., Vallée & Bastien 1996):

$$I(\theta) = 0.5I(\mathrm{total}) + 0.5I(\mathrm{polar}) \cdot \cos(4\theta - 2\theta_{\mathrm{source}})$$

Rotating the wave plate angle θ through 360 degrees allows the detection of the unique angle θ_{source} where the emission is maximum. This unique direction θ_{source} is perpendicular to the direction of the magnetic field (perpendicular to the photon's polarization position angle θ_{source} of maximum intensity). For computing, one often uses a quantitative representation known as the Stokes parameters *I, Q, U, V*, where

$$2\theta_{\mathrm{source}} = \arctan[U/Q],\ I(\mathrm{polar}) = [Q^2 + U^2]^{0.5},$$

and *V* is the circular polarization. The Stokes parameters are linearly additive.

The observations of the polarization angle (PA) can provide a vital test of the model-predicted shape of the magnetic field. Let θ_{source} be the photon's electric vector, coming from an interstellar source. To see if the source's magnetic field *B* is parallel or perpendicular to the elongation of an object (a 90° difference), at a 5 r.m.s. level (i.e., r.m.s. = 90/5 = 18°), one only needs to integrate until the 'error in polarization position angle' $\Delta\ \theta_{\mathrm{source}}$ is ±18°. In general, the probability function for θ_{source} is approximatively gaussian and sharp-peaked, and the error in θ_{source} follows the polarization percentage p_{obs} according to the statistical law:

$$\Delta\theta_{source} = 28.6^{\circ}[p_{obs}/\Delta p_{pobs}]^{-1}.$$

Thus for $\Delta\theta_{source}$ = 18° , one needs to observe only long enough at the telescope until one reaches p_{obs} / Δp_{obs} = 1.6 (e.g., Greaves et al. 1995a; Greaves et al. 1995b; Greaves et al. 1994).

6. PREDICTED MAGNETIC FIELDS IN PROTOSTELLAR DISKS (OUT TO ~ 2000 AU OR SO; ~ 10^{-2} PARSEC) AND DENSE INTERSTELLAR STARFORMING CLOUDLETS (0.1 TO 1 PC)

6.1. Distinctions of sizes

There are some distinctions between protostellar disks and interstellar cloudlets. A protostellar object often has a flattened dense disk out to ≈ 50 - 100 AU *and* an *infalling* nebular envelope out to $r_e \approx$ 2000 AU (r_e = 1400 AU in Weintraub et al. 1992; $r_e \leq$ 2000 AU in Heyer et al. 1996; r_e = 1400 - 10000 AU in Whitney et al. 1997). Here 2000 AU ~ 3×10^{11} km ≈ 0.01 pc. Thus, a protostellar disk (0.001 - 0.01 pc) differs in size from a cloudlet (0.1 - 1 pc). Second, a protostellar disk will have exactly *one* protostar (emitting at IR wavelengths), while a cloudlet can have either none, *one*, or maybe two protostellar disks within a total size < 1 pc. Third, a cloudlet may have associated gas distributed (i) partly in a circumstellar envelope or shell < 200 AU, (ii) partly in a flat halo above and below a protostellar disk < 2000 AU, *and* (iii) partly in a slightly distant interstellar volume < 1 pc (weakly or not yet gravitationnally bound).

Below, these objects will be lumped together, since their small sizes fit completely inside a radio telescope beam (a 10 arcsec beam corresponds to a size of 0.05 pc at a nearby distance of 1 kpc; or a 0.5 pc size at a distance of 10 kpc).

6.2. Magnetic Fields and Star Formation Onsets

6.2.1. *Spontaneous processes*

As reviewed in Elmegreen (1998), spontaneous processes probably dominate the onset of star formation on a galactic scale, but triggered star formation processes sustain, amplify and disperse what large-scale instabilities begin. Triggers include (i) direct compression of clouds (a 3-dimensional squeezing), (ii) collection and compression of clouds at the edges of HII regions or supernovae or giant rings and shells in galaxy disks (a 2-dimensional push), and (iii) cloudlet-cloudlet collisions and cloud-cloud collisions (2-dimensional effect with possible lateral squirting).

6.2.2. *Cloudlet Collisions*

Theoretical models of cloudlet collisions with magnetic fields are in their infancy (e.g., Elmegreen 1998). Small cloudlets in inelastic collisions may coalesce to form larger cloudlets. A sufficiently massive cloudlet (= clump by now) may then undergo a gravitational collapse. Globally, the large gas compression following many inelastic collisions might enhance the star formation rate. Cloudlet-cloudlet collisions have been discussed theoretically as strong collisions (such as with magnetic tangling) or as weak collisions (such as with magnetic oscillation) (e.g., Elmegreen 1988). The morphology of the cloudlets after collisions is strongly dependent on both the presence of a magnetic field and the elasticity defined as the ratio of the final to the initial kinetic energy of the cloudlets (e.g., Ricotti et al. 1997). Stone (1970a , 1970b) has identified three main evolutionary stages (compression, expansion and lateral outflow, collapse). The presence of a magnetic field parallel to the shock front between two clouds will lower the compression of the postshock gas, decrease the dissipation energy, increase the elasticity of the collision, and prevent the shattering of the clouds (Ricotti et al. 1997). In the magnetized collision case, Elmegreen (1985) has shown that energy dissipation by Alfvén wave radiation can be important at least for some clouds.

Observationally, cloudlet-cloudlet collisions have been categorized with a *12-point observational test* for their easy recognition (see Table 3 in Vallée, 1995b). The application of the 12-point test, made for the observations of the cloud collision giving rise to the infrared source IRAS 2306+1451, supports the collision model of Stone (1970a, 1970b).

6.3. Collapse models

6.3.1. *Simple collapse models*

Earlier reviews of the theoretical status of our knowledge on protostellar disk magnetic fields, with some applications to observations, are summarized below.

Galli (1995) used a theoretical size for a protostellar disk as characterized by a radius defined as the radius inside which infalling gas lands on its equatorial plane:

$$r_{\rm disk}/{\rm AU} = 600[B_{\rm initial}/30\mu{\rm Gauss}]^{4/3}[{\rm sound\ speed}/0.35{\rm km\ s^{-1}}]^{-1/3}[{\rm time}/10^5{\rm years}]^{7/3}$$

A radius of 600 AU corresponds to 0.003 pc. Many protostellar disks with gas density 10^6 to 10^7 cm^{-3} may have a magnetic field strength around 1 to 10 milliGauss.

Pudritz (1986) thus envisioned the magnetic fields in starforming cloudlets to be oriented parallel to the direction of the twin bipolar outflows (be it molecular or ionized), and suggested a picture where magnetic fields could dominate all aspects of cloud dynamics. Rotating outflows, corotating with an underlying object, is probable evidence for a hydromagnetic wind mechanism. Only a strong magnetic field can force accelerating gas at large distances to corotate out to 20 disk radii.

Königl & Ruden (1993) thus discuss the possibility that a significant magnetic flux is carried by the inflowing matter onto a protodisk, removing some of the angular momentum of the accreted matter. They pointed to meteoritic evidence for a ~ 1 Gauss magnetic field at a distance of 3 AU from the center of the early protosolar nebula. The young protostellar object itself could then develop a stronger magnetic field by dynamo action when it becomes convective. Magnetic braking of the stellar rotation could ensue, as well as disruption of the circumstellar disk out to a few stellar radii. Magnetic driving is proposed as the mechanism for launching the high-momentum neutral winds that give rise to the bipolar molecular lobes outside the disk.

Shu et al. (1987) discussed, among other things, the relative importance of turbulence versus magnetic field pressure in starforming cloudlets. The observed well ordered alignment of magnetic fields over the dimensions of cloudlets demonstrates that turbulence cannot be totally dominant over magnetic fields. Otherwise, a more tangled field configuration would result. Thus the observed turbulent motions are more probably wavelike than eddylike, and the magnetic field still has a well-defined mean direction. Their model favors a decoupling of the magnetic field from the gas density by ambipolar diffusion for gas density $n > 10^{11}$ cm^{-3} (e.g., their Equation 17). Recent observational data shows that significant magnetic flux loss is not seen at $n < 10^{12}$ cm^{-3} (e.g., Fig. 2 in Vallée 1995a).

6.3.2. *Complex Collapse Models*

Embedded disks are often needed by theories. Protostellar disks around protostars have dust, molecules, and magnetic fields inside, and protostars often (but not always) have a twin outflow (or twin jet) going away perpendicular to the protostellar disks (on both sides). These twin outflows/jets may be turned on or off by a 'magnetic switch', depending if gravitational forces dominate or not over magnetic forces in the hot tenuous corona close to the dense thin protostellar disk, i.e., if $B_{\rm corona}$ is above or below $[4\pi\, gas\ density]^{0.5}V_{\rm escape}$, (e.g., Meier et al. 1997). *Embedded disks* are also observed. In L1551-IRS5, a large diffuse elongated envelope or protostellar disk (~ 20000 AU, ~ 0.1 parsec) has been seen around a small dense protostellar disk (~ 1400 AU, ~ 0.01 parsec) at its center, both with the same orientations, with a twin outflow going away perpendicular to these disks (e.g., Tamura et al. 1995). In HL Tau, a diffuse protostellar disk (~ 4000 AU, ~ 0.02 parsec) has been seen around a very small dense protostellar disk (~ 100 AU, ~ 0.0004 parsec) at its center, both with the same orientations, with a twin outflow going away perpendicular to these disks (e.g., Tamura et al. 1995). The *tidal interaction between* a protostellar disk and a nearby massive companion has been modelled (without magnetic fields), predicting gaps in the protostellar disk and tidal truncation (e.g., Lin & Papaloizou 1993; Shu et al. 1993).

What is the spatial orientation of twin outflows with respect to the galactic plane? Some *pre main sequence* stars with outflows seem to have their outflow axis roughly perpendicular to the galactic plane (Cohen et al. 1984). Some *post main sequence* stars with outflows seem to have their outflow axis roughly parallel to the galactic plane (Phillips 1997). Various mechanisms have been suggested to explain this situation, including the influence of the galactic magnetic field. None of these seem entirely plausible (the galactic magnetic field energy density is 10^{-4} times that of the kinetic energy density of twin outflows). Since we are dealing with relatively few well-defined outflows, then we may have to wait for bigger statistical studies in these areas.

Molecular disks around protostars are threaded by magnetic fields. In most models, the interstellar magnetic field lines frozen in the large parent cloud are advected inward, either (i) early on during the gravitational collapse of the cloud core/center, or (ii) later on during the subsequent accretion to the disk around the core/center (Königl, 1995). Magnetic waves are expected inside molecular cloudlets. Carlberg and Pudritz (1990) thus predicted excited hydromagnetic waves, with large velocity differences between resolved clumps (clump size < 2000 AU) as material oscillates between vibrating magnetic field lines, and a velocity coherence with density as material accumulates at the wave nodes. Thi spredicted velocity coherence is not seen with HPBW from 0.2 pc out to 100 pc (e.g., Heyer et al. 1996), indicating that the magnetic field is not dominant.

6.4. Magnetic Disk Classes

There are various theories on magnetic field in dusty molecular disks around protostars, with different predictions for the

direction and strength of the magnetic field. *I* group them here into a simple classification of 'magnetic disk classes' - a simple classification scheme using (a) magnetic field shape, (b) the disk's thickness, and (c) nearby companion(s). Such a simple classification can be complexified later, i.e., by combining two classes along or across the line of sight, and by adding different shapes above and below the disk.

6.4.1. ***Magnetic Class I: B shape parallel to disk, thick disk, no companion***

Figure 10 shows a sketch of this magnetic class.

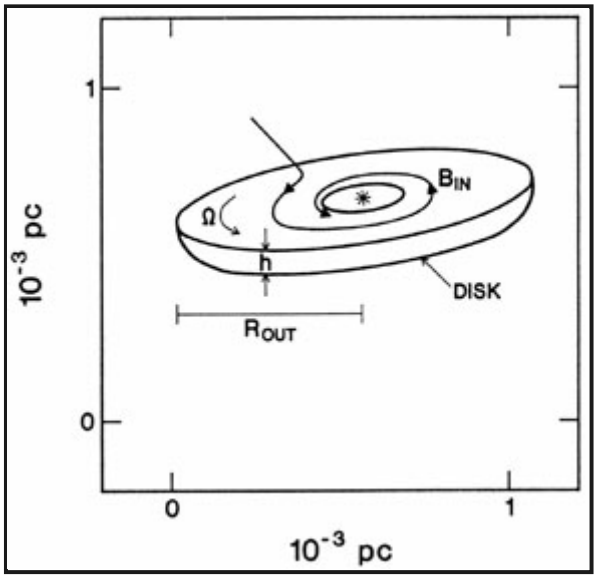

Figure 10. Magnetized molecular disk, with parallel *B* shape, thick disk (disk height/outer radius ~ 0.1). *B* lines are drawn into the disk by differential rotation. Adapted from Uchida & Shibata (1985).

The 'magnetic twist' model of Uchida and Shibata (1985) predicts a large scale poloidal magnetic field direction, that can be twisted by disk rotation to give a small scale *toroidal* magnetic field *parallel* to the disk major axis (their Fig. 2) to within 30 degrees. The theory of Uchida and Shibata (1985) also predicts a warm disk heated by magnetic field slippage (Joule heating), by adiabatic compression, and by stellar radiation, giving a disk temperature $T_{disk} = T_{corona} / 400$, which covers a wide range of hundreds of degrees K (after their Equ. 32 and their Fig. 6), with a minimum field strength B = 10 mG for a gas density $n \sim 10^7$ cm^{-3} and a maximum B = 100 G for a gas density 10^{13} cm^{-3} (after their Equ. 4).

A similar model uses a radial contraction of a rotating disk to twist the *B* field lines in the disk plane, with or without differential rotation in the disk (e.g., Fig. 6 in Kaifu et al. 1984). The 'dynamo' theory is another model (Stepinski & Levy 1990; Vishniac et al. 1990; Stepinski 1995) employing a *B* field direction parallel to the disk elongation, with substantial differential rotation in the disk. Here magnetic field amplitudes of 100 to 1000 Gauss are needed at the near edge of the disk, very much higher than expected from the submillimeter continuum observations and from the B vs n^k relation with k = 0.5.

The 'cored-apple' model or 'circulation' model of Henriksen & Valls-Gabaud (1994) uses a toroidal magnetic field in a disk, an empty outflow cavity with a poloidal magnetic field, and a tangled magnetic field elsewhere within a large sphere. With a large telescope beam, the net polarization would come from the *toroidal* magnetic field in the disk.

Inside the disk: what happens to the magnetic field lines (inside the width of the disk) ? Variations of the geometry of the magnetic field in the disk can be thought. Thus in the 'twist' model, while the magnetic field turns around the disk center, the magnetic field lines are undulating, going slightly below the middle plane of the disk and than going slightly above the middle plane of the disk, as discussed further in Hildebrand (1996).

Main model advantages: the submm radio power from the dusty protostellar disk should be large in this class; differential rotation in the disk is normally included, with its effect on the magnetic field; twin jets out of the disk center can be accommodated; model can be followed theoretically. Main model disadvantage: many protostellar disks have one or more nearby companions, possibly affecting the primary disk in some way (gravitational and magnetic).

6.4.2. ***Magnetic Class II : B shape parallel to the disk, thin disk, no companion***

Figure 11 shows a sketch of this magnetic class.

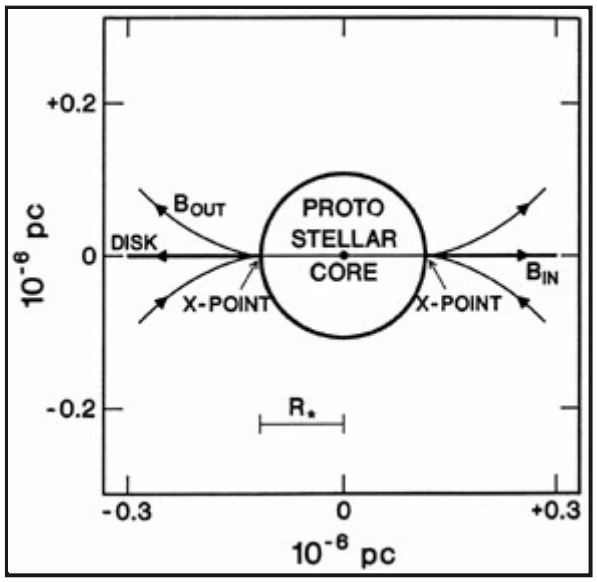

Figure 11. Magnetized molecular disk, with parallel *B* shape, thin disk (disk height/outer radius ~ 0.01). Adapted from Shu et al. (1988).

The theory of Shu et al. (1988) employs a magnetic field parallel to a very thin and long accretion disk (their Fig. 1), but the dust is not thick enough to emit much continuum radiation. Above the disk, the magnetic field lines are drawn outward by a centrifugally driven magnetic wind. In the disk, the magnetic field lines follow spirals aligned by differential rotation.

The thin disk model of Shu et al. (1997) could explain X-ray emission, notably during flares, due to interaction between an accretion disk and the magnetosphere of a central star, in the part of the disk closest to the star. Here in their modeled protostars, the gas density ~ 10^{10} cm^{-3}, the magnetic field ~ 1000 Gauss, X-ray flares have a magnetic loop size ~ 10^{7} km from the protostar, and these flares can heat the chondrules in the protodisk as well as release cosmic rays to bombard primitive rocks in the protodisk and induce short-lived radioactivities.

Main model advantages: differential rotation in the disk is normally included, with its effect on the magnetic field; model can be followed theoretically; twin jets out of the disk center can easily be accomodated by the central wind; can explain some characteristics of chondrules. Main model disadvantages: the submm radio power from the dusty protostellar disk should be small in this class; many protostellar disks have one or more nearby companions, possibly affecting the primary disk in some way (gravitational and magnetic).

6.4.3. ***Magnetic Class III : B shape perpendicular to the disk, thick disk, no companion***

Figure 12 shows a sketch of this magnetic class.

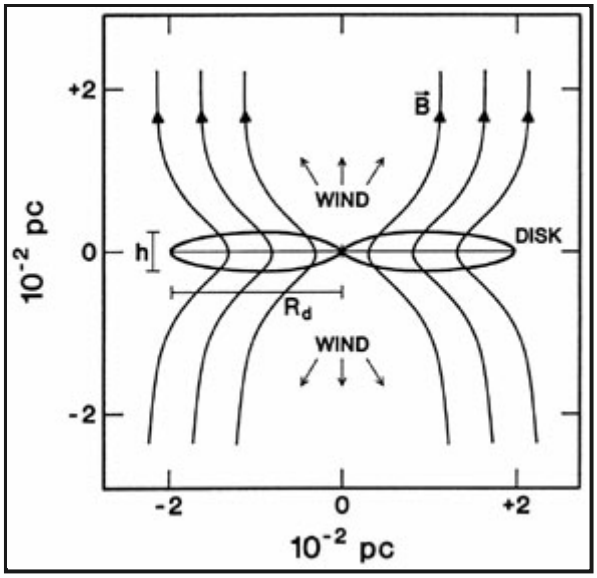

Figure 12. Magnetized molecular disk, with perpendicular *B* shape, thick disk (disk height/outer radius ~ 0.4). Adapted from Pudritz (1985) and Pudritz & Norman (1983).

The 'disk-wind' model of Pudritz and Norman (1983) predicts a *B* field direction in the disk's surroundings and in the disk to be perpendicular to the disk major axis (their Fig. 1) to within 30 degrees. The theory of Pudritz and Norman (1983) also predicts, among other things, a cool disk temperature covering a range in the tens of degrees K (their Equ. 4), with a *B* strength of about 1 milliGauss (after their Equ. 69).

A similar model uses a spherical disk collapsing in 1-dimension along the regional *B* lines to give a disk (e.g., Fig. 1 in Pudritz 1985; Fig. 1 in Pudritz and Silk 1987). The ambient/regional *B* field direction outside the disk is nearly parallel to the *B* field in the disk. Such a *B* structure is partially supported by polarimetric observations at 0.8mm wavelength by Minchin & Murray (1994).

The 'cloud-collapse' model of Holland et al. (1996, their Fig. 7) for high-mass sources predicts a poloidal magnetic field in two cases (original; slighly compressed field), and a toroidal magnetic field in one case (highly compressed field). There is no mention of an outflow in this model (but it is assumed to lie along the external magnetic field lines).

Off the disk: what happens to the magnetic field lines outside the disk ? Variations of the geometry of the magnetic field outside of the disk can be thought. Thus in the '*hourglass*' model the magnetic field lines start by stretching out radially away from the disk center, then go vertically away perpendicular to the disk. In the 'bulge' model the magnetic field lines start by concentrating towards the outflow axis, then go vertically away perpendicular to the disk. And in the 'torus' model, the magnetic field lines always go vertically away perpendicular from the disk. These models are discussed further in Hildebrand (1996).

Main model advantages: The submm radio power from the dusty protostellar disk should be large in this class; twin outflows out of the disk center can be accommodated; can be followed theoretically; can be adapted off the disk to the hourglass model. Main model disadvantages: differential rotation in the disk is not easily included, with its effect on the magnetic field; many protostellar disks have one or more nearby companions, possibly affecting the primary disk.

6.4.4. ***Magnetic Class IV: B shape perpendicular to the disk, thin disk, no companion***

Figure 13 shows a sketch of this class.

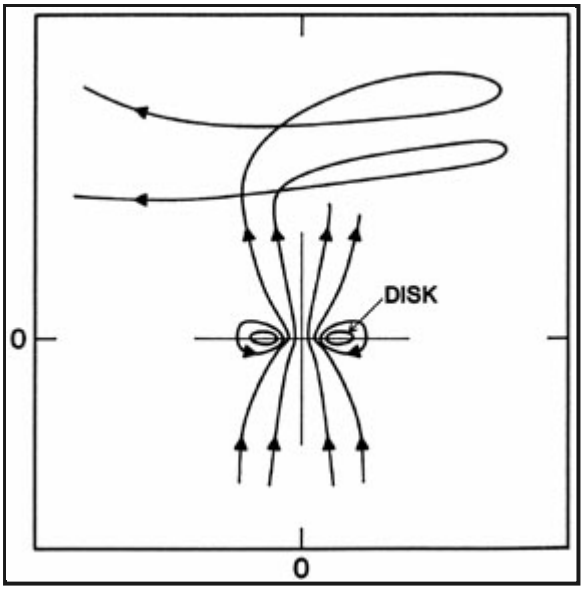

Figure 13. Magnetized molecular disk, with perpendicular *B* shape, thin disk (disk height/outer radius < 0.1). Here the distance scale is in arbitrary units. Adapted from Newman et al. (1992) and Lovelace et al. (1991).

The 'magnetic-pinch' models of Lovelace et al. (1991), Wang et al. (1990), and Newman et al. (1992) use a *B* field direction perpendicular to a thin accretion disk, with twisting of the *B* lines above and below the disk to drive a bipolar outflow. The bipolar flow and the disk are both very close to the star at the center, so it is unlikely that dust grains will survive in large quantity. The initial poloidal magnetic field could arise from dynamo processes in the protodisk. Differential rotation is included here. Super-Kleperian rotation of the gas at large radii is predicted for a strong magnetic field.

Warp stability has been studied by Lovelace & Zweibel (1997) in a cold, magnetically-supported ($\approx$ 50 μ Gauss), thin (minor/major axis $\approx$ 0.1), non-rotating, disk of size $\approx$ 0.1 parsec and mass ~ 1 solar mass, without a central protostar (preceding star formation). Differential rotation is not included here. They found the disks to be stable against thermal or dissipative instabilities, for magnetic fields strong enough to control the environment (gas density ~ 10^3 cm^{-3}).

Main model advantages: twin outflows out of the disk center can be easily accommodated; can be followed theoretically. Main model disadvantages: the submm radio power from the dusty protostellar disk should be small in this class; strong magnetic control required; many protostellar disks have one or more nearby companions, possibly affecting the primary disk.

6.4.5. ***Magnetic Class V: B shape perpendicular to the disk, thick main disk, with companion(s)***

Figure 14 shows a sketch of this magnetic class.

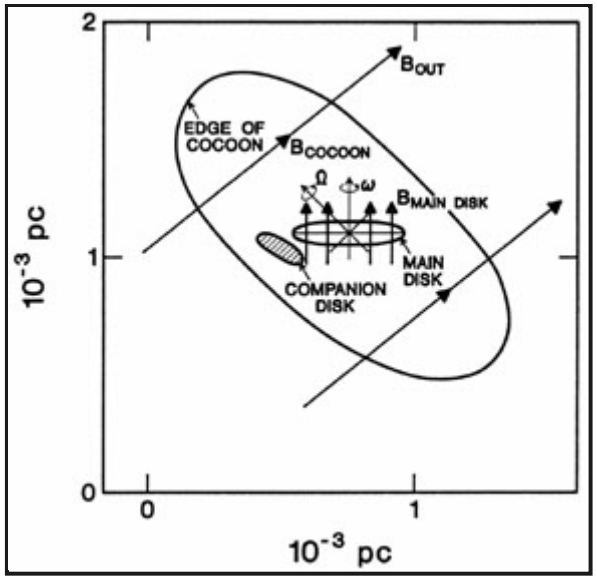

Figure 14. Magnetized molecular disk, with predominently perpendicular *B* shape, thick main disk (disk height/outer radius ~ 0.2), with one secondary disk companion. Some tidal interaction has caused precession of the main rotating disk.

To get a magnetic field direction perpendicular to a disk elongation, a binary origin of the major object (disk) and minor object (companion) must be envisioned in the plane of the larger thin cocoon. With the common onset of gravitational collapse, the disk and cocoon have initially parallel axes of elongation. If the gas in the cocoon collapses along the ambient magnetic field lines, the magnetic field in the main disk is initially perpendicular to the main disk elongation. The companion object may or may not have fragmented later on from the main disk object.

Later interaction between the two objects (main disk and companion) could cause gravitational torques, changing the direction of the main disk elongation, and causing a precession of the main disk. Here, the magnetic field direction (perpendicular to the main disk elongation) may no longer be aligned with the ambient magnetic field direction (outside the cocoon). A fragmentation theory - without magnetic fields - by Bonnell & Bastien (1991; 1992a; 1992b) employs two companions (each with its own disk) embedded in a larger disk/cocoon. Each companion disk can be at an arbitrary angle with respect to the larger cocoon elongation. One needs to observe each disk to get the whole picture. The magnetic field does not have to dominate the interaction, which could be entirely gravitational in character, leaving the magnetic field to be a tracer of what goes on.

Main model advantages: the submm radio power from the dusty protostellar disk should be large in this class; there should be a dust companion nearby; twin outflows should be easily accommodated; differential rotation in the primary disk is normally included, with its effect on the magnetic field. Main model disadvantage: more difficult to follow theoretically and to make suitable predictions; need to observe both primary and secondary components to deduce the interaction history.

Figure 15 shows a simple model case for 2 clumps in a cloudlet. Here the two small propostellar disks are placed side by side within a common envelope, all the components having the same elongation perpendicular to the magnetic field lines.

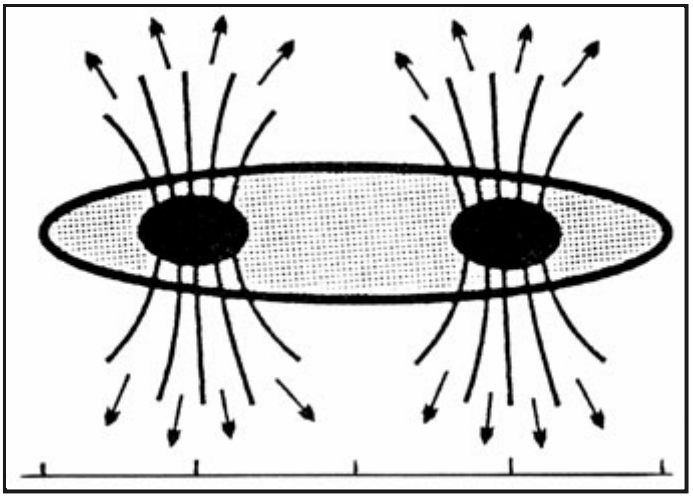

Figure 15. Magnetic field model for 2 clumps in a cloudlet. Arrows show the directions of the model magnetic field lines, roughly parallel to the minor axis of the gas elongation.

Figure 16 shows a more complex model case for 5 clumps in a cloudlet. In this cloudlet, a central concentration of gas and dust along a ridge has formed, with gas peaks or dust cores located where future star(s) may form inside the ridge.

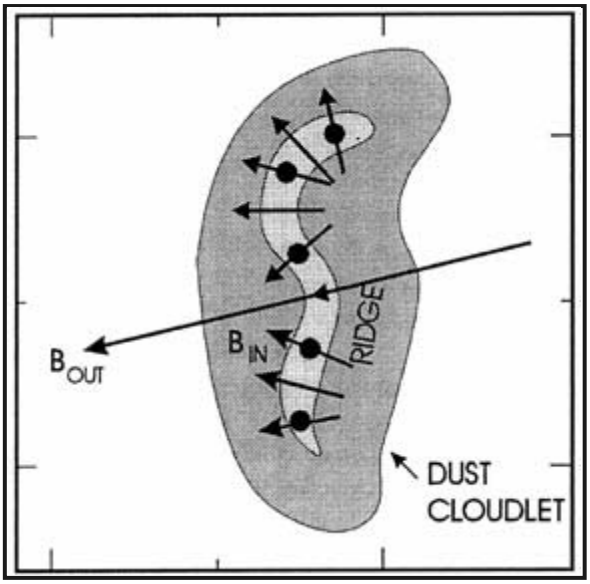

Figure 16. Model magnetic field as predicted for 5 clumps in a dusty molecular cloudlet. Note the dust cores/peaks along the cloudlet ridge.

6.5. Expected *B* with Time

Figure 17 shows a sketch of the predicted evolution with time of the magnetic field in a dusty molecular cloudlet.

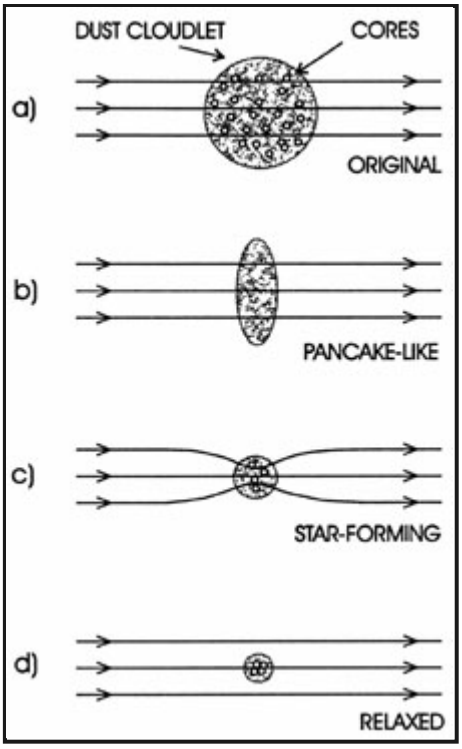

Figure 17. Time evolution of the predicted magnetic field in a dusty molecular cloudlet. (a) Stage 0. Hypothetical initial state of gas and magnetic field with $n \sim 1$ cm^{-3}. Some initial dust cores/peaks of higher density gas are embedded. (b) Stage I. The gas is allowed to move freely along the magnetic field lines and to coalesce into a pancake-like cloud, with $B \sim n^{0.0\text{-}0.2}$, with $n <$ 100 cm^{-3} . (c) Stage II. Self-gravity starts, with gas and magnetic field collapsing into several cloudlets inside the cloud, with $B \sim n^{0.4\text{-}0.6}$ and $n >$ 100 cm^{-3} . In this stage, short-lived twin outflows may be ejected perpendicular to the protostar disks (not shown). (d) Stage III. Diffusion of the magnetic field lines out of the starforming sites, due to a decrease in its ionic content. Here B in the cloudlets tends to low values, with $n > 10^{12}$ cm^{-3}.

6.5.1. *Stage 0 - Initial*

Initially (see Fig. 17a), the magnetic field is assumed to be roughly parallel to the galactic plane, where concentrations of gas and dust abound, with $B \sim 10^{-6}$ Gauss and $n \sim 1$ cm^{-3}. Also, interstellar turbulences, waves and shocks can travel in the galactic plane.

If the magnetic field strength is much smaller than 1 microGauss, insignificant with respect to existing interstellar turbulences, it could not act as a guide for the dust and gas.

6.5.2. *Stage I - Gliding*

Many theoreticians have proposed that, at a low gas density, interstellar gas and dust can accumulate or glide along magnetic field lines into denser regions, driven by magnetic instabilities, but without a noticeable increase in magnetic field strength.

Thus in this Stage I (see Fig. 17b), one could expect a gas sphere to become a gaseous sheet-like cloud, with $B \sim n^{0.0\text{-}0.2}$ for $n <$

100 cm^{-3}. If the magnetic field strength is much larger than 10 mGauss, it could stop the cloudlet from concentrating further and collapsing at its center due to gravitational forces, preventing the formation of substructures, i.e., cloudlets.

Our limited magnetic field observations of large scale gas are consistent with Stage I ($k \approx 0.1$) (e.g., Vallée 1995a; Vallée 1997).

6.5.3. *Stage II - Starforming*

Later, self-gravity starts, giving several elongated cloudlets inside the main cloud. Hence in this Stage II (see Fig 17c), one expects a large increase in B, with a $B \sim n^{0.4\text{-}0.6}$ law for $n > 100$ cm^{-3}. In Stage II, a simple model with strict mass-conserved collapse ($n \sim r^{-3}$) and magnetic flux conservation ($B \sim r^{-2}$) would lead to a predicted law $B \sim n^{2/3}$ (excluding collisions of any kind). This is contrary to what is observed in Stage II ($B \sim n^{1/2}$). So some limited flux removal mechanism may be at play in Stage II.

The observed $\sim n^{0.5}$ law is predicted by many basic equilibrium models (mechanical, hierarchical, etc). In this stage, a short-lived twin outflow may appear, perpendicular to the protostellar disk. Some flux removal mechanisms in Stage II could be associated with twin magnetized bipolar outflows, magnetized disks, limited ambipolar diffusion, etc.

Some comparison can be made. Our magnetic field observations of smaller scale gas densities to date are consistent with Stage II ($k \sim 0.5$) (e.g., Vallée 1995a).

6.5.4. *Stage III - Relaxing*

Much later (see Fig. 17d), a rapid decoupling of the field strength is likely to occur at a 'critical gas density' (decoupling régime, with a critical gas density $n > 10^{12}$ cm^{-3}). After a while, the magnetic field lines will slowly diffuse out of the disk, and the disk itself will slowly collapse toward the emerging protostar at its center, possibly forming some planets around the star(s). In Stage III, there are no observations yet, only observational limits.

6.5.5. *Discussion*

In this research area, there is a plethora of theories on magnetic field strength and shape, yet still not enough observations. Mouschovias (1985) argues that for non-self-gravitating gas with gas density n up to $n \approx 75$ cm^{-3} one should first allow for the accumulation of matter along field lines, and that the $B \sim n^{0.5}$ law cannot apply there.

There is confusion about the meaning of ambipolar diffusion. A difference of opinion and of results arises when using two *different* definitions for ambipolar diffusion (e.g., Shu et al. 1987, p.43). (i) The orthodox definition is that ambipolar diffusion is the process of decoupling and removal of the magnetic field from the gas, with the ensuing relatively *rapid collapse* of the gas to form substructures, and with *strong departure* from the $B \sim n^{0.5}$ law in the substructures, so ambipolar diffusion starts with $n > 10^{11}$ cm^{-3} in the substructures, while there is a *decrease* with time of the magnetic field. (ii) The unorthodox definition is that ambipolar diffusion can be equated with relatively *slow motions* even when the evolution proceeds quasi-hydrostatically, *without departing* from the existing $B \sim n^{0.5}$ law, at $n > 10^6$ cm^{-3}, even if the magnetic field increases with time and gas density due to contraction. The use of both definitions for ambipolar diffusion in the literature can be confusing to readers.

Mouschovias et al. (1985) employed (unorthodox) ambipolar diffusion to solve the problem that the predicted magnetic fluxes of typical stars with gas density $\sim 10^{25}$ cm^{-3} (made from assuming flux-freezing and mass-conserving laws of the observed magnetic fluxes of corresponding masses at interstellar gas densities of $\sim 10^5$ cm^{-3}), are far greater than the ~ 10 Gauss observed. They advocate significant ambipolar diffusion at moderately low critical gas density starting at $n \sim 10^6$ cm^{-3} (unorthodox definition), stop their computing near $n \sim 10^9$ cm^{-3}, and argue that significant magnetic flux has been taken out of the central core by then. Core collisions are not included here.

This low critical gas density n for unorthodox ambipolar diffusion is not strictly in contradiction to observational data indicating that a high critical density $n > 10^{11}$ cm^{-3} in substructures is needed for strong departure from the $B \sim n^{0.5}$ law (orthodox definition) (e.g., sect. 3.3 in Davies 1994; fig. 3 in Vallée 1995a; equ. 17 in Shu et al. 1987). But processes other than ambipolar diffusion could also be at play in gas density $n > 10^6$ cm^{-3}, such as core collisions with field amplification, magnetic line reconnections, etc.

Morton et al. (1994) gave the set of numerical equations, and a proposed numerical adaptive mesh method to solve them, for the time evolution of model cloud cores or cloudlets in a magnetic molecular cloud, at the onset of the Stage II (gas already setted in

a pancake cloud; unorthodox definition of ambipolar diffusion used; no core collisions). They also found slow ambipolar diffusion, no departure from the $B \sim n^{0.5}$ law, and stopped computing near $n \sim 3 \times 10^9$ cm^{-3} (hence no stars yet).

The ambipolar diffusion timescale depends on many factors, notably charged particles (various ions, electrons, and grains of various size and charge). In cloudlets with small B values, smaller than necessary for magnetic control, grains are not lost out of the cloudlets during ambipolar diffusion (Nakano et al. 1996). In cloudlets with large B values, larger than necessary for magnetic control, grains are lost out of the cloudlets along with the magnetic field due to ambipolar diffusion in the course of cloudlet contraction by a factor 4 (e.g., Nakano 1998), because even large grains are frozen-in to the magnetic field; it follows that stars formed at the cloudlet centers, then the heavy elements in these new stars must be much less abundant than in the surrounding molecular cloudlets, and these predictions are not supported by any observations.

Christodoulou et al. (1997) reappraised the formal equations for gravitational collapse in cloudlets and the viability of forming stars via core collisions inside a cloud through coalescence. They verified that the mass estimates correctly predict the onset of Jeans instability in the nearby Orion starforming region as well as in the CO cores in the disk of the Large Magellanic Cloud galaxy. The importance of core collisions inside a cloud is thus strengthened. For core collisions inside a cloud of volume V, having N cores each of radius R and a velocity dispersion ν (inside the cloud), the time t between any two core collisions is derived as

$$t(\mathrm{Gyr}) \approx V\,(\mathrm{kpc}^3)[N/10]^{-2}[R/10\ \mathrm{pc}]^{-2}[\nu/30\ \mathrm{km/s}]^{-1}$$

In addition, they found that this process predicts very little starforming activity in the halo of the Milky Way and in the halo of the Magellanic Clouds, and very little is observed (no ambipolar diffusion used).

Theoretical studies of star formation, including the magnetic fields involved, tend to use an environment made up of dense cool clouds in pressure balance with a hotter intercloud medium, while denser cores are found inside each cloud. Some of these cores may be self-gravitating, while others may be in pressure equilibrium with its surrounding. Core-core collisions followed by coalescence is expected to built up the initial core masses. Core rotation is expected, and may lead to further fragmentation (e.g., Monaghan 1983).

6.6. Other Theoretical Ideas

Magnetic theories already published are based on different assumptions and link various magnetic field directions to compressible turbulences, to energy balance, to fragmentation, self-gravity and star formation, and to other physical processes (chaotic behaviour, fractals, etc).

6.6.1. *Magnetism - dominant or not ?*

Scalo (1987) proposed that turbulences can explain many scaling relations, such as the velocity dispersion in clumps being proportional to the inverse square root of the gas density. In this picture, turbulence (not magnetic fields) is the dominant mechanism in clouds. The magnetic field may be important for the support and line broadening in some clouds, but it seems likely that such a dominance is restricted.

Theoretical studies have hinted that a small magnetically supported cloudlet should have an oblate core (Lizano and Shu, 1989), whereas some cloudlets show a prolate core, requiring another physical process, such as a rotationally supported cloud (Bonnell & Bastien, 1991).

In contrast, Myers and Goodman (1990) proposed that magnetic fields are dominant in cloudlets, requiring triple equipartition between magnetic energy, gravitational energy, and kinetic energy. Subtracting the thermal part of the line width (proportional to the cloudlet temperature), the remainder (nonthermal part) is attributed entirely to magnetic origins.

In this picture, hydromagnetic waves are expected to be significant. Myers and Khersonsky (1995) proposed that MHD waves, chaotic motions, and clumps are probably more pervasive in clouds than would be expected from cosmic-ray ionization alone, implying a very long time scale for ambipolar diffusion $\sim 10^8$ years. This suggests that ambipolar diffusion *alone* may be too slow a process for low-mass star formation in nearby dark clouds. They also pointed out that the assumption of dominant magnetic support in cores may not be real, since for low mass cores (i) the thermal motions inside the cloud appear observationally energetically sufficient to support the cores against gravity (Fuller & Myers, 1993) and (ii) the required field strength for magnetic support (~ 40 μGauss in TMC-1C) is 10 times larger than the 1 rms observed OH Zeeman upper limit (~ 4 μGauss; Goodman 1992).

Starting from the virial equation for an axisymmetric oblate magnetic cloud of mass M and semimajor axis R and semiminor axis

Z embedded in an external medium of pressure P_0 and external magnetic field B_0 with the radius R_0 being the radius far from the cloud of the magnetic tube penetrating the cloud with flux freezing ($B_0 R_0^2 = BR^2$), one gets (Equ. 1 in Nakano, 1998):

$$0.5 d^2 I/dt^2 = M[(3kT/\mu m_{\rm H}) + V_{\rm turb}^2] - aGM^2/R + b[B^2R^3 - B_0^2 R_0^3] - 4\pi R^2 Z P_0$$

where I is the generalized moment of inertia of the cloud, t is the time, k is Boltzmann constant, T is the mean cloud temperature, μ is the mean molecular weight of the gas, $m_{\rm H}$ is the hydrogen atom mass, $V_{\rm turb}$ is the mean turbulent velocity, B is the mean cloud magnetic field, a and b are dimensionless coeficients of order unity. Solutions of this equation have been worked out for different boundary conditions and geometrical assumptions. The same equation can be used for cores, clumps, or cloudlets, provided that the external parameters B_0, R_0, P_0 are those of the cloud or interclump medium.

Nakano (1998) points out that there are no cloud cores which have been confirmed to be magnetically subcritical, defined as having enough or more magnetic field than needed to prevent cloud contraction due to gravity. Also, published lists of magnetic fields in molecular clouds and cores contain mainly upper limits to the field strengths, and these observational upper limits are below the values needed to have magnetic support of the clumps and clouds (e.g., Bertoldi & McKee 1992; Nakano 1998).

Crutcher et al. (1992) made OH Zeeman observations towards 12 cloud cores, and obtained a definite detection in only 1 out of 12; the other 11 gave only upper limits, all several times smaller than required for magnetic control; even the one detection (the B1 core) out of 12 gave a magnetic field value below that required for magnetic control (Heiles et al. 1993; Nakano 1998). Crutcher et al. (1996) also obtained observational upper limits for CN Zeeman observations in 2 cloud cores, still way below that required for magnetic control.

Here we can estimate the amount of magnetic support against the gravitational energy in some clumps. For total magnetic support against gravity, one derives the equation (Equ. 25 in Myers & Goodman, 1988; Equ. 1 in Myers & Goodman, 1990):

$$[B_{\rm control}/\mu G] = 15[\Delta v/{\rm km\ s^{-1}}][[{\rm Radius/pc}]^{-1}$$

The clumps in the cloud M17-SW have been well studied observationally, and from Extreme-IR continuum emission at 800 μ m, Vallée and Bastien (1996) estimated a clump radius $\approx$ 0.17 pc and a clump density $\approx 3 \times 10^5$ cm^{-3}, while from ^{12}CO line data Bergin et al. (1994) estimated a line width $\approx$ 4 km/s, giving a nonthermal line width Δv ~ 3.7 km/s. Entering these data in the above equation for magnetic control gives $B_{\rm control}$ = 1.2 mG.

We can also estimate the expected magnetic to be observed from observations of magnetic fields in many other cloudlets and clouds, having obtained the statistical relation (e.g., Fig. 1 in Vallée 1997):

$$[B_{\rm stat\ obs}/\mu G] = 0.4[n/{\rm cm^{-3}}]^{0.5}$$

giving again for the clumps in M17-SW a value $B_{\rm stat\ obs} \approx$ 0.3 mGauss.

Preliminary Zeeman data near clump P4 in M17-SW by Brogan et al. (1998) gave a magnetic field $B_{\rm Zeeman} \approx$ 0.2 mG.

Thus in the clumps of M17-SW the $B_{\rm stat\ obs}$ and $B_{\rm Zeeman}$ give an average of ~ 0.3 mG, while the assumption of magnetic control gives $B_{\rm control}$ ~ 1.2 mG, hence we have $B_{\rm stat\ obs}$ / $B_{\rm control} \approx$ 25% and the statistical and observed magnetic energy density is roughly $[0.3 / 1.2]^2 \approx$ 6% of the large magnetic energy density needed when assuming magnetic control against gravity.

Hence in addition to the weak magnetic energy density, there is a need for another non-magnetic process to provide the 94% of energy density needed against gravity. The most likely candidates would be turbulences, clump collisions, shocks from travelling clumps, stellar outflows near embedded protostars, convective motions due to IR photon heating near embedded protostars, thermal instabilities due to time-dependent shielding variations near embedded protostars, etc.

6.6.2. ***Fractals and Waves***

Can magnetic field structures be represented with 'fractals' ? There have been some hints that a fractal nature of molecular cloudlets is real, i.e., the number of clouds N of size L is proportional to the size elevated to some fractal power D, like $N(L) \sim L^{-D}$ where D is near 2.7 (Henriksen 1991; Henriksen 1986). Then it follows that the gas density n varies as $n(L) \sim L^{-E}$ where E is

near 1.0 In a similar vein, it is not yet known if the magnetic field structures is showing a fractal behaviour with size, like $B(L) \sim L^{-F}$.

Are there many 'wavy' magnetic field structures in the interstellar medium ? Magnetic field structures are known to display a uniform and a random component. In some departures from this view, wavy transverse vibrations of an otherwise uniform component have been observed (Shuter & Dickman 1990; Moneti et al. 1984). The degree of this magnetic wavyness is not known, but it could be a strong indicator of the existence of Alfvén-type magnetic disturbances, with potential consequences for subsequent star formation (e.g., magnetic braking by an uniform component, see Fig. 10 in Warren-Smith et al. 1987). In turn, these magnetic disturbances would predict increased CO line widths (e.g., Blitz 1991).

Martin et al. (1997) proposed theoretically that small molecular clouds or cloudlets are supported along the magnetic field lines by an Alfvén wave pressure force. The origin of these Alfvén waves would be the orbital motions of clumps (clump size ~ 0.1 pc) within a small cloud (cloud size ~ 1 pc). For a gas density ~ 1000 cm^{-3} and a cloud magnetic field ~ 100 μGauss, their model requires a minimum wavelength $\nu_{\rm Alfven} \cdot \tau_{\rm min}$ (= 4.5 km / s × 0.3 Myr $\approx$ 1.4 pc, after their Equ. 43) and smaller than a maximum equal to the cloud thickness ($\approx$ 5 pc, after their Equ. 44). Also, their wave model requires the magnetic wave pressure to be strong, about 30 times the isothermal gas pressure, hence $\Delta B / B_0 \approx 0.6$, after their Equ. 69 and 70. Thus their wavelength range is quite limited, and their strong Alfvén wave would imply a nearly random overall magnetic field B_0($\Delta PA \approx \Delta B / B_0 = 30°$), much larger than what observations of small clouds show. Their model excludes non-magnetic supports, such as (i) clump collisions, (ii) internal cloud hydrodynamic (micro) turbulence, (iii) cloud rotation, (iv) outflows from embedded protostars, (v) shocks from traveling clumps or outflows, (vi) convective motions due to gas heating by IR photons from embedded protostars, and (vii) thermal instabilities due to time-dependent shielding variations of photons from embedded protostars, etc.

Nakano (1998) studied the possibility of having MHD waves travelling inside clouds or clumps. He found that in most cases the waves' dissipation time $t_{\rm wave}$ is significantly smaller than the free-fall time, typically $t_{\rm wave}$ is $\approx$ 10% of the free-fall time, yet the whole clump or cloud may last much longer than the free-fall time (because of various supports against gravity). In addition, any such MHD wave in weak B field could be supersonic and super-Alvénic so shock dissipation must then occur in a timescale $t_{\rm shock}$ much smaller than $t_{\rm wave}$.

7. OBSERVED MAGNETIC FIELDS IN PROTOSTELLAR DISKS (OUT TO ~ 200 AU OR SO; ~ 10^{-2} PC) AND DENSE INTERSTELLAR STARFORMING CLOUDLETS (0.1 TO 1 PC)

7.1. Excess line width for small objects (sizes < 1 parsec)

One of the most important signatures of small scale turbulence is the presence of a spectral line width $W_{\rm observed}$ having an excess of (i) the thermal width (expected from the gas temperature) and of (ii) the line broadening due to large scale motions such as expansion or contraction. The large scale motion is generally subtracted out linearly first. The thermal line width is given by the relation

$$W_{\rm thermal} = 0.214 T_k^{0.5} [m_a/m_H]^{-0.5} \ {\rm km/s},$$

where $T_{\rm k}$ is the kinetic temperature in kelvins and $m_{\rm a}$ / $m_{\rm H}$ is the atomic mass (in units of the hydrogen atom mass). The excess line width $W_{\rm excess}$ (often called the non-thermal line width) is given by the quadratic subtraction thus:

$$W_{\rm excess}^2 = W_{\rm observed}^2 - W_{\rm thermal}^2 = 8 \ln 2 \langle V_{\rm turb} \rangle^2 / 3$$

where $<V_{\rm turb}>$ is the equivalent turbulent rms speed; here $<V_{\rm turb}> = 0.74\ W_{\rm excess}$. All line widths W are measured or expressed as full widths between half-intensity points (FWHP).

A relation between the excess line width (= $W_{\rm excess}$) and the object size (= R), of the form $W_{\rm excess} = R^{\rm q}$, has been known since the late 1970s, in both radio molecular studies and in optical HII region studies (e.g., Larson 1979). Objects in this category encompass molecular/dust cores with stars inside ($W_{\rm excess}$ = 0.25 km/s, R = 0.1 pc), large low-brightness molecular/dust cloudlets (0.38 km/s, 0.1 pc), α Ori cloudlets (0.38 km/s, 0.3 pc), some globules (0.6 km/s, 0.3 pc), high galactic latitude molecular/dust cloudlets (2.4 km/s, 0.7 pc), ionized carbon interfaces between molecular clouds and HII regions (4.2 km/s, 1.0 pc), etc.

A well-known separation occurs for object sizes R = 1 pc, in the log W_{excess} - log R plane. At small sizes, taking all types of objects with R < 1 pc, one finds the relation $W_{excess} \sim R^{0.7}$. Splitting these objects by mass, it seems that q = 0.7 (Fuller & Myers 1992) or 0.5 (Caselli & Myers 1995) for low-mass cores ~ 1 $M_\odot$ (using density ~ 10^4 cm^{-3}, radius = 0.1 pc) , while q = 0.2 (Caselli & Myers 1995) for high mass cores ~ 100 $M_\odot$ (using density ~ 10^5 cm^{-3}, radius = 0.2 pc). More data are needed on small objects with $R \approx$ 0.1 pc to 0.01 pc, and future improvements are expected there. W_{excess} could be due physically to cascading/macroscopic turbulences, to energetic stellar outflows, to collisions of cores, or else to magnetic turbulences. This small scale behaviour differs from the behaviour at larger scale. For all types of objects with R > 1 pc, one typically finds $W_{excess} \sim R^{0.5}$ (e.g., Vallée 1994) in objects like small molecular clouds (~ 10^3 $M_\odot$), cloud complexes (~ 10^4 $M_\odot$) and others, indicative of gravitational and other equilibrium supports.

7.2. Magnetic Field Strengths

What is the statistical B strength inferred from dust emission? In the dust thermal emission method, the magnetic field strength B is not measured directly but it can be deduced to first order by various mechanisms. (1) Deduced by scaling the theoretical polarization amplitude (predicted by model equations) to match the observed polarization amplitude. (2) Deduced by using the turbulent scatter in the polarization position angle $\Delta\Theta$ from a mean in a map of a dusty object, such as with the equation

$$B_{\rm Gauss} \approx 2.7 \times 10^{-7} [n/{\rm cm}^{-3}]^{0.5} [v_{\rm turb}/{\rm km\ s}^{-1}] [\Delta\Theta_{\rm rad}]^{-1}$$

(e.g., Hildebrand 1989; Heiles et al. 1991; Chrysostomou et al. 1994). (3) Deduced by using the gas density n through the appropriate $B \sim n^k$ law, such as with the equation (e.g., Vallée 1995a):

$$B_{\rm Gauss}/ \approx 4 \times 10^{-7} [n/{\rm cm}^{-3}]^{0.5}$$

How about real Zeeman detections ? Zeeman detections of B > 100 μGauss are now being made. Using the Zeeman method at the VLA interferometer near the HI line at 21 cm, an hourglass-shaped magnetic field has been observed in the cloudlet W3 Core, consisting of the components W3a (-47 μGauss) and W3b (+103 μGauss) separated by 0.6 parsec (e.g., Fig. 1 and 6 in Roberts et al. 1993). Using the VLA at HI 21 cm, several localized hot spots are seen by the Zeeman method within the large 30" (= 0.3 pc) DR21 region, with hot spot magnetic field ~ 400 μGauss aligned along the edges of a conical V-shaped cavity caused by an outflow from a young star (Roberts et al. 1997).

Can weak magnetism be typical? Using the Zeeman method with the IRAM 30m telescope at the CN gas 3mm line, only upper limits of 200 μGauss were placed in cloudlets which were expected by strong virial equilibrium arguments to be around 600 μGauss (e.g., Crutcher et al. 1996). This shows that one *cannot* assume a strong magnetic energy, in equilibrium with gravitational and kinetic energies. We may still assume the simple virial equilibrium (grav. energy $\approx$ kinetic energy), both being much larger than the magnetic energy. This would entail rejecting strong magnetic field models.

Using the Zeeman method with the Hat Creek 26m single-dish telescope at the HI 21 cm line, Goodman and Heiles (1994) claim the detection of B ~ 10 μGauss in the Ophiuchus Dark Cloud Complex. The HI profile are comprised of multiple (~ 4) components, which are tentatively identified as arising from different régimes along the line of sight; their telescope beamwidth is ~ 36 arc minutes, and could thus convolve multiple components across the line of sight as well as along the line of sight. Their deconvolution requires multiple input assumptions, and yields low magnetic field values obtained using single-dish telescopes.

Caveat: measurements by the Zeeman splitting method are difficult. Claimed Zeeman detections in nearby dust cores and cloudlets must always come with proper corrections for instrumental sidelobe effects and self-correction for source brightness gradient effects; these effects are specially large for the Zeeman detections of *low magnetic field values* (< 100 μGauss) using *single-dish telescopes*. For the OH line (ν = 1.665 GHz), the split is 0.02 km/s for a B strength of 100 μGauss, far smaller than the full OH line width. Exemple: after pointing single dishes at the HI 21 cm line toward cloudlets H0928+02, MBM12, and MBM40, all of sizes ~ 1 parsec, uncorrected HI Zeeman claims of B ~ 5 μGauss become after corrections ~ 0.2 μGauss (e.g., Table 5 in Verschuur 1995). This amounts to a sizable reduction of ~ 625 in observed magnetic energies (~ B^2).

Future trends: the advent of the detection of Zeeman effects with the VLA and other interferometers at the HI 21 cm line (with a synthesized beamwidth of ~ 25 arc seconds in the C and D configurations) should help to establish reliable magnetic field strengths, free of the large instrumental and angular limitations of single-dish data.

7.3. Polarization Percentages and Physical Parameters

Magnetic fields play a significant role in the collapse of protostellar cloudlets. But they are difficult to observe, and it appears that submillimeter polarimetry is perhaps the best way to observe them reliably. This new technique is in its infancy. A significant improvement is needed to put on solid ground the observational constraints inferred from theoretical models. For example, the observational errors need to be improved from typically 0.3% down to 0.1% which is now becoming possible. In the following, I describe briefly the tentative physical correlations which have been obtained so far, concerning the submillimeter/Extreme IR polarization percentage. These correlations have important implications for testing the many theories of star formation with magnetic fields.

7.3.1. ***Percentage Correlation 1 (Pol. percent vs grain chemistry)***

The ratio of the polarization amplitude of dust emission at two different wavelengths varies with grain composition, i.e., silicate grains give a constant ratio of polarization percentages while graphite grains give a polarization percentage increasing at longer wavelengths (e.g., Hildebrand 1988). Thus graphite/metallic grains seem to predominate near DR21, since at λ800 μm one sees only $\approx$ 2.5% polarization while at λ1100 μm one sees $\approx$ 4% ±1% polarization (quite a change, e.g., Minchin and Murray 1994). New observations of DR21 at λ1300 microns indicate 1.7% ±0.2%, supporting silicate graphite grains (Glenn et al. 1997a). Silicate grains seem to predominate near OMC-1, since at λ100 μm one also sees $\approx$ 3.7% polarization while at λ1300 μm one sees $\approx$ 4.6% polarization (about the same, e.g., Leach et al. 1991). More observational work remains to be done to firm up this correlation.

7.3.2. ***Percentage Correlation 2 (Pol. percent vs angular distance)***

A simple trend in polarization percentage as a function of angular distance from a source center has been claimed. A small decrease in polarization percentage, relative to its immediate surroundings, termed a "polarization hole", has often been observed; it has been variously attributed physically to "a change in the magnetic field alignment" within the beam (e.g., Minchin and Murray 1994; Aitken et al. 1997; Rao et al. 1998) or to "gas-grain collisions" near the dust density maximum (e.g., Minchin et al. 1996). However, a calibrated plot of percentage versus telescope beam size for DR21 (see Fig. 3 in Glenn et al. 1997a) shows no evidence of a decrease or increase, from HPBW = 13" out to 42". Yet Greaves et al. (1997) find that the polarization percentage increases from 1% for nearby objects (at ~ 100 pc) up to 4% for more distant ones (at ~ 400 pc). More observational work remains to be done to firm this up.

7.3.3. ***Percentage Correlation 3 (Pol. percent versus time evolution)***

Two opposite variations of polarization percentage with source age or time have been claimed. "The magnetic field becomes more ordered as a young stellar object moves towards the main sequence" (Holland et al. 1996), and "the magnetic field lines must first be more ordered around younger protostars" (Greaves et al. 1997). In this last reference, the polarization percentage decreases from 4% for young objects (outflow opening angle ~ 10° ; small ratio of bolometric luminosity / 1.3mm luminosity) down to 1% for older objects (outflow opening angle ~ 60°; large ratio of bolometric luminosity / 1.3mm luminosity).

7.4. Polarization Position angles and Physical Parameters

The Extreme IR polarization data for these dusty objects can reveal the magnetic field direction (from polarization position angle), and the degree of polarization (from polarization amplitude and total continuum), and can permit testing physical models. The total continuum emission allows the derivations of the 'optical' depth and thermal density upon reasonable physical assumptions (e.g. McCutcheon 1992).

In the following I describe briefly the physical correlations obtained so far in the submillimeter / Extreme IR, involving the position angle of polarization. More observations would certainly improve and extend these correlations, and then a proper testing of these correlations against the theoretical model predictions could be done better.

7.4.1. ***Angle Correlation 1 (B shape and companionship)***

An interaction effect among companion disks is possible. In Table 1, the presence or absence of a cold gas companion nearby (within two source radii) seems to be correlated with the angular difference between the magnetic field direction and the source elongation. Most sources in this Table 1 having 'a poloidal magnetic field direction' also have 'a nearby companion within two source radii', and those having 'a toroidal magnetic field direction' are more likely to be isolated. A similar correlation for 3 low-mass sources has been noted by Holland et al. (1996): two sources with companions have a poloidal magnetic field, one source without companion has a toroidal magnetic field. More data are badly needed.

Table 1. Magnetism in Protostellar Disks and Interstellar Cloudlets

Object	B PA o	Source PA o	|PA(B) - PA(source)| o	ref	Total Dens. 10^6 cm^{-3}	Source diam. pc	Gas Temp. o	Cold gas comp.[(a)] yes=1;no=0	Note
(i) *B toroidal*									
AFGL490	126	135	09	(b)	1000.	0.01	75	no	(b)
SVS13	053	035	18	(b)	100.	0.01	50	no	(b)
AFGL989	110	110	00	(b)	0.1	0.15	28	no	(b)
AFGL2591	170	180	10	(b)	20.	0.2	43	no	(b)
W75N-IRS1	145	145	00	(i)	3	0.12	--	no	(i)
V645 Cyg	038	040	02	(b)	0.005	1.0	--	no	(b)
NGC2071	142	135	07	(c)	0.1	1.0	35	no	(c)
R Mon	101	070	31	(c)	0.002	0.6	28	no	(c)
HL Tau	140	135	05	(k)	1	0.02	--	binary	(k)
AFGL2136	046	045	01	(b)	-	0.04	--	triple	(n)
S106-IRS4	079	080	01	(m)	0.04	0.04	--	binary	(m)
Median:			02		0.7	0.1	40	no	
Mean:			08		112	0.3	43	0.3	
s.d. of mean:			03		99	0.1	07	0.1	
(ii) *B poloidal*									
SgrB2-N+S	082	012	70	(q)	0.5	0.2	35	cluster	(q)
W49N-F	125	005	60	(q)	0.1	0.1	--	ridge	(q)
W51e1-IRS1	059	161	78	(q)	0.1	0.2	46	binary	(q)
L1551-IRS5	055	135	80	(k)	50	0.01	15	no	(k)
N1333-IR4A	042	132	90	(l)(p)	9000	0.02	--	binary	(l)
N1333-IR4B	010	132	58	(l)	920	0.02	--	binary	(l)
OMC1-IRc2	032	122	90	(o)(q)	0.1	0.1	--	bin 1.5'S	(o)
Mon R2-IRS2	170	045	55	(b)	0.02	0.7	29	SW ext.	(f)
IR16293-242	044	150	74	(d)	200	0.01	40	Comp.B	(e)
DR21	116	170	54	(j)(q)	1 0.5	--	flows	(j)	
S140-IRS1	011	100	89	(b)	3	0.25	70	Arc	(h)
N7538-IRS1	142	050	88	(j)	0.1	0.3	--	IRS2,3	(j)
N7538-IRS11	148	055	87	(j)	0.1	0.3	--	ridge	(j)
Median:			76		0.5	0.2	38	yes	
Mean:			75		780	0.2	39	0.9	
s.d. of mean:			04		690	0.1	07	0.1	

(a): Cold gas companion located nearby, no more than two source radii away.
(b): Aitken et al. (1993), and references therein. Mid IR polarization data.
(c): Sato et al. (1985), and references therein. Near IR polarization data. These data may be due to a magnetic field or to multiple scattering. They are kept for statistical purposes.
(d): Vallée & Bastien (1998). Extreme IR polarization data.
(e): Mundy et al. (1992), their Fig. 1.
(f): Wolf et al. (1990), their Fig. 4.
(g): Vogel et al. (1984), their Fig. 3.
(h): Hayashi et al. (1985), their Fig. 4.
(i): Vallée & Bastien (1995). Extreme IR polar. data.
(j): Minchin & Murray (1994).
(k): Tamura et al. (1995)
(l): Minchin et al. (1995)

(m): Holland et al. (1994).
(n): Minchin et al. (1991).
(o): Leach et al. (1991)
(p): Akeson et al. (1996)
(q): Kane et al. (1993)

7.4.2. *Angle Correlation 2 (B shape and viewing angle)*

A viewing angle effect is claimed by Minchin et al. (1996), whereas poloidal magnetic field lines parallel to the minor axis of a cloudlet (or disk) can be well detected, but toroidal magnetic field lines parallel to the major axis of a cloudlet (or disk) will be subject to wide misinterpretations. Greaves et al. (1977) found with 7 sources that a small viewing angle (outflow direction close to the line-of-sight to Earth) yields a poloidal magnetic field, while a large viewing angle (outflow direction orthogonal to the *l-o-s* to Earth) yields a toroidal magnetic field. More observational work would help.

7.4.3. *Angle Correlation 3 (B shape and beam size)*

A beam size effect is claimed by Holland et al. (1996), i.e. for *nearby* sources the telescope beamwidth can detect well the *toroidal* magnetic field lines (parallel to the major axis of the cloudlet), but for *distant* sources the telescope beamwidth includes both the toroidal magnetic field in the denser part of the cloudlet (or disk) and the poloidal magnetic field in the huge thin envelope/outflow (above and below the elongated cloudlet/disk) thus leading to a net poloidal magnetic field. More data are needed. Figure 18 shows the possible misunderstanding due to the beam size effect. The inner circle represents a telescope beamwidth englobing a *nearby* cloudlet/disk (square) with a toroidal magnetic field inside (horizontal arrows) - leaving out the outer diffuse gas in the envelope/outflow above and below the disk, thus yielding a toroidal magnetic field answer. The *outer* circle represents a telescope beamwidth englobing a *distant* cloudlet/disk and its envelope/outflow (twin cones, above and below the disk) having a poloidal magnetic field (vertical arrows), thus yielding a poloidal magnetic field answer (diffuse gas over a large volume wins over dense gas over a minuscule volume).

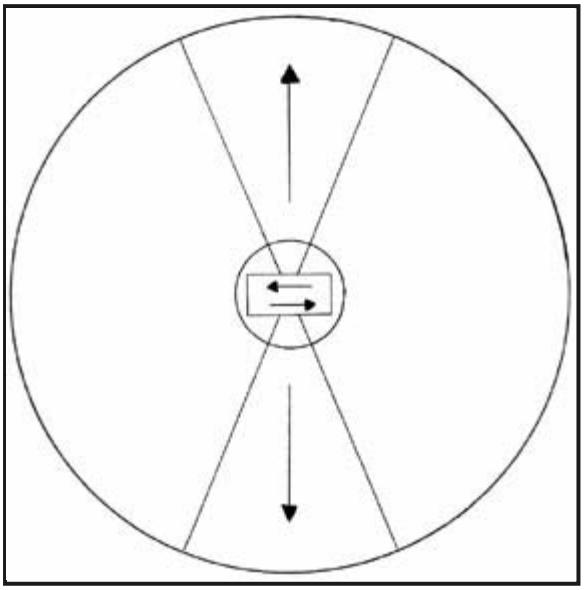

Figure 18. Illustration of the "beam size effect", in which a small telescope beam (inner circle) sees mostly the magnetic field in the core/cloudlet/protostellar disk (rectangle), while a large telescope beam (outer circle) sees both the magnetic fields in the twin outflow/envelope (twin cones) and in the core (rectangle). For a fixed telescope beam (in angle), the cores of nearby sources are mostly seen, while the full extent of distant sources are mostly seen in the beam. Adapted from Holland et al. (1996).

7.4.4. *Angle Correlation 4 (B shape and time evolution)*

A time evolution may be at play. At a young age, the protostellar disk and its surroundings may both have a poloidal/vertical magnetic field. At a later age, differential rotation sets in the protostellar disk, so a toroidal magnetic field would be seen in the protostellar disk while a poloidal magnetic field would still be seen in the surroundings. More observations would help.

7.5. Some Mapping Results So Far (~ 10^{-3} Gauss)

Published data on the observed protostellar disks and cloudlets with observed magnetic fields have been culled from the literature, and preliminary statistics have been performed on them.

Table 1 shows the accumulation of the published data (Vallée & Bastien 1998). The first columns give the disk or cloudlet name, position angle of the magnetic field direction, position angle of the source elongation, and angular difference between these two. Other columns give the total (gas plus dust) density, source diameter ($\leq$ 1 pc), gas temperature, and whether there is or not a cold gas companion of similar temperature (between 10 K and 100 K) located nearby (no more than two disk radii away). The sources are placed in either of two categories: (i) those with *B* field direction roughly *parallel* to the source elongation (angle difference less than 45°), and (ii) those with *B* field direction roughly *perpendicular* to the source elongation (angle difference greater than 45°).

There is a relative absence of sources with a difference in angles between 30° and 60°. Statistics were performed separately on each category, to yield the mean values and their standard deviations. The results showed that, for most of the physical parameters (see columns) listed in this Table, the sources in the two categories could easily come from the same original parent distribution (same median source density of ~ 10^6 cm^{-3}, same mean source diameter ~ 0.2 pc, same median source gas temperature ~ 40 K). However, a good trend could be seen in the absence of a companion for most sources (8/11) with a toroidal *B*, and the presence of a companion/nearby object for most sources (12/13) with a poloidal *B*.

Figure 19, using data from Table 1, shows the current status of the angle correlation with companionship. There is a surplus of sources with a poloidal magnetic field having a nearby companion (at right), and a surplus of sources with a toroidal magnetic field being isolated (at left).

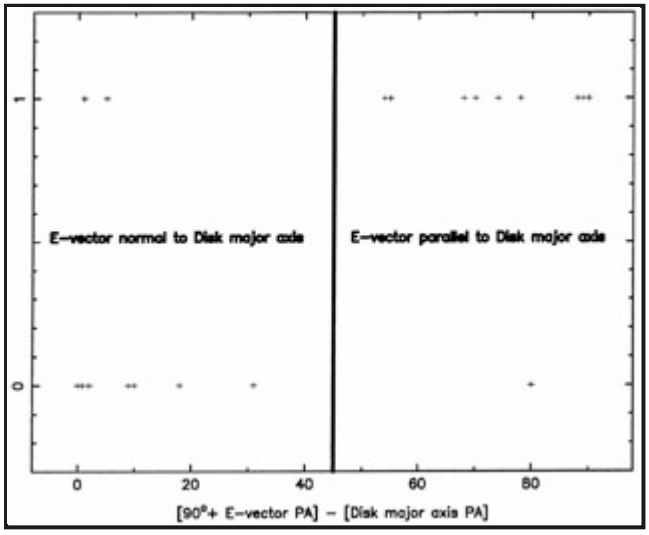

Figure 19. Observed difference between the Source magnetic field direction (90° + *E*-vector PA) minus the Source elongation, versus the absence (bottom) or presence (top) of a nearby cold companion (within 2 disk radii). There is a surplus of sources with a poloidal magnetic field having a nearby companion (at right), and a surplus of sources with a toroidal magnetic field being isolated (at left).

Figure 20 shows the area around the cloudlet W75N-IRS1, which was observed bolometrically and polarimetrically (Vallée & Bastien 1995) at 800 μm. They found that the continuum flux density and moderate source size (0.12 pc) gave a mean total density of 3 × 10^6 cm^{-3}, at a dust temperature of 45 K. They also found that, on this size scale, the magnetic field is roughly *parallel* (*B* toroidal) to the major axis of the dust/molecular cloudlet (i.e., *B* is toroidal), and nearly *perpendicular* to a CO outflow from this object, with a field strength ~ 1 milliGauss. On this scale in W75N-IRS1, the polarimetric data at 800 μm are

best interpreted by the following magnetic models: *Y*-shaped *B* lines in clump, *X*-shaped *B* lines in clump, or *B* lines in clump perpendicular to *B* lines outside clump. More data at submillimeter wavelengths are needed to further narrow these possibilities. Near-IR polarimetric maps of W75N-IRS1 are dominated by multiple scattering and may not reveal anything about the magnetic field direction.

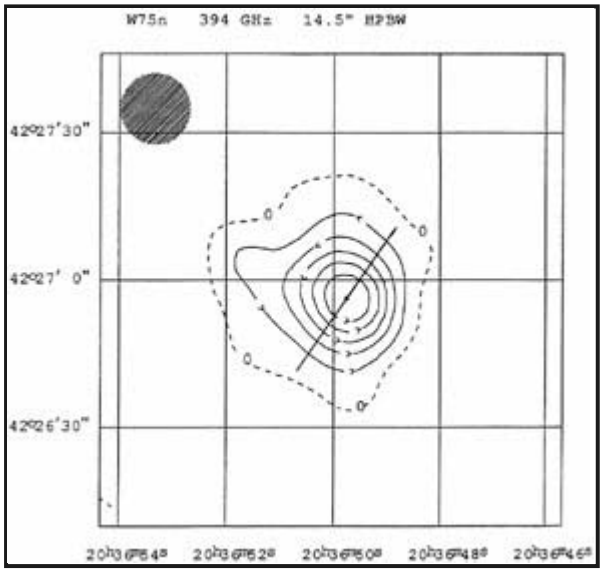

Figure 20. Observed magnetic field lines in the interstellar cloudlet W75-IRS1, as seen at the JCMT at a wavelength of 800 microns (Vallée and Bastien, 1995). The magnetic field line (bar) is roughly parallel to the major axis of the cloudlet. At 2 kpc away, 1 arcmin corresponds to 0.6 pc.

On a smaller scale, Zeeman observations of OH masers at λ18 cm by Hutawarakorn and Cohen (1996) clustering on a small scale (~ $6000\,AU$ ~ 9×10^{11} km ~ 0.03 pc) near the protostar in W75N near IRS1/HII(B) indicated a magnetic field ~ 5 milliGauss oriented *parallel* (B poloidal) to the CO outflow. This apparent misunderstanding (poloidal; toroidal) may be explained by the beam size effect. They also find some evidence in their data for a magnetic field reversal, indicative of another, toroidal component perpendicular to the outflow.

Figure 21 shows an example of the magnetic fields in two close clumps, located in source IRAS 4 within the object NGC 1333. The arrows show the direction of the magnetic fields. The magnetic field goes roughly perpendicular to the line joining the two clumps. Here the magnetic fields are observed to point perpendicular to the gas and dust ridge. Typical amplitudes of the magnetic field strength in molecular cloudlets are near 1 mGauss.

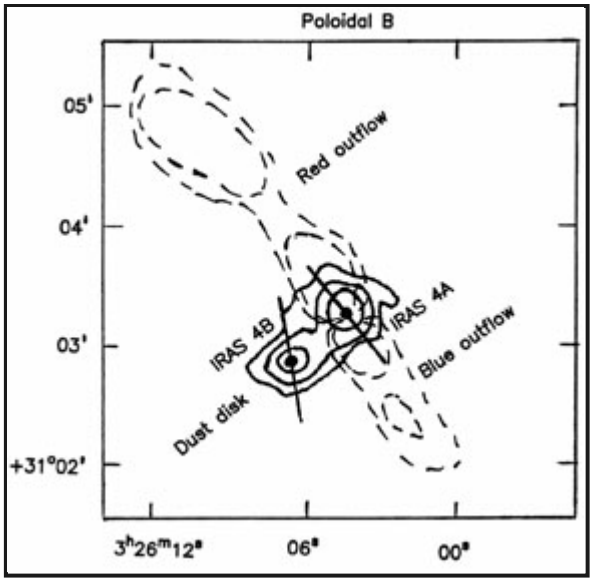

Figure 21. Magnetic field observed in source IRAS 4 within the object NGC 1333. Dust emission contours near 870 μm (solid curves) and CO gas line emission near 870 μm (dashed curves) are shown. The bars show the direction of the magnetic fields, measured near 800 μm. In both IRAS4a (at right) and IRAS 4b (at left), the magnetic field goes roughly perpendicular to the line joining the two clumps. At 220 pc away, 1 arcmin corresponds to 0.06 pc. Adapted from Minchin and Murray (1995).

Figure 22 shows the area around the cloudlets S106-IR and S106-FIR. They were observed near 800 microns (adapted from Holland et al. 1996). A magnetic field roughly *parallel* to the overall elongation is seen (toroidal magnetic field). This region has been observed in the Zeeman splitting of HI and OH by Roberts et al. (1995), who measured ~ 400 μGauss about 0.1 pc NE and 0.2 pc SW of the Extreme IR core, suggesting a magnetic field *perpendicular* (B poloidal) to the Extreme IR core elongation. This apparent misunderstanding (poloidal, toroidal) may be explained by the beam size effect mentioned above.

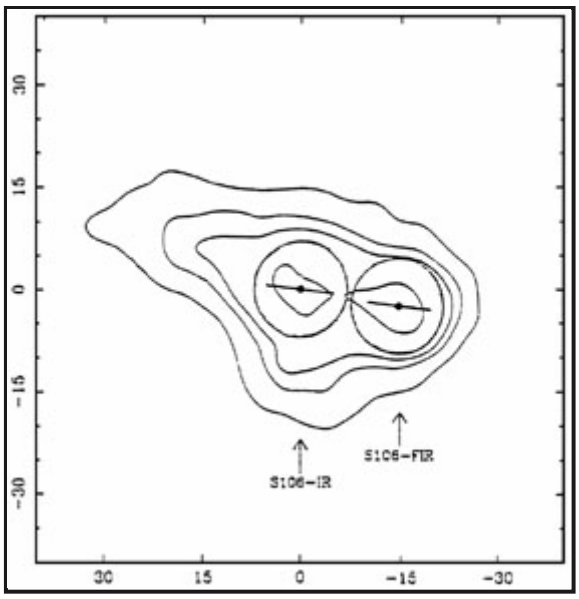

Figure 22. Observed magnetic fields in the interstellar cloudlets S106-IR and S106-FIR, as seen at the JCMT near 800 μm (adapted from Holland et al. 1996). The two circles represent the JCMT beams of 13.5". The units in x and y axes are in arcsec, with the (0,0) at RA = 20h 25m 34.3s, Dec = + 37° 12' 50.0". Two bars represent the magnetic field lines, which are roughly parallel to the major axis of the cloudlet. At 600 pc away, 1 arcmin corresponds to 0.2 pc.

Figure 23 shows the area around the cloudlet MonR2, with sources IRS2 and IRS3, from 800 microns data (adapted from Greaves et al. 1995a). Here the magnetic field lines at first glance may appear to be roughly perpendicular to the overall major axis of the cloudlet (*B* poloidal). A detailed view shows that the magnetic field lines enter from the left, bend in the central area as measured at the telescope (circles), and exit at top right. Outside of the cloudlet, the polarization of field stars was taken from Hodapp (1987). It is interesting that a group of protostars has formed near the bend/gradient in the magnetic field - perhaps the details of the gravitational collapse process may affect how many protostars can form. Yao et al. (1997) refer to this magnetic structure as having an 'hourglass' morphology, because on the cloud scale the magnetic field seems to be oriented along the twin gas outflows (blue lobe 2'NW, red lobe 2' SE), and because on the small scale they see a tight pinching of the magnetic field near the IRS1/IRS2 starforming areas due to a supercritical collapse of a part of the the original cloud.

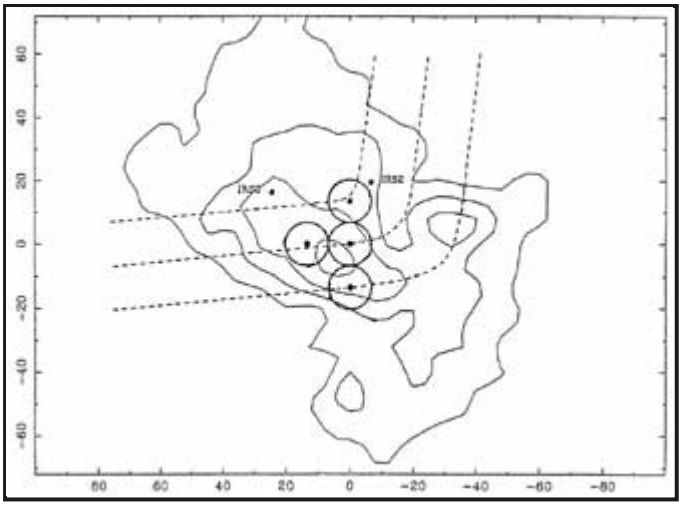

Figure 23. Observed magnetic field lines in the interstellar cloudlet MonR2, as seen at he JCMT near 800 μm (adapted from Greaves et al. 1995c). Dashes represent the magnetic field lines, which very roughly follow the minor axis, but are seen in detail to bend near the cloudlet centre. The units in x and y axes are in arcsec, with (0,0) at RA = 06h 05m 19.8s, and Dec = - 06° 22'40.7". At 950 pc away, 1 arcmin corresponds to 0.3 pc.

Aitken et al. (1997) proposed both a poloidal magnetic field for the elongated cloudlet OMC-1 at 450 pc with size ~ 80" (0.17 pc), as well as a toroidal magnetic field for an embedded core/disk with size ~ 5" (0.01 pc).

From the limited number of Extreme IR polarimetric maps available for cloudlets/protostellar disks, there is no clear preference in favour of any of the proposed theoretical models, and all the potential percentage correlations and angle corrrelations still remain to be rigorously proven.

7.6. Many Unanswered Questions

There are many questions yet to be answered in this area. These include:

- What are the most likely magnetic field structures in interstellar cloudlets ? Many theories abound (see above), but a firm global observational picture is needed.
- How is the magnetic field structure affected by the formation of a high-mass star ? Many theories predict magnetic field curvature, field twisting, and field disorder.
- What is the magnetic field structure of cold 10 K dark cloudlets ? Many such cloudlets are too faint for current instrumental sensitivities. Many theories predict some magnetic support of these cloudlets.
- What is the magnetic field structure of cold cloudlets having just started to produce a single protostar ? This could give some clues to the early stage of star formation.
- Do magnetic fields collimate protostellar outflows, and do they interconnect the cloudlet with the surrounding interstellar material ? Many theories predict the removal of angular momentum from the protostellar cloudlet to the environment, and the observational details are lacking.
- Etc.

8. STRIPES AND CLOUDLETS AT NEAR-INFRARED, OPTICAL, AND ULTRAVIOLET WAVELENGTHS (~ 10^{-6} GAUSS)

8.1. Gas Stripes near Planetary Nebulae

Some planetary nebulae seem to be located near gaseous stripes, with the orientation of the narrow (~ 0.1 pc), long (~ 2 pc) stripes being parallel to the Galactic Plane. The stripes could have come from stripping of the gas previously in the halo of planetary nebulae, due to the relative motion of the central star ~ 20 km/s. The stripes could also be ionized by the central star of the planetary nebulae at a distance ~ 0.5 pc away, and be oriented by the shape of the galactic magnetic field (~ 10^{-6} Gauss) reconnecting in the gas behind the planetary nebula's motion (e.g., Soker and Zucker 1997; Soker and Dgani 1997).

8.2. Cloudlets in Filaments

Messinger et al. (1997) have studied the variations of linear polarization percentages and position angles at wavelengths from 0.36 μm up to 2.0 μm, of 3 stars located behind the filamentary Taurus Molecular Cloud-1, located way off the Galactic Plane. They assigned the observed variations to cloudlets (subclouds) located within the filament. Each cloudlet has a gas density ~ 10^4 cm^{-3}, radius ~ 0.1 pc, gas temperature ~ 10 K, and a mass ~ $2M_{\odot}$, and may harbor a site of low-mass star formation inside. They used a deconvolution technique, separating the Stokes parameters Q and U into a linear sum of cloudlets 1 and 2, to subtract a low-density foreground cloudlet 1 from the higher-density cloudlets 2 and 3, and thus obtain grain information inside each cloudlet. The data for the heavily reddeded star HD 29647 imply grains inside cloudlet 2 to be 1.3 times larger than grains outside (~ 0.1 μm), with icy mantles on the grains, and to have an internal magnetic field roughly perpendicular to the elongation of the overall filament TMC-1. The low-density filament has a magnetic field parallel to the galactic magnetic field outside the filament.

8.3. Diffuse Interstellar Dust Near and in between Stars

Photons at near-IR, optical, and ultraviolet wavelengths, from 2.2 μm down to 0.12 μm, can be absorbed by dust. The observed polarization amplitude is a function of wavelength and varies with 2 parameters (λ_{max}, p_{max}) in the modified Serkowski relation:

$$p(\lambda) = P_{max} \cdot e^{-k.u}, \quad \text{with } k \approx 1.66\lambda_{max} + 0.01, \quad \text{and } u = \ln^2(\lambda_{max}/\lambda),$$

and p_{max} in % is the maximum amplitude of the polarization found at λ_{max} in μm (e.g., Whittet 1996; Clayton et al. 1995; Whittet et al. 1992; Serkowski 1973). This $p(\lambda)$ form is purely empirical but still reminiscent of Mie scattering theory. Typical values are $p_{max} \approx 3\%$ and $\lambda_{max} \approx 0.55$ μm.

It was suggested by Martin and Whittet (1990) that in the near-IR ($\lambda > 2.2$ μm) an alternative law $p(\lambda)$ λ^{β} with $\beta \approx -1.8$ might be more representative locally.

In the far ultraviolet (~ 1500 Å; ~ 0.15 μm), half of the polarization data have an observed value close to that predicted by the Serkowski relation, and half of the polarization data have an excess above the predicted value (e.g., Anderson et al. 1996), which may imply that a small modification of the parameter k may be required in the UV ($k \approx 2.8$ λ_{max}).

Physically, p_{max} is related directly to the extinction, and thus indirectly to the distance of the star. The $p(\lambda)$ curves of stars seen through dark cloud complexes tend to exhibit a larger $\lambda_{max} \approx 0.75$ μm (e.g., Breger et al. 1981). Physically, λ_{max} is related to the mean size of the polarized grain.

Dust grains are in an active, dynamic/turbulent environment, so to keep them aligned with a magnetic field would require a significant field strength. The alignment of dust grains by the interstellar magnetic field is thought to be due to the Davis-Greenstein mechanism (paramagnetic relaxation of the spin axis of the aspherical dust grain to the direction of the ambient magnetic field), modified to include suprathermal spinup (repeated formations of H_2 at the same site on a grain allowing the grain to spin up, like a spinning rocket) and superparamagnetic inclusions (small clumps of iron in a grain will give it a greater magnetic susceptibility, like a supermagnet) (e.g. Jones 1996). Hildebrand (1988a) also favors alignment of superparamagnetic grains by the modified Davis-Greenstein mechanism. Some evidence for superparamagnetic inclusions have been discussed by Martin (1995). An alternative model, that the alignment of elongated grains along the streaming motion of gas à la Gold (putting the long axis of the grain along the gas motion)or the streaming motion of photons, can be rejected (e.g., Hildebrand 1988b), since streaming of gas along the galactic plane would put the long axis of the grain along the galactic plane, hence the E-vector of the optical polarization observed will be perpendicular to the galactic plane due to preferential absorption of light, contrary to what is observed (e.g., Hildebrand 1989).

Chemically, the respective amounts of carbonaceous and graphite grains (optical hump effects) versus silicate grains (near-IR

and optical effects) and their effects on λ_{max} are still being debated. In the Far-UV, the extinction data seem to require the presence of a mixture of many PAH (Polycyclic Aromatic Hydrocarbons) (e.g., Li and Greenberg 1997).

To *B* or not to *B* ? Some optical/near-infrared polarization maps were made of nearby cloudlets, notably Ophiuchi (e.g., Bastien and Ménard 1990; Goodman et al. 1990), using stars at specified locations. Linear polarization maps of Young Stellar Objects with a pattern of aligned polarization vectors at optical wavelengths as observed very close to the central object have been interpreted in terms of multiple scattering in flattened optically thick structures, not in terms of magnetically aligned elongated grains (Bastien and Ménard 1990). These optical patterns provide direct evidence for circumstellar disks around YSO. Optical/near-infrared polarization mapping can indicate large dust scattering effects, saying nothing about the magnetic field. Optical polarization mapping can best be done for the more nearby cloudlets (distant from the Earth by < 1 kpc). Optical polarization maps due to dust scattering can tell us more about the distribution and structure of dust grains (polarization position angles) and about grain sizes (polarization percentages) (e.g., Fischer 1995), *but nothing on magnetic fields.* Casali (1995) observed at near-IR (λ1.25 μm to λ2.2 μm) some 33 young stellar objects in L1641 dark cloud (size of 10 × 40 pc), and found a huge random orientation of the *E*-vector polarization position angles, telling us *nothing on the link between these YSO and the cloud's magnetic field* in most clouds (Goodman et al. 1995). Carlqvist and Kristen (1997) summed up a numerical study of magnetic fields in filaments as seen at optical and near IR wavelengths, by finding that it is difficult to figure out the geometry of the magnetic field from optical/near IR polarization observations, and also difficult to determine the strength of the magnetic field.

There are exceptions. Tamura et al. (1996) have found one cloud where they claim the opposite, namely that near Infrared polarimetry does reveal the magnetic field in the dark cloud. The existing bank of optical polarization observations of stars near cloudlets along 8000 lines of sight (e.g., Axon and Ellis 1976 ; Bastien 1996) could be of use in comparing with radio polarization data, althought optical stars exactly behind dark cloudlets will not be seen at optical wavelengths. This comparison is not often made.

Fortunately, Extreme-IR (submillimeter), Far IR, and mid-IR wavelength polarization observations, and all mapping at long wavelengths λ, involve no dust scattering, since scattering varies with the wavelength λ as λ^{-4} (e.g., Tamura et al. 1988 Tamura et al. 1993; Bhatt and Jain 1992). Thus the emission component seen is the true component, along the line of sight.

9. CONCLUSION

Starting with magnetic phenomena on Earth (e.g., Fig. 1), a brief summary of our observational knowledge of the magnetic fields has been presented for the interplanetary medium (Fig. 5), for objects therein (Figs. 2, 3), and their association with angular momentum (Fig. 4). The methodology of signal detection from Earth has been discussed (Figs. 7 , 8). Remanent magnetism (random shape) or dynamo magnetism (dipolar shape) can explain the maintenance of magnetism in most solar system objects. In a few cases, a dead or dying dynamo may be involved. The interplanetary medium supports an Archimedean spiral-shaped magnetic field, usually with 4 magnetic sectors (e.g., Fig. 6).

Outside the solar system, the magnetism of normal stars can be mostly explained by a large scale dipolar dynamo, with the possible addition of small scale loop-type magnetism localized on the stellar surfaces. In a few cases, a quadrupolar shape field is necessary. For compact degenerate stars, a frozen dipolar magnetic field is found.

Over recent years, direct measurements of the magnetic field strength and direction in dusty protostellar disks and dusty molecular cloudlets have shown that hydromagnetic processes are essential to understanding their internal physics and evolution. The ultimate goal of obtaining a full understanding of the magnetic field in the formation and evolution of molecular disks and cloudlets is a challenging task. Is the magnetic field a strong player/guide or else a weak player/tracer ? A preliminary answer favours a moderately strong (but not dominant) magnetic field.

Observational studies have been mainly limited by numerous practical difficulties of measuring magnetic fields in astronomical objects, *via* dust emission (weighted by grain properties), or *via* Faraday rotation (weighted by electron density) or *via* Zeeman effect (with instrumental sensitivity effects) (e.g., Davies 1994).

A succinct review and a short classification of various magnetic field models for protostellar disks has been made (Figs. 10 to 14), and a time evolution discussed (Fig. 17). Although the geometry of the magnetic field could be partially preserved (e.g., poloidal) when clouds contract from the interstellar medium (Fig. 21; e.g., Jones et al. 1992), after a while the increasing differential rotation of the protostellar disk may completely change the *B* lines to become spiral (toroidal). Cool protostellar disks and cloudlets are only detected in emission at Extreme IR and Far IR wavelengths, and their low polarized flux density values present a technical challenge for such telescopes (e.g., Fig. 9).

Magnetic protostellar models involve "twist", "circulation", "cloud collapse", "disk-wind", "magnetic pinch", "hourglass", as

well as "dynamo".

A list of observational data for magnetism in cloudlets/protostellar disks has been presented (Table 1). Possible correlations have been discussed: polarization percentage correlating with wavelength, with beam size, with source age, and polarization position angle correlating with companion presence (Fig. 19), with viewing angle, with beam size, and with source age. For disks/cloudlets, the main predictions (Fig. 15, 16) and the effect of telescope beams (Fig. 18) have been noted and used in comparing selected observational maps (Figs. 20, 22, 23).

Future trend: polarimetry at Extreme IR and Far IR is the most effective way to determine unambiguously the direction (position angle) of the magnetic field in protostellar disks and in molecular cloudlets, since it measures the emission of polarized radiation. Scattered light is not a problem at long wavelengths. Extreme-IR (submillimeter), Far IR, and mid-IR wavelength polarization observations are not affected by dust scattering since light scattering varies as $(\text{wavelength})^{-4}$.

Clearly this research area at Extreme-infrared wavelengths is in its infancy, much in need of more polarimetric data, and has a potential for a rapid growth in our physical understanding. The time is ripe for a major observational advance, with the recent improvements in polarimetric technology in the Extreme IR and Far IR. At these wavelengths, polarimetry is a powerful method to study circumstellar, protostellar, and interstellar magnetic fields. and it is limited by the Earth's atmosphere, observing time required, and lack of polarimetric instruments at many telescopes.

A good polarimetric map in the Extreme IR and Far IR will in itself say a good deal, and it may inspire new theoretical work. Magnetic field orientations are crucial in most models of formation and evolution of disks and cloudlets and in star formation. Sensitive array receivers could open up a rich and exciting field of study in polarimetry. A reasonable 10 × improvement in sensitivity would result in a decrease in observing time by a factor 100, when aiming for the same signal to noise ratio.

Acknowledgements

I thank Ms. Lyne Séguin (NRCC-Ottawa) for creative help in drawing Figures 10 to 14 and 16, Mr. David Duncan (NRCC-Victoria) for drawing Figures 1, 2, 3, 5, 7, 8, 17, while I used the PGPLOT software for Figures 4 and 19. I thank a referee (anonymous) for thoughtful and valuable advice, and Dr. D. C. Morton (NRCC-Victoria) for a reading of an early version.

REFERENCES

1. Acuna, M.H., Connerney, J.E., Wasilewski, P., Lin, R.P., Anderson, K.A., Carlson, C.W., McFadden, J., Curtis, D.W., Mitchell, D., Reme, H., Mazelle, C., Sauvaud, J.A., d'Uston, C., Cros, A., Medale, J.L., Bauer, S.J., Cloutier, P., Mayhew, M., Winterhalter, D., Ness, N.F. 1998, Science, 279, 1676-1680.
2. Aitken, D.K., Wright, C.M., Smith, C.H., Roche, P.F. 1993, M.N.R.A.S., 262, 456-464.
3. Aitken, D.K., Smith, C.H., Moore, T.J., Roche, P.F., Fujiyoshi, T., Wright, C.M. 1997, Monthly Not. Roy. Astron. Soc., 286, 85-96.
4. Akeson, R.L., Carlstrom, J.E., Phillips, J.A., Woody, D.P. 1996, Ap. J., 456, L45-L48.
5. Anderson, C.M., Weitenbeck, A.J., Code, A.D., Nordsiek, K.H., Maede, M.R., Babler, B.L., Zellner, N.E., Bjorkman, K.S., Fox, G.H., Johnson, J.J. 1996, A.J., 112, 2739-2743.
6. Arce, H.G., Goodman, A.A., Bastien, P., Manset, N., Sumner, M. 1998, Ap. J., 499, L93-L97.
7. Axon, D.J., Ellis, R.S. 1976, Monthly Not. Roy. Astron. Soc., 177, 499-511.
8. Babel, J., Montmerle, T. 1997, Astron. & Astrophys., 323, 121-138.
9. Babel, J., North, P. 1997, Astron. & Astrophys., 325, 195-202.
10. Bagenal, F., Cravens, T.E., Luhmann, J.G., McNutt, R.L., Cheng, A.F. 1997, in "Pluto and Charon", ed. S.A. Stern and D.J. Tholen, Univ. Ariz. Press, Tucson, p. 523-555.
11. Bailey, J., Chrysostomou, A., Hough, J.H., Gledhill, T.M., McCall, A., Clark, S., Ménard, F., Tamura, M. 1998, Science, 281, 672-674.
12. Barvainis, R., Clemens, D.P., Leach, R. 1988, A.J., 95, 510-515.
13. Barvainis, R., McIntosh, G., Predmore, C.R. 1987, Nature, 329, 613-615.
14. Bastien, P. 1996, private communication.
15. Bastien, P. 1988, in "Polarized Radiation of Circumstellar Origin", ed. by Coyne, G.V., Magalhães, A.M., Moffat, A.F., Schulte-Ladbeck, R.E., Tapia, S., Wickramasinghe, D.T., Vatican Observatory, Vatican City State, p. 541-582.
16. Bastien, P. 1996, in "Polarimetry of the Interstellar Medium", ed. by Roberge, W.G., & Whittet, D.C., Astron. Soc. Pacific, San Francisco, USA - A.S.P. Confer. Ser., 97, 297-314.
17. Bastien, P., Ménard, F. 1990, Ap.J, 364, 232-241.
18. Baudry, A., Diamond, P.J. 1998, Astro. & Astrophys., 331, 697-708.
19. Baumgärtel, K., Sauer, K., Bogdanov, A. 1994, Science, 263, 653-655.

20. Baumgärtel, K., Sauer, K., Story, T.R., McKenzie, J.F. 1997, Icarus, 129, 94-105.
21. Bergin, E.A., Goldsmith, P.F., Snell, R.L., Ungerechts, H. 1994, Ap. J., 431, 674.
22. Bertoldi, F., McKee, C.F. 1992, Ap.J., 395, 140.
23. Bhatt, H.C., Jain, S.K. 1992, M.N.R.A.S., 257, 57-61.
24. Bianda, M., Solanki, S.K., Stenflo, J.O. 1998, Astron. & Astrophys., 331, 760-770.
25. Blackett, P.M. 1947, Nature, 159, 658-666.
26. Blitz, L. 1991, in "Molecular Clouds", ed. by R.A. James & T.J. Millar, Cambridge Univ. Press, Cambridge, U.K., p. 49-68.
27. Bloemhof, E.E., Reid, M.J., Moran, J.M. 1992, Astrophys. J., 397, 500-519.
28. Bonnell, I., Bastien, P. 1991, Ap.J., 374, 610-622.
29. Bonnell, I., Bastien, P. 1992a, Ap.J., 400, 579.
30. Bonnell, I., Bastien, P. 1992b, Ap. J, 401, 654.
31. Borra, E.F., Landstreet, J.D. 1978, Ap. J., 222, 226.
32. Brearley, A. 1997, Science, 278, 76-77.
33. Breger, M., Gehrz, R.D., Hackwell, J.A. 1981, Ap.J., 248, 963-976.
34. Brogan, C.L., et al., 1998, Ap. J., in preparation.
35. Buchanan, M. 1997, New Scientist, 26 July issue, p. 42-43.
36. Burnham, R. 1994, Astronomy, April issue, 39.
37. Burwitz, V., Reinsch, K., Beuermann, K., Thomas, H.-C. 1997, A & A, 327, 183-190.
38. Buzasi, D.L. 1997, Astrophys. J., 484, 855-861.
39. Campbell, C.G. 1997, "MagnetoHydroDynamics in Binary Stars", Kluwer Acad. Publ., Dordrecht, Netherlands (xii+306 pages).
40. Carlberg, R.G., Pudritz, R.E. 1990, Monthly Not. Roy.Astron. Soc., 247, 353.
41. Carlqvist, P., Kristen, H. 1997, Astron. & astrophys., 324, 1115-1122.
42. Casali, M.M. 1995, MNRAS, 277, 1385-1392.
43. Caselli, P., Myers, P.C. 1995, Ap.J., 446, 665-686.
44. Christodoulou, D.M., Tohline, J.E., Keenan, F.P. 1997, Ap. J., 486, 810-817.
45. Chrysostomou, A., Hough, J.H., Burton, M.G., Tamura, M. 1994, MNRAS, 268, 325-334.
46. Claussen, M.J., Frail, D.A., Goss, W.M., Gaume, R.A. 1997, Astrophys. J., 489, 143-159.
47. Clayton, G.C., Wolff, M.J., Allen, R.G., Lupie, O.L. 1995, Ap.J., 445, 947-957.
48. Clemens, D. 1996, in "Polarimetry of the Interstellar Medium", ed. by Roberge, W.G., & Whittet, D.C., Astron. Soc. Pacific, San Francisco, USA - ASP Confer Ser, 97, p. 95-99.
49. Clemens, D.P., Leach, R.,W., Barvainis, R., Kaine, B.D. 1990, P.A.S. Pacific, 102, 1064-1076.
50. Cohen, P. 1997a, New Scientist, 27 Sept. issue, p. 22.
51. Cohen, R.J. 1997b, in "High-Sensitivity Radio Astronomy", ed. by Jackson, N., & Davis, R.J., Cambridge Univ. Press, Cambridge, UK- page 65-72.
52. Cohen, R.J., Rowland, P.R., Blair, M.M. 1984, MNRAS, 210, 425.
53. Cole, K.C. 1997, Victoria times Colonist, 4 Oct. issue, p. D18.
54. Crutcher, R.M. 1994, in "Cloud, Cores, and low-mass stars", ed. D.P. Clemens & R. Barvainis, Astron. Soc. Pacific, San Francisco, USA - Astron. Soc. Pac. Conf. Series, 65, 87-96
55. Crutcher, R.M., Troland, T.H., Lazareff, B., Kazès, I. 1996, Ap. J., 456, 217-224.
56. Curren, R. 1997, Victoria Times-Colonist, B.C., 6 April issue, p. A11.
57. Davidson, J.A., Schleuning, D., Dotson, J.L., Dowell, C.D., Hildebrand, R.H. 1995, in "Airborne Astronomy Symposium on the Galactic Ecosystem", ed. by M.R. Haas et al., Astron. Soc. Pacific, San Francisco, USA - A. S. P. Conf. Ser., 73, 225-234.
58. Davies, R.D. 1994, in "Cosmical Magnetism", ed. by D. Lynden-Bell, Kluwer Acad. Publ., Dordrecht, Netherlands - NATO ASI Series C, 422, 131-141.
59. Donati, J.-F., Cameron, A.C. 1997, Monthly Not. R. Astron. Soc., 291, 1-19.
60. Donati, J.-F., Semel, M., Carter, B.D., Rees, D.E., Cameron, A.C. 1997, Monthly Not. Roy. Astron. Soc., 291, 658-682.
61. Eastlund, B.J., Miller, B., Michel, F. C. 1997, Astrophys. J., 483, 857-867.
62. Elitzur, M. 1982, Rev. Modern Physics, 54, 1225-1260.
63. Elitzur, M. 1992, Annual Rev. Ast. & Ap., 30, 75-112.
64. Elmegreen, B.G. 1985, Astrophys. J., 299, 196.
65. Elmegreen, B.G. 1988, Astrophys. Lett & Communic., 26, 207-216.
66. Elmegreen, B.G. 1993, in "Protostars & Planets III", ed. by E.H. Levy & J.I. Lumine, Univ. of Ariz. Press, Tucson, USA, p.97-124.
67. Elmegreen, B.G. 1998, in "Origins of Galaxies, Stars, Planets & Life", ed. Woodward, C.E., Thronson, H.A., Shull, M., Astron. Soc. Pacific, San Francisco, Calif. - Astron. Soc. Pac. Conf. Ser., 148, 150-183.
68. Elmegreen, B.G., Genzel, R., Moran, J.M., Reid, M.J., Walker, R.C. 1980, Astrophys. J., 241, 1007-1013.
69. Fiebig, D., Gusten, R. 1989, Astron. & Astrophys., 214, 333-338.
70. Fiedler, R.L., Dennison, B., Johnston, K.J., Hewish, A. 1987, NAture, 326, 675.

71. Fischer, O. 1995, Rev. in Modern Astronomy, 8, 103-123.
72. Fischer, O., Henning, Th., Yorke, H.W. 1994, A & A, 284, 187-209.
73. Flett, A.M., Murray, A.G. 1991, M.N.R.A.S., 249, 4p-6p.
74. Forsyth, R.J., Balogh, A., Horbury, T.S., Erdös, G., Smith, E.J., Burton, M.E. 1996, A & A, 316, 287-295.
75. Frail, D.A., Vasisht, G., Kulkarni, S.R. 1997, Ap.J., 480, L129-L132.
76. Fuller, G.A., Myers, P.C. 1992, Ap.J., 384, 523-527.
77. Fuller, M., Dobson, J., Gregor-Wieser, H., Moser, S. 1995, Brain Res. Bull., 36, 155-159.
78. Fuller, G.A., Myers, P.C. 1993, Ap. J., 418, 273.
79. Galli, D. 1995, Rev. Mex. A & A, Ser. de Confer., 1, 179-186.
80. Geim, A. 1998, Physics Today, 51, no. 9, 36-39.
81. Glanz, J. 1997, Science, 278, 387-388.
82. Glatzmaier, G.A., Roberts, P.H. 1996, Science, 274, 1887-1891.
83. Glenn, J., Walker, C.K., Jewell, P.R. 1997a, Ap.J., 479, 325-331.
84. Glenn, J., Walker, C.K., Bieging, J.H., Jewell, P.R. 1997b, Astrophys. J., 487, L89-L92.
85. Gloeckler, G., Fisk, L.A., Geiss, J. 1997, Nature, 386, 374-377.
86. Goodman, A.A. 1992, quoted in Myers & Khersonsky (1995, Section 3.2).
87. Goodman, A.A. 1995, in "Airborne Astronomy Symposium on the Galactic Ecosystem", ed. by M.R. Haas et al., Astron. Soc. Pacific, San Francisco, USA - A. S. P. Conf. Ser., 73, 45-52.
88. Goodman, A.A., Barranco, J.A., Wilner, D.J., Heyer, M.H. 1998, Ap.J., 504, 223-246.
89. Goodman, A.A., Bastien, P., Myers, P.C., Ménard, F. 1990, Ap.J., 359, 363-377.
90. Goodman, A.A., Jones, T.J., Lada, E.A., Myers, P.C. 1995, Astrophys. J., 448, 748.
91. Goodman, A.A., Heiles, C. 1994, Ap. J., 424, 208-221.
92. Gould, J.L. 1996a, Nature, 380, 593-594.
93. Gould, J.L. 1996b, Nature, 383, 123-124.
94. Greaves, J.S., Holland, W.S. 1998, Astron. & Astrophys., 333, L23-L26.
95. Greaves, J.S., Holland, W.S., Friberg, P., Dent. W. 1996, JCMT Newsletter, 6, 31-32.
96. Greaves, J.S., Holland, W.S., Murray, A.G. 1995a, A & A, 297, L49-L52.
97. Greaves, J.S., Holland, W.S., Murray, A.G., Nartallo, R. 1995b, Month. Not. R. A. S., 272, L1-L4.
98. Greaves, J.S., Holland, W.S., Ward-Thompson, D. 1997, Ap.J., 480, 255-261.
99. Greaves, J.S., Murray, A.G., Holland, W.S. 1994, A & A, 284, L19-L22.
100. Greaves, J.S., Bastien, P., Emerson, J.P., Holland, W.S., Minchin, N.R., Robson, E.I., Russell, S.C., Vallée, J.P., Ward-Thompson, D. 1997, Scientific Case for a Polarimeter for the BOL Instrument on FIRST, Joint Astronomy Center, Hilo, USA
101. Gurnett, D.A., Kurth, W.S., Roux, A., Bolton, S.J. 1997, Nature, 387, 261.
102. Hayashi, M., Omodaka, T., Hasegawa, T., Suzuki, S. 1985, Ap. J., 288, 170-174.
103. Heiles, C., Goodman, A.A., McKee, C.F., Zweibel, E.G. 1991, in "Fragmentation of molecular clouds & Star formation", ed. by E. Falgarone et al., Kluwer Acad. Pub., Dordrecht, Neth.- I.A.U. Symp. 147, 43-60.
104. Heiles, C., Goodman, A.A., McKee, C.F., Zweibel, E.G. 1993, in "Protostars & Planets III", ed. by E.H. Levy & J.I. Lunine, Univ. Ariz. Press, Tucson, AZ., USA, p. 279.
105. Henriksen, R.N. 1986, Ap.J., 310, 189-206.
106. Henriksen, R.N. 1991, Ap.J., 377, 500-509.
107. Henriksen, R.N., Valls-Gabaud, D. 1994, Monthly Not. Roy. Astron. Soc., 266, 681.
108. Heyer, M.H., Carpenter, J.M., Ladd, E.F. 1996, Astrophys. J., 463, 630-641.
109. Hildebrand, R.H. 1983, Q.J.R.A.S., 24, 267-282.
110. Hildebrand, R.H. 1988a, Ap. Lett. & Comm., 26, 263-275.
111. Hildebrand, R.H. 1988b, Q.J.R.A.S., 29, 327-351.
112. Hildebrand, R.H. 1989, in "Interstellar Dust", ed. by Allamandola, L.J., & Thielens, A.G., Kluwer, Dordrecht, Netherlands - I.A.U. Symp., 135, 275-281.
113. Hildebrand, R.H. 1996, in "Polarimetry of the Interstellar Medium", ed. by Roberge, W.G., & Whittet, D.C., Astron. Soc. of the Pacific, San Francisco, USA - A.S.P. Confer. Ser., 97, 254-268.
114. Hildebrand, R.H., Dotson, J.L., Dowell, C.D., Platt, S.R., Schleuning, D., Davidson, J.A., Novak, G. 1995, in "Airborne Astronomy Symposium on the Galactic Ecosystem", ed. by M.R. Haas et al., Astron. Soc. Pacific, San Francisco, USA - A.S.P. Conf. Ser., 73, 97-103.
115. Hodapp, K.-W. 1987, A & A, 172, 304-310.
116. Holland, W.S., Greaves, J.S., Ward-Thompson, D. 1994, JCMT Newsletter, 3, 51-53.
117. Holland, W.S., Greaves, J.S., Ward-Thompson, D., André, Ph. 1996, A & A, 309, 267-274.
118. Hubbard, W.B. 1984, "Planetary Interiors", van Nostrand Reinhold Co., New York, USA.
119. Hubbard, W.B., Stevenson, D.J. 1984, in "Saturn", ed. by Gehrels, T., Matthews, M.S., University of Arizona Press, Tucson, Ariz,, USA, p. 47-87.
120. Hutawarakorn, B., Cohen, R.J. 1996, in "Polarimetry of the Interstellar Medium", ed. by Roberge, W.G., & Whittet, D.C., Astron. Soc. Pacific, San Francisco, USA - A.S.P. Confer. Ser., 97, 532-536.

121. Ignace, R., Nordsieck, K.H., Cassinelli, J.P. 1997, Ap. J., 486, 550-570.
122. Israelian, G., Chentsov, E., Musaev, F. 1997, Monthly Not. Roy. Astron. Soc., 290, 521-532.
123. Jeanloz, R., Romanowicz, B. 1997, Physics Today, August ed., 22-27.
124. Jones, T.J. 1996, in "Polarimetry of the Interstellar Medium", ed. by Roberge, W.G., & Whittet, D.C., Astron. Soc. Pacific, San Francisco, USA - A.S.P. Confer. Ser., 97, 381-395.
125. Jones, T.J., Klebe, D.I., Dickey, J.M. 1992, Ap. J., 389, 602-615.
126. Jones, B.F., Fischer, D.A., Stauffer, J.R. 1996, Astron. J., 112, 1562.
127. Kaifu, N., Suzuki, S., Hasegawa, T., Morimoto, M., Inatani, J., Nagane, K., Miyazawa, K., Chikada, Y., Kanzawa, T., Akabane, K. 1984, A & A, 134, 7-12.
128. Kane, B.D., Clemens, D.P., Barvainis, R., Leach, R.W. 1993, Ap. J., 411, 708-719.
129. Kemball, A.J., Diamond, P.J. 1997, Ap.J., 481, L111-L114.
130. Kerr, R.A. 1997, Science, 277, 1924.
131. Khurana, K.K., Kivelson, M.G., Russell, C.T., Walker, R.J., Southwood, D.J. 1997, Nature, 387, 262.
132. Kiernan, V. 1997, New Scientist, 1 Feb. issue, p.10.
133. Kirschvink, J.L. 1997, Nature, 390, 339-340.
134. Kivelson, M.G., Wang, Z., Joy, S., Khurana, K.K., Polanskey, C., Southwood, D.J., Walker, R.J. 1995, Adv. Space Res., 16, no.4, 59-68.
135. Kivelson, M.G., Khurana, K.K., Russell, C.T., Walker, R.J., Warnecke, J., Coroniti, F.V., Polanskey, C., Southwood, D.J., Schubert, G. 1996a, Nature, 384, 537-541.
136. Kivelson, M.G., Khurana, K.K., Walker, R.J., Russell, C.T., Linker, J.A., Southwood, D.J., Polanskey, C. 1996b, Science, 273, 337-340.
137. Kivelson, M.G., Khurana, K.K., Walker, R.J., Warnecke, J., Russell, C.T., Linker, J.A., Southwood, D.J., Polanskey, C. 1996c, Science, 274, 396-398.
138. Kivelson, M.G., Khurana, K.K., Joy, S., Russell, C.T., Southwood, D.J., Walker, R.J., Polansky, C. 1997, Science, 276, 1239.
139. Klebe, D.I., Dahm, M.A., Stencel, R.E. 1996, in "Polarimetry of the Interstellar Medium", ed. by Roberge, W.G., & Whittet, D.C., Astron. Soc. Pacific, San Francisco, USA - ASP Confer Ser, 97, p. 79-84.
140. Königl, A. 1995, Rev. Mex. A & A Ser. Confer., 1, 275-283.
141. Königl, A., Ruden, S.P. 1993, in "Protostars & Planets III", ed. by E.H. Levy & J.I. Lumine, Univ. of Ariz. Press, Tucson, USA, p. 641-687.
142. Kouveliotou, C., Dieters, S., Strohmayer, T., van Paradijs, J., Fishman, G.J., Meegan, C.A., Hurley, K., Kommers, J., Smith, I., Frail, D., Murakami, T. 1998, Nature, 393, 235-237.
143. Kulkarni, S.R., Thompson, C. 1998, Nature, 393, 215-216.
144. Kulsrud, R.M. 1997, in "Critical Dialogues in Cosmology", ed. By N. Turok, World Scientific, Singapore, pages 328-340.
145. Kylafis, N. 1983, Ap. J., 267, 137-150.
146. Lai, D., Salpeter, E.E. 1997, Ap. J., 491, 270-285.
147. Lamb, D.Q., Melia, F. 1988, in "Polarized Radiation of Circumstellar Origin", ed. by Coyne, G.V., Magalhães, A.M., Moffat, A.F., Schulte-Ladbeck, R.E., Tapia, S., Wickramasinghe, D.T., Vatican Observatory, Vatican City State, p. 45-84.
148. Landstreet, J.D. 1990, Ap. J., 352, L5-L8.
149. Lang, K.R. 1992, "Astrophysical Data - Planets and Stars", Springer-Verlag, New York, USA. p. 45-47.
150. Lanzerotti, L.J., Krimigis, S.M. 1985, Physics Today, 38, no. 11, 24-34.
151. Lapointe, S.M., Vallée, J.P. 1970, J. Geophys. Research, 75, 6991-6998.
152. Larson, R.B. 1979, M N R A S., 186, 479-490.
153. Lazarian, A., Goodman, A.A., Myers, P.C. 1997, Ap. J., 490, 273-280.
154. Leach, R.W., Clemens, D.P., Kane, R.D., Barvainis, R. 1991, Ap.J., 370, 257-262.
155. Leroy, J.-L. 1985, in "Measurements of Solar Vector Magnetic Fields", ed. By Hagyard, M.J., NASA Conf. Publ., 2374, p. 121.
156. Levy, E.H., Sonett, C.P. 1978, in "Protostars & Planets", ed. by T. Gehrels, Univ. Ariz. Press, Tucson, USA - p.516-532.
157. Li, A., Greenberg, J.M. 1997, Astron. & Astrophys., 323, 566-584.
158. Lin, D.N., Papaloizou, J.C. 1993, in "Protostars & Planets III", ed. E.H. Levy & J.I. Lunine, Univ. of Ariz. Press, Tucson, Ariz., USA, pages 749-835.
159. Lin, R.P., Mitchell, D.L., Curtis, D.W., Anderson, K.A., Carlson, C.W., McFadden, J., Acuna, M.H., Hood, L.L., Binder, A. 1998, Science, 281, 1480-1484.
160. Little, L.T., Heaton, B.D., Dent, W.R. 1990, Astron. & Astrophys., 232, 173-183.
161. Lizano, S., Shu, F.H. 1989, Ap.J., 342, 834-854.
162. Lohmann, K.J., Lohmann, C.M. 1996, Nature, 380, 59-61.
163. Lovelace, R.V., Zweibel, E. G. 1997, Astrophys. J., 485, 285-289.
164. Lovelace, R.V., Berk, H.L., Contopoulos, J. 1991, Ap.J, 379, 696-705.
165. Mac Low, M.-M. 1998, in "The Orion Complex Revisited", Astron. Soc. Pacific Conf. Ser., in press

166. Main, P. 1997, New Scientist, 12 April issue, p.13.
167. Manset, N., Bastien, P. 1995, Publ. Astron. Soc. Pacific, 107, 483-487.
168. Martin, P.G. 1995, Astrophys. J., 445, L63-L66.
169. Martin, P.G., Whittet, D.C. 1990, Astrophys. J., 357, 113.
170. Martin, C.E., Heyvaerts, J., Priest, E.R. 1997, Astron. & Astrophys., 326, 1176-1186.
171. Mathys, G., Hubrig, S. 1997, Astron. Astrophys. Suppl. Ser., 124, 475-497.
172. Mathys, G., Hubrig, S., Landstreet, J.D., Lanz, T., Manfroid, J. 1997, Astron. & Astrophys. Suppl. Ser., 123, 353-402.
173. Mazelle, C., Rome, H., Neubauer, F.M., Glassmeier, K.-H. 1995, Adv. Space Res., 16, no.4, 41-45.
174. McCutcheon, W.H. 1992, J.R.A.S. Canada, 86, 195-209.
175. McIntosh, G.C., Predmore, C.R. 1996, in "Polarimetry of the Interstellar Medium", ed. by Roberge, W.G., & Whittet, D.C., Astron. Soc. Pacific, San Francisco, USA - ASP Confer Ser, 97, p. 207-211.
176. Meier, D.L., Edgington, S., Godon, P., Payne, D.G., Lind, K.R. 1997, Nature, 388, 350-352.
177. Melatos, A., Johnston, S., Melrose, D.B. 1995, MNRAS, 275, 381-397.
178. Merrill, R.T. 1997, Nature, 389, 678-679.
179. Messinger, D.W., Whittet, D.C., Roberge, W.G. 1997, Astrophys. J., 487, 314-319.
180. Mikhajlov, Y.M., Maslenitsyn, S.F. 1995, Solar System Res., 29, 369-378.
181. Minchin, N.R., Murray, A.G. 1994, A & A, 286, 579-587.
182. Minchin, N.R., Hough, J.H., Burton, M.G., Yamashita, T. 1991, MNRAS, 251, 522-528.
183. Minchin, N.R., Sandell, G., Murray, A.G. 1995, A & A, 293, L61-L64.
184. Minchin, N.R., Bonifacio, V.H., Murray, A.G. 1996, A & A, 315, L5-L8.
185. Moffat, A.F. 1988, in "Polarized Radiation of Circumstellar Origin", ed. by Coyne, G.V., Magalhães, A.M., Moffat, A.F., Schulte-Ladbeck, R.E., Tapia, S., Wickramasinghe, D.T., Vatican Observatory, Vatican City State, p. 539-540.
186. Monaghan, J.J. 1983, Proc. Astron. Soc. Austral., 5, 163-165.
187. Moneti, A., Pipher, J.L., Helfer, H.L., McMillan, R.S., Perry, M.L. 1984, Astrophys. J., 282, 508-515.
188. Moran, C., Marsh, T.R., Dhillon, V.S. 1998, Mont. Not. Roy. Astron. Soc., 299, 218-222.
189. Morton, S.A., Mouschovias, T. Ch., Ciolek, G.E. 1994, Ap. J., 421, 561-569.
190. Mouschovias, T.C. 1985, A & A, 142, 41-47.
191. Mouschovias, T. Ch., Paleologou, E.V., Fiedler, R. A. 1985, Ap. J., 291, 772-797.
192. Mukherjee, S., Kembhavi, A. 1997, Ap. J., 489, 928-940.
193. Mundy, L.G., Wootten, A., Wilking, B.A., Blake, G.A., Sargent, A.I. 1992, Ap. J., 385, 306-313.
194. Murray, A.G. 1991, JCMT-UKIRT Newsletter, 2, 19-19.
195. Myers, P.C. 1991, in "Molecular Clouds", ed. James, R.A., Millar, T.J., Camb. Univ. Press, Cambridge, U.K. - p.133-139.
196. Myers, P.C., Goodman, A.A. 1988, Ap. J., 329, 392-405.
197. Myers, P.C., Goodman, A.A. 1990, in "Galactic and Intergalactic magnetic fields", ed. Beck, R. et al., Kluwer, Dordrecht, Netherlands - I.A.U. Symp., 140, 309-311.
198. Myers, P.C., Khersonsky, V.K. 1995, Ap. J., 442, 186-196.
199. Nakano, T. 1998, Astrophys. J., 494, 587-604.
200. Nakano, T., Nishi, R., Umebayashi, T. 1996, in "The Role of Dust in the Formation of Stars", ed. by H.U. Käufl & R. Siebenmorgen, Springer-Verlag, Berlin, Germany, p. 393.
201. Navarro, J., Manchester, R.N., Sandhu, J.S., Kulkarni, S.R., Bailes, M. 1997, Astrophys. J., 486, 1019-1025.
202. Nedohula, G.E., Watson, W.D. 1994, Ap. J., 423, 394.
203. Ness, N.F., et al. 1979, Science, 204, 982.
204. Newman, W.I., Newman, A.L., Lovelace, R.V. 1992, Ap.J., 392, 622-627.
205. Novak, G., Predmore, R., Goldsmith, P.F. 1990, Ap.J., 355, 166-171.
206. Olson, P. 1997, Nature, 389, 337-338.
207. Ossendrijver, A.J., Hoyng, P. 1997, Astron. & Astrophys., 324, 329-343.
208. Parker, E.N. 1958, Astrophys. J., 128, 664.
209. Parker, E.N. 1979, "Cosmical Magnetic Fields", Clarendon Press, Oxford, UK, xviii+842 p.
210. Parker, E.N. 1983, Scientific American, August issue, 249, no.2, 44-54.
211. Parker, E.N. 1993, Astrophys. J., 408, 707.
212. Payne, J.M., Emerson, D.T., Jewell, P.R. 1993, NRAO Newsletter, 57, 5-5.
213. Phillips, J.P. 1997, Astron. & Astrophys., 325, 755-757.
214. Podolak, M., Hubbard, W.B., Stevenson, D.J. 1991, in "Uranus", ed. Bergstralh, J.T., Miner, E.D., Matthews, M.S., Univ. Ariz. Press, Ticson, Ariz., USA, p. 29-61.
215. Pudritz, R.E. 1985, Ap.J., 293, 216-229.
216. Pudritz, R.E. 1986, Publ. Astron. Soc. Pacific, 98, 709-731 (erratum, 98, 894-895).
217. Pudritz, R.E., Norman, C.A. 1983, Ap.J, 274, 677-697.
218. Pudritz, R.E., Silk, J. 1987, Ap.J, 316, 213-226.
219. Radhakrishnan, V., Cooke, D.J. 1969, Astrophys. lett., 3, 225.
220. Raloff, J. 1998, Science News, 153, 29-31.

221. Rao, R., Crutcher, R.M., Plambeck, R.L., Wright, M.C. 1998, Ap. J., 502, L75-L78.
222. Ratkiewicz, R., Barnes, A., Molvik, G.A., Spreiter, J.R., Stahara, S.S., Vinokur, M., Venkateswaran, S. 1998, Astron. & Astrophys., 335, 363-369.
223. Ricotti, M., Ferrara, A., Miniati, F. 1997, Astrophys. J., 485, 254-262.
224. Roberts, D.A., Crutcher, R.M., Troland, T.H., Goss, W.M. 1993, Ap. J., 412, 675-683.
225. Roberts, D.A., Crutcher, R.M., Troland, T.H. 1995, Ap. J., 442, 208-227.
226. Roberts, D.A., Dickel, H.R., Goss, W.M. 1997, Ap.J., 476, 209-220.
227. Romani, R.W. 1990, Nature, 347, 741.
228. Russell, C.T. 1978, Nature, 272, 147-148.
229. Saint-Germain, M. 1996, L'Actualité, Québec, 1 Dec., 60.
230. Sandford, S.A. 1996, in "Polarimetry of the Interstellar Medium", ed. by Roberge, W.G., Whittet, D.C., Astron. Soc. Pacific, San Francisco, USA - Astron. Soc. Pacific Conf. Series, 97, 29-47.
231. Sarson, G.R., Jones, C.A., Zhang, K., Schubert, G. 1997, Science, 276, 1106-1108.
232. Sato, S., Nagata, T., Nakajima, T., Nishida, M., Tanaka, M., Yamashita, T. 1985, Ap.J., 291, 708-715.
233. Scalo, J.M. 1987, in "Interstellar Processes", ed. Hollenbach, D.J., Thronson, H.A., Reidel Publ. Co., Dordrecht, Netherlands - Ap. & Sp. Sci. Lib., 134, 349-392.
234. Scanlan, R. 1997, New Scientist, 10 May issue, p.16.
235. Schleuning, D.A. 1998, Ap. J., 493, 811-825.
236. Schleuning, D.A., Dowell, C.D., Hildebrand, R.H., Platt, S.R., Novak, G. 1997, Publ. Astron. Soc. Pacific, 109, 307-318.
237. Schubert, G., Ross, M.N., Stevenson, D.J., Spohn, T. 1988, in "Mercury", ed. by Vilas, F., Chapman, C.R., Matthews, M.S., Univ. Ariz. Press, Tucson, Ariz., USA, p. 429-460.
238. Schubert, G., Solomon, S.C., Turcotte, D.L., Drake, M.J., Sleep, N.H. 1992, in "Mars", ed. by Jakosky, B.M., Snyder, C.W., Matthews, M.S., Univ. Ariz. Press, Tucson, Ariz., USA, p. 147-183.
239. Schulte-Ladbeck, R.E. 1988, in "Polarized Radiation of Circumstellar Origin", ed. by Coyne, G.V., Magalhães, A.M., Moffat, A.F., Schulte-Ladbeck, R.E., Tapia, S., Wickramasinghe, D.T., Vatican Observatory, Vatican City State, p. 319-352.
240. Seaquist, E.R., Taylor, A.R., Button, S. 1984, Astrophys. J., 284, 202.
241. Serkowski, K. 1973, I.A.U. Symp. 52, 145.
242. Serkowski, K. 1974, in "Planets, Stars and Nebulae Studied with Photopolarimetry", ed. T. Gehrels, Univ. Ariz. Press, Tucson, USA, p. 135.
243. Shi-Hui, Y. 1994, "Magnetic fields of celestial Bodies", Kluwer Acad. Publ., Dordrecht, Netherlands - Astrophys. & Space Science Library, 198, p. xvi +340.
244. Shu, F.H., Adams, F.C., Lizano, S. 1987, Annual Rev. A & A, 25, 23-81.
245. Shu,F.H., Lizano, S., Roden, S.P., Najita, J. 1988, Ap.J, 328, L19-L23.
246. Shu, F.H, Najita, J., Galli, D., Ostriker, E., Lizano, S. 1993, in "Protostars & Planets III", ed. E.H. Levy & J.I. Lunine, Univ. Ariz. Press, Tucson, Ariz, USA, p. 3-45.
247. Shu, F.H., Shang, H., Glassgold, A.E., Lee, T. 1997, Science, 277, 1475-1479.
248. Shuter, W.L., Dickman, R.L. 1990, in "Galactic and intergalactic magnetic fields", ed. Beck, R., et al., Kluwer, Dordrecht, Netherlands - I.A.U. Symp., 140, 314-314.
249. Smith, C.H., Moore, T.J., Aitken, D.K., Fujiyoshi, T. 1997, Publ. Astron. Soc. Australia, 14, 179-188.
250. Soker, N., Dgani, R. 1997, Astrophys. J., 484, 277-285.
251. Soker, N., Zucker, D.B. 1997, Monthly Not. Roy. Astron. Soc., 289, 665-670.
252. Solanski, S.K., Motamen, S., Keppens, R. 1997, Astron. & Astrophys., 324, 943-948.
253. Spinrad, H., Brown, M., Johns, C.M. 1994, A.J., 108, 1462-1470.
254. Stenflo, J.O. 1982, Solar Physics, 80, 209.
255. Stepinski, T.F. 1995, Rev. Mex. A & A Ser Confer, 1, 267-274.
256. Stepinski, T.F., Levy, E.H. 1990, Ap.J, 350, 819-826.
257. Stone, M.E. 1970a, Astrophys. J., 159, 277.
258. Stone, M.E. 1970b, Astrophys. J., 159, 293.
259. Sugiura, N., Strangway, D.W. 1988, Chapt. 8 in "Meteorites and the Early Solar System", ed. by Kerridge, J.F., & Matthews, M.S., University of Arizona Press, Tucson, USA, p.595-615
260. Tamura, M., Hasegawa, T., Ukita, N., Gatley, I., McLean, I.S., Burton, M.G., Rayner, J.T., McCaughrean, M.J. 1988, Ap.J., 326, L17-L21.
261. Tamura, M., Hayashi, S., Itoh, Y., Hough, J.H., Chrysostomou, A. 1996, in "Polarimetry of the Interstellar Medium", ed. Roberge, W.G., & Whittet, D.C., Astron. Soc. Pacific, San Francisco, USA - A.S.P. Confer. Ser., 97, 372-377.
262. Tamura, M., Hayashi, S.S., Yamashita, T., Duncan, W.D., Hough, J.H. 1993, Ap.J, 404, L21-L24.
263. Tamura, M., Hough, J.H., Hayashi, S.S. 1995, Ap. J., 448, 346-355.
264. Taubes, G. 1997, Science, 4 July edition, p. 29.
265. Taylor, J.H., Cordes, J.M. 1993, Ap. J., 411, 674-684.
266. Thompson, C., Duncan, R.C. 1996, Ap.J., 473, 322-342.

267. Thompson, I.B., Landstreet, J.D. 1985, Astrophys. J., 289, L9-L13.
268. Tomisaka, K. 1998, Ap. J., 502, L163-L167.
269. Uchida, Y., Shibata, K. 1985, Publ. A.S. Japan, 37, 515-535.
270. Umebayashi, T., Nakano, T. 1984, "Origin and dissipation of magnetic fields in protostars and in the primitive solar nebula", in Proc. 16th ISAS Lunar Planet. Symp., 118-121.
271. Vallée, J.P. 1969, "Identification Possible des Régions Solaires Responsables des Orages Géomagnétiques Récurrents", M.Sc. (Physics) Thesis, Université de Montréal, Montréal, Québec, Canada.
272. Vallée, J.P. 1982, Astrophys. J., 261, L55-L58.
273. Vallée, J.P. 1994, Astrophys. & Space Sci., 220, 289-297.
274. Vallée, J.P. 1995a, Astrophys. & Space Sci., 234, 1-10.
275. Vallée, J.P. 1995b, Astronom. J., 110, 2256-2260.
276. Vallée, J.P. 1997, Fundamentals of Cosmic Physics, 19, 1-89.
277. Vallée, J.P., Bastien, P. 1995, Astron. & Astrophys. 294, 831-834.
278. Vallée, J.P., Bastien, P. 1996, Astron. & Astrophys., 313, 255-268.
279. Vallée, J.P., Bastien, P. 1998, JCMT Time Allocation Proposal M-98B-C39.
280. Verschuur, G.L. 1995, Ap.J., 451, 624-644.
281. Vishniac, E.T., Jin, L., Diamond, P. 1990, Ap.J, 365, 648-659.
282. Vogel, S.N., Wright, M.C., Plambeck, R.L., Welch, W.J. 1984, Ap. J., 283, 655-667.
283. Walker, M.M., Diebel, C.E., Haugh, C.V., Pankhurst, P.M., Montgomery, J.C., Green, C.R. 1997, Nature, 390, 371-376.
284. Wang, J.C. 1997, Astrophys. J., 486, L119-L122.
285. Wang, J.C., Sulkanen, M.E., Lovelace, R.V. 1990, Ap.J., 355, 38.
286. Wang, Z., Kivelson, M.G. 1996, J. Geophys. Res., 101, 24479-24493.
287. Warren-Smith, R.F., Draper, P.W., Scarrott, S.M. 1987, Monthly Not. R.A.S, 227, 749-771.
288. Weindler, P., Wiltschko, R., Wiltschko, W. 1996, Nature, 383, 158-160.
289. Weintraub, D.A., Kastner, J.H., Zuckerman, B., Gatley, I. 1992, Astrophys. J., 391, 784-804.
290. Westendorp Plaza, C., del Toro Iniesta, J.C., Cobo, B.R., Pillet, V.M., Lites, B.W. and Skumanich, A. 1997, Nature, 389, 47-49.
291. Whitney, B.A., Kenyon, S.J., Gomez, M. 1997, Astrophys. J., 485, 703-734.
292. Whittet, D.C. 1996, in "Polarimetry of the Interstellar Medium", ed. by Roberge, W.G., & Whittet, D.C., Astron. Soc. Pacific, San Francisco, USA - ASP Confer Ser, 97, p. 125-142.
293. Whittet, D.C., Martin, P.G., Hough, J.H., Rouse, M.F., Baily, J.A., Axon, D.J. 1992, Ap.J., 386, 562.
294. Wickramasinghe, D.T. 1988, in "Polarized Radiation of Circumstellar Origin", ed. by Coyne, G.V., Magalhães, A.M., Moffat, A.F., Schulte-Ladbeck, R.E., Tapia, S., Wickramasinghe, D.T., Vatican Observatory, Vatican City State, p. 3-44.
295. Willson, L.A. 1988, in "Polarized Radiation of Circumstellar Origin", ed. by Coyne, G.V., Magalhães, A.M., Moffat, A.F., Schulte-Ladbeck, R.E., Tapia, S., Wickramasinghe, D.T., Vatican Observatory, Vatican City State, p. 453-460.
296. Wolf, G.A., Lada, C.J., Bally, J. 1990, A.J., 100, 1892-1902.
297. Woloschuk, M. 1997, Ottawa Citizen, 12 April issue, p.A1.
298. Yao, Y., Hirata, N., Ishii, M., Nagata, T., Ogawa, Y., Sato, S., Watanabe, M., Yamashita, T. 1997, Ap. J., 490, 281-290.
299. Yuan, Y.F., Zhang, J.L. 1998, Astron. & Astrophys., 335, 969-972.
300. Zwaan, C. 1978, Sol. Phys., 60, 213.